12-14-2002

Seasonal Biogeochemistry And Mineral Cycling Of The Middle Rio Grande Alluvial Aquifer, New Mexico

David Stewart Vinson

THE UNIVERSITY OF NEW MEXICO
ALBUQUERQUE, NEW MEXICO 87131

POLICY ON USE OF THESES AND DISSERTATIONS

Unpublished theses and dissertations accepted for master's and doctor's degrees and deposited in the University of New Mexico Library are open to the public for inspection and reference work. *They are to be used only with due regard to the rights of the authors.* The work of other authors should always be given full credit. Avoid quoting in amounts, over and beyond scholarly needs, such as might impair or destroy the property rights and financial benefits of another author.

To afford reasonable safeguards to authors, and consistent with the above principles, anyone quoting from theses and dissertations must observe the following conditions:

1. Direct quotations during the first two years after completion may be made only with the written permission of the author.

2. After a lapse of two years, theses and dissertations may be quoted without specific prior permission in works of original scholarship provided appropriate credit is given in the case of each quotation.

3. Quotations that are complete units in themselves (e.g., complete chapters or sections) in whatever form they may be reproduced and quotations of whatever length presented as primary material for their own sake (as in anthologies or books of reading) ALWAYS require consent of the authors.

4. The quoting author is responsible for determining "fair use" of material he uses.

This thesis/dissertation by David Stewart Vinson has been used by the following persons whose signatures attest their acceptance of the above conditions. (A library which borrows this thesis/dissertation for use by its patrons is expected to secure the signature of each user.)

NAME AND ADDRESS	DATE

David Stewart Vinson
Candidate

Earth and Planetary Sciences
Department

This thesis is approved, and it is acceptable in quality and form for publication on microfilm:

Approved by the Thesis Committee:

, Chairperson

Accepted:

Dean, Graduate School

12·14·02

Date

SEASONAL BIOGEOCHEMISTRY AND MINERAL CYCLING OF THE MIDDLE RIO GRANDE ALLUVIAL AQUIFER, NEW MEXICO

BY

DAVID STEWART VINSON

B.S.Geo., Geology / American Studies,
The University of Alabama, 2000

THESIS

Submitted in Partial Fulfillment of the
Requirements for the Degree of

Master of Science
Earth and Planetary Sciences

The University of New Mexico
Albuquerque, New Mexico

December, 2002

ACKNOWLEDGEMENTS

This project would not have been possible without the wells that were installed by Bruce Allen (New Mexico Tech), Susan Block, Laura Crossey, and Rick Ortiz. The Belén research site was established by the UNM Hydrogeology Group with the cooperation of the Middle Rio Grande Conservancy District, on whose land it sits. My research was preceded and enhanced by the great work done in the bosque by Susan Block. I thank my thesis committee, Drs. Laura Crossey, Cliff Dahm, and Adrian Brearley, for their guidance and advice.

Lab and field collaborators were Susan Block, Bethany Burnett, Danielle Clemons (PURSUE), Crystal Dodson (PURSUE), Andy DuFrane, Jim Karner, Dorothella Littlepage (SHARP), Nadia Madden, Alaina Pershall (PURSUE), Marybeth Riley (PURSUE), Jeff Tepper, Kate Ziegler, Mindy Zimmer, and the friendly staff at Burritos Alinstante. Without their enthusiastic toil, none of the work in this thesis would have been possible.

Jim Thibault, UNM Biology, provided a huge amount of hydrologic data that immeasurably helped my work. Diana Northup showed me how to use the autoclave. John Craig helped me with the organic carbon analyzer. Jim Karner and Mike Spilde spent countless hours training me on the SEM. Dr. John Bloch ran several X-ray samples and provided great advice at every turn.

Other UNM lab facilities were generously made available for my work: the Soils Lab (Dr. Les McFadden), the Scanning Electron Microscope Lab (Mike Spilde), the Gas Chromatography Lab (Dr. Tobias Fischer), and the Biology Annex Lab (John Craig). Finally, I must thank John Husler, SSU, for patience, advice, meals, the use of his lab, and boundless assistance.

And to Andy, Jaime, Amanda, Susan, Lynne, Laura, Melissa, Mike G., Lysa, Toti, Mindy, Rachel, Danielle, Mike T., Rick, Lea Anne, and Heather....You know what you did.

Lab and field assistance was funded in part by the UNM-NASA PURSUE Program (PAIR), Grant # NCC5-350, funded by the NASA MURED Division; and NASA SHARP PLUS. Hydrologic data from Biology was funded in part by NASA contract NAG5-6999. Much of my time at UNM was generously funded by the Caswell Silver Foundation.

SEASONAL BIOGEOCHEMISTRY AND MINERAL CYCLING OF THE MIDDLE RIO GRANDE ALLUVIAL AQUIFER, NEW MEXICO

BY

DAVID STEWART VINSON

ABSTRACT OF THESIS

Submitted in Partial Fulfillment of the
Requirements for the Degree of

Master of Science
Earth and Planetary Sciences

The University of New Mexico
Albuquerque, New Mexico

December, 2002

SEASONAL BIOGEOCHEMISTRY AND MINERAL CYCLING OF THE MIDDLE RIO GRANDE ALLUVIAL AQUIFER, NEW MEXICO

by

David Stewart Vinson

B.S.Geo., Geology / American Studies, The University of Alabama, 2000

M.S., Earth and Planetary Sciences, The University of New Mexico, 2002

ABSTRACT

The Rio Grande in central New Mexico flows through a semi-arid, historically aggrading Quaternary rift basin. Flow regulation measures include dams, irrigation diversions, levees, and bank stabilization. These have caused severe impairment including incision, lowered water tables, and less overbank flooding; disrupted groundwater – surface water interactions; altered seasonal organic carbon dynamics; and declining native biota. Previously dynamic flowpaths in the shallow alluvial aquifer (hyporheic corridor) have become are less reversible due to parallel drain ditches with lower beds than the river. These ditches impose relatively static hydraulic gradients on the alluvial aquifer that force water to flow from the river to the drains.

A water sampling campaign from May 2001 through April 2002 established seasonal major element and redox chemistry using dialysis multi-level samplers, wells, and surface water sampling. Sediment extractions quantified and characterized authigenic Fe/Mn oxyhydroxides, as well as solid phase P, all of which were more widespread in intermittently wetted sediments near the water table. Filter papers were

incubated in the aquifer to grow seasonal precipitates and examined by scanning electron microscopy with chemical characterization by energy-dispersive X-ray spectroscopy.

Oxygen is rapidly depleted from Rio Grande water shortly after it enters hyporheic corridor sediments. A series of terminal electron-accepting processes, including denitrification, manganese reduction, iron reduction, and sulfate reduction, occurs under anoxic conditions as microorganisms metabolize organic carbon. These reactions occur down-flow from the Rio Grande through the alluvial aquifer toward the drainage ditch system. These redox processes depend on changes in hydraulic head driven by diel, seasonal, interannual, and irregular (anthropogenic) variations in river stage. Oxic – anoxic cycling produces Fe/Mn oxyhydroxide and Fe sulfide minerals near the water table. Stalky, helical, and spherical oxide morphologies and cubic sulfide morphologies were observed. These phases grow on the scale of weeks, probably as microbial respiration products. Seasonal mineralogy and organic carbon dynamics may affect water quality and the success of potential restoration efforts. Restoration should include geochemical and hydrologic monitoring of groundwater – surface water interactions.

Table of Contents

List of Figures

List of Tables

Introduction

Interactions between channels and alluvial aquifers are mutual and bidirectional, rather than the traditional "pipe" model of a channel carrying solutes and sediments to the ocean (Bencala, 1993). Groundwater-surface water interactions among alluvial rivers may occur rapidly, depending on geomorphic, sedimentological, and hydrologic factors. Sandy riparian aquifers may exchange with the channel on the scale of hours, producing an area of high biogeochemical activity termed the hyporheic corridor (Stanford and Ward, 1993). These shallow sediments host geochemical processes between solutes and solids, including oxidation – reduction, precipitation – dissolution, hydration – dehydration, and microbial competitive relationships driven by shifting supplies of oxidants, organic carbon, and nutrients (Drever, 1997; Groffman and Crossey, 1999; Baker et al., 2000a).

An understanding of the relationships between surface water, groundwater, and aquatic and terrestrial ecosystems in the hyporheic corridor can be applied to such diverse problems as nutrient dynamics, water resources, flood management, fire management, aquatic ecology, and disturbed lands restoration. Over geologic time, these processes are crucial to the diagenetic transition from alluvial sediments to sedimentary rocks seen in the ancient record. This research seeks to identify biogeochemical redox zones in a disturbed alluvial system, the Middle Rio Grande of New Mexico.

Geologic and hydrologic setting

The Rio Grande heads in the Sangre de Cristo Mountains of southern Colorado and receives tributary inputs from northern mountains and a large, linear group of structural basins in central New Mexico that collectively represent the Rio Grande Rift

(Figure 1). This long-lived (> 10 Ma) tectonic feature has produced basins up to 7000 m deep, shed large volumes of sediment from uplifted areas, and produced abundant Quaternary volcanic rocks (Lozinsky et al., 1991; Russell and Snelson, 1994).

The southern Albuquerque Basin, where this study was conducted, contains a deep graben under the present-day Rio Grande, bounded by shallower blocks separated by normal faults (Figure 2; Russell and Snelson, 1994). Within this basin flowed the ancestral Rio Grande and Rio Puerco. The oldest Tertiary – Quaternary Santa Fe Group deposits are dominated by low-energy closed-basin facies, with large areas of fine sediments and evaporites. Upper Santa Fe Group sediments were deposited by higher energy, through-flowing rivers. These sediments are sandier and serve as the primary water-supply aquifer for the region (Lozinsky et al., 1991; Hansen and Gorbach, 1997).

In the Middle Rio Grande catchment, sediment sources are diverse. Lithologies are plutonic (granitoids); volcanic (basalt, tuff, and glass); metamorphic (quartzite, pelitic schist, and gneiss); and sedimentary (limestone, sandstone, evaporites, and unconsolidated basin-fill sediments). Modern sources of sediment include major tributaries such as the Jemez River, as well as floods carrying basin-fill material from ephemeral tributaries (Rittenhouse, 1944). In the past fifty years, sediment has become unavailable due to upstream dam construction (Baird, 2001), so the study is being conducted on a non-aggrading or incising alluvial plain.

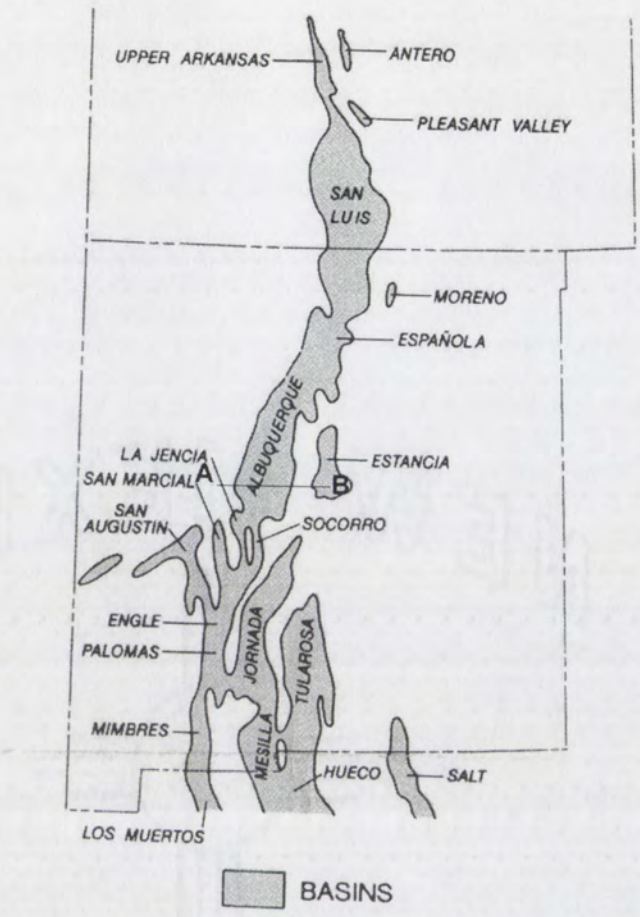

Figure 1. Sedimentary basins of the Rio Grande Rift, including the Albuquerque Basin (Woodward, 1984).

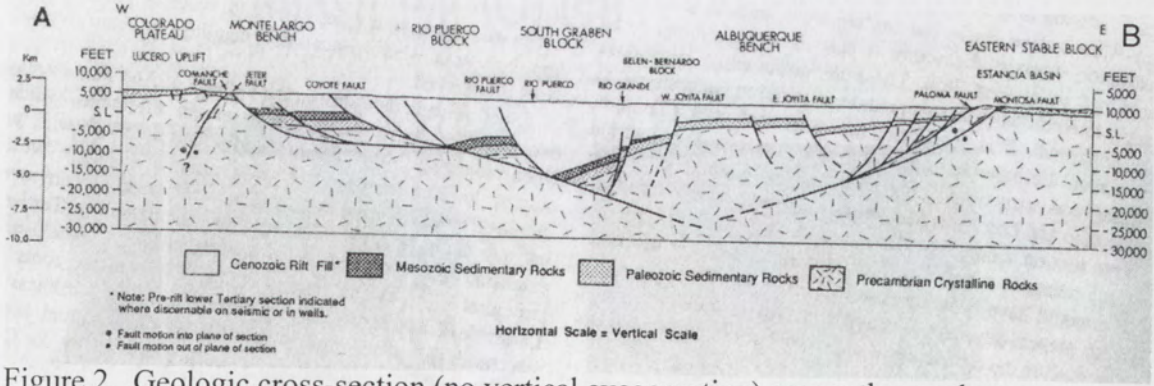

Figure 2. Geologic cross-section (no vertical exaggeration) across the southern Albuquerque Basin along a line from the southern Lucero Uplift to the southern Manzano Mountains. The study area is along the Rio Grande, at center (Russell and Snelson, 1994).

The study location (Figure 3-Figure 5) is along the eastern bank of the Rio Grande between Belén and Casa Colorada, New Mexico, at 34° 35' 25" N, 106° 45' 02" W, and elevation 1460 m. The sediments immediately up-gradient from the floodplain at Belén include Holocene – Pleistocene alluvial and eolian sand and gravel, older Quaternary alluvium recycled from Santa Fe Group basin-fill sediments, and Quaternary terraces representing past Rio Grande aggradation (Love, 2000). These bluffs and slopes adjacent to the channel represent one of two critical "recharge windows" between Isleta Pueblo and Bernardo. Recharge windows are locations at which surface water is most effective at recharging the basin-fill aquifer used for water supply (Hawley and Whitworth, 1996; Hansen and Gorbach, 1997). The valley-fill sediments involved in this study are highly conductive and connected to the river. The well hydrograph responds to changes in river stage within a few hours. These rapid groundwater-surface water interactions are characteristic of the hyporheic corridor as defined by Stanford and Ward (1993).

The shallow, alluvial valley-fill aquifer represents the Rio Grande's Pleistocene – Holocene aggradational phase as it deposited sediments in a valley approximately 20 m deep. This aggradation probably resulted from climate change, as the region has become more arid in the past few thousand years, with lower streamflow, less vegetation, and greater sediment loads (Kelley, 1977). In the Albuquerque Basin, valley-fill sediments are 15-29 m thick to the contact with the Santa Fe Group (Connell and Love, 2001). Prior to large-scale regulation efforts, mean aggradation rates along the MRG were estimated at 5.8 cm yr^{-1} from 1936-41 (Rittenhouse, 1944). This rate has probably varied greatly, since arroyos deliver sediment episodically on the scale of tens to hundreds of years (Bull, 1997).

Figure 3. Aerial photograph of the study site, taken February 2001. SJMC: San Juan Main Canal: an irrigation-supply ditch, seasonal use only; USJRD: Upper San Juan Riverside Drain: A drain ditch with no surface connection to other ditches. Its only source of water is intercepted groundwater; RRD: River-return ditch from drainage system (U.S. Bureau of Reclamation, Albuquerque, N.M., unpub. georectified photo, frame 40, 2001).

Figure 4. The Rio Grande, facing west from its confluence with RRD (see Figure 3, above) on 10 Oct 2001, showing banks stabilized by Russian olive (short, light green trees) and even-aged cottonwood bosque beyond (tall, dark green trees).

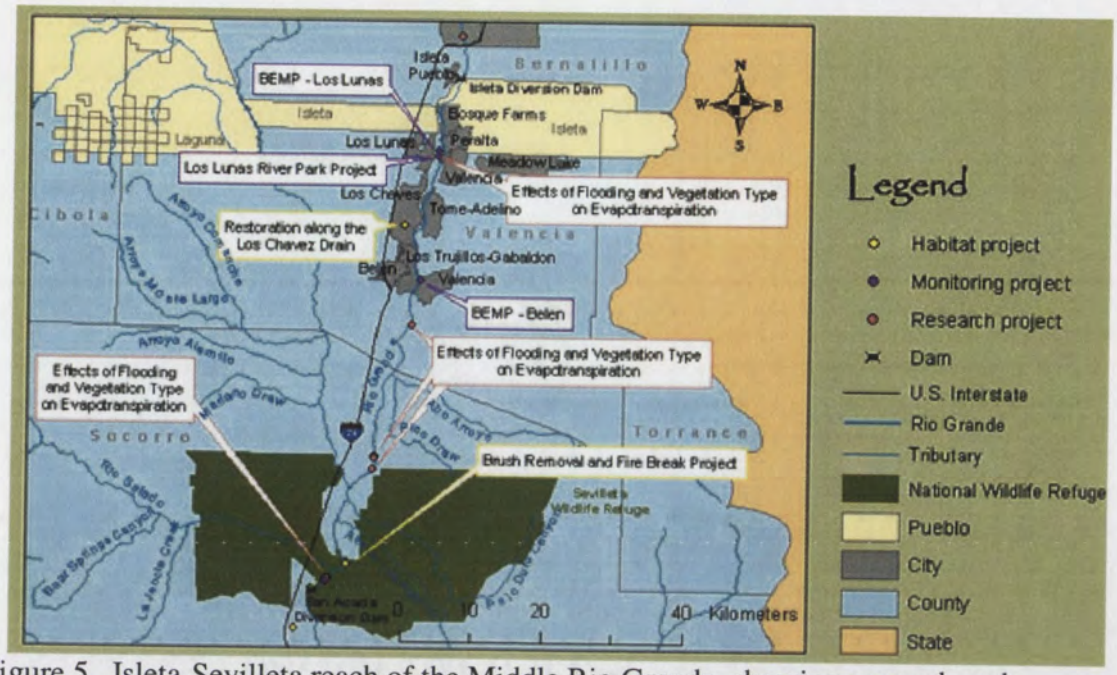

Figure 5. Isleta-Sevilleta reach of the Middle Rio Grande, showing research and restoration projects (U.S. Fish and Wildlife Service, 2002). This study was conducted at the evapotranspiration site 10 km south of Belén.

The Middle Rio Grande hydrograph naturally shows seasonal variability. The largest input is snowmelt from mountain tributaries, peaking in May or June (Figure 6). During the study period, 2000-01 snowpack was slightly above average, facilitating a high flow in May, but 2001-02 snowpack was substantially below average. The other primary input is the fall monsoon season from July through September. Interannual climate variability produces wide changes in stage from year to year (Molles and Dahm, 1990; Molles et al., 1992). Within each year, seasonal pulses caused by snowmelt and the North American Monsoon produce days to weeks of high stage. The relationship between snowpack and monsoon rain is complex and may be inverse in many years (Gutzler and Preston, 1997; Costigan et al., 2000). Human releases and irrigation diversions overprint these natural pulses. The water table at Belén does not exactly track the river hydrograph due to upstream diversions at Isleta Pueblo or varying amounts of water in the irrigation system and riverside return ditch.

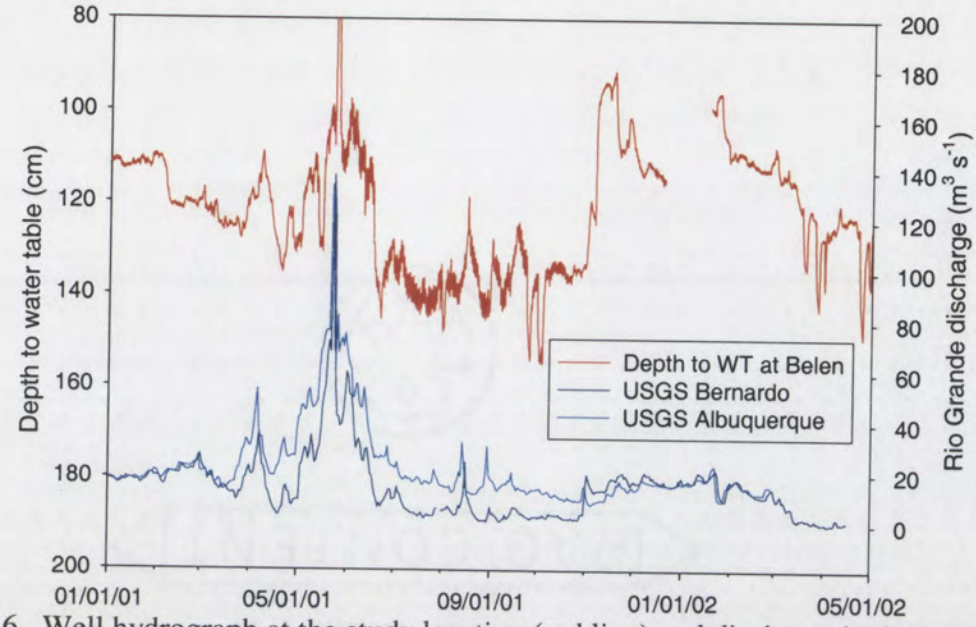

Figure 6. Well hydrograph at the study location (red line) and discharge hydrographs for the Rio Grande at Albuquerque, 60 km upstream and Bernardo, 22 km downstream (blue and purple lines) showing losing nature of the Rio Grande during irrigation season. Well data provided by J.R. Thibault et al. (unpub. data). Discharge data provided by U.S. Geological Survey, Water Resources Division.

River regulation

An elaborate irrigation and drainage system was constructed along the MRG during the twentieth century. Water is diverted at several locations along the reach of river and travels through high-line canals parallel to the river at the upper edge of the floodplain. Smaller distribution ditches then carry water by gravity flow into the fields. Irrigation structures at the Belén site are different from elsewhere in the MRG due to the narrowness of the floodplain. In 1947 (Figure 7a), water was diverted directly from the river to the local irrigation system at San Juan Heading (the nearby study site may have been a channel or scoured bank). By the 1970s, a riverside canal was constructed from Belén to San Juan Heading, where water is currently diverted from the canal into a ditch that serves the local area from the upper edge of the floodplain. In the same area begins a separate ditch with no surface connection, the Upper San Juan Riverside Drain (USJRD;

Figure 3). The riverside drains steepen the hydraulic gradient beneath the bosque, lower water tables below the floodplain, and reduce the waterlogging of fields, returning this water to the Rio Grande via surface flow (Titus, 1963; Hansen and Gorbach, 1997). Because the riverside drains have lower bed levels than the corresponding river bed, relatively static flow directions are imposed from river to drain (Peter, 1987), rather than the bidirectional flows expected in the hyporheic corridor of an undisturbed alluvial river (Bencala, 1993).

Since the 1942 flood season, the MRG has undergone flow regulation measures that include upstream dam building, bank stabilization, and levee construction. Prior to regulation, the Rio Grande frequently flooded into adjacent fields and wetlands. Flood sedimentation raised the water table, enabled native cottonwoods to reproduce on freshly deposited sediments, and damaged cropland (Crawford et al., 1993). Research based on the 1941 flood season indicated that levees and drainage alone would not be able to stop crop damage or aggradation; however, the sediment load of the Rio Grande could be reduced by stabilizing the erosion-prone banks of arroyos or by constructing sediment-detention dams on major tributary streams (Happ, 1948). Ultimately, the U.S. Army Corps of Engineers built dams on Galisteo Creek, the Jemez River, the Santa Fe River, and the upper Rio Grande itself. This had the effect of removing every major sediment-contributing tributary from the upper reach of the MRG by 1975 (Table 1).

Additional projects, begun in 1948, sought to convert the MRG from a braided, shifting bed to a stable, incised channel that was less flood-prone. Most widespread was the installation of jetty jacks, steel structures connected by cables, which slowed flows, trapped debris, and encouraged permanent vegetation to take root (Lagasse, 1981;

Table 1. Major tributary contributions of water and sediment to upper MRG before regulation. Numbers in parentheses indicate range of possible values after effects of minor tributaries are estimated.

Tributary	Water contribution to Bernalillo-Bernardo reach, percent [1]	Sediment contribution to Bernalillo-Bernardo reach, percent [2]	Date of dam completion [3]
Upper Rio Grande	90.	45 (11-37)	1975
Santa Fe River	0.71	2 (1-2)	1975
Galisteo Creek	0.25	8 (2-6)	1970
Jemez River	5.2	45 (21-40)	1953
Abq. Stormwater canals	0.62	No data	N/A
Tijeras Arroyo	0.03	No data	N/A
Abq. wastewater plant (from deep groundwater)	3.6	N/A	N/A

[1]- Action Committee of the Middle Rio Grande Water Assembly, 1999
[2]- Rittenhouse, 1944
[3]- Scurlock, 1998

Crawford et al., 1993; Grassel, 2002). At the time, incision was regarded as a beneficial engineered effect because it would prevent the river from shifting laterally into agricultural land (Pemberton, 1964; Grassel, 2002). These measures have resulted in a 65-77% decrease in width and a 45-125% increase in depth, and drastically reduced sediment loads during the twentieth century (Baird, 2001).

Historical maps (Figure 7) reveal changes in vegetation which have occurred throughout the MRG since the 1940s. Historical conditions along the river include scattered and uneven-aged native riparian forests on a dynamic floodplain, interspersed with scoured sand and active deposition. Flow regulation, reflected on the 1991 map (Figure 7b), has made possible a continuous even-aged riparian forest of cottonwood (*Populus deltoides* var. *wislizenii*) with native understory such as coyote willow (*Salix exigua*; Dahm et al., 2002). For the most part, this forest is no longer reproducing because of the lack of flooding and is being invaded by non-native saltcedar

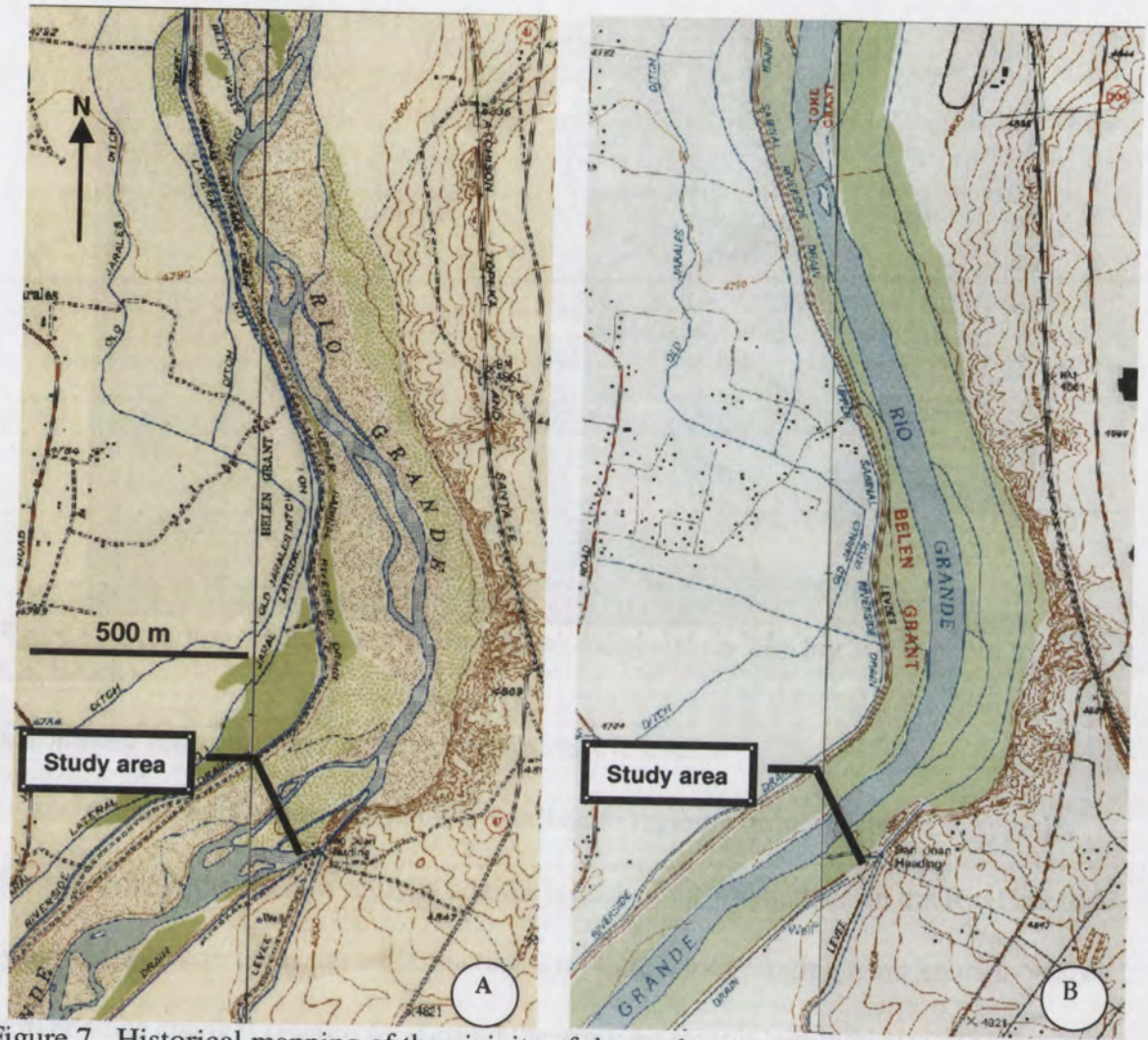

Figure 7. Historical mapping of the vicinity of the study area. From 1947 aerial photos (A) and 1991 photos (B). Vegetation patterns: solid green - forest, green dots - scrub or scattered trees, brown dots - unvegetated sand, no pattern - grass or agricultural (USGS Veguita and Turn 7.5 minute quadrangles: 1952, 1991). Elevations in feet.

(*Tamarix chinensis*) and Russian olive (*Eleagnus angustifolia*; Howe and Knopf, 1991). Although the Belén site floods occasionally, most recently in May 2001, these floods are brief and low-energy, without enough power to produce the sedimentary features seen in the past. For example, the May 2001 flood left signs of standing water at Belén (salts and mud cracks) but no noticeable scour or deposition (Figure 8). Similarly, manipulated floods at Bosque del Apache National Wildlife Refuge in 1993-1995 did not remove accumulated forest debris (Molles et al., 1998).

Figure 8. Standing water from flooding at the study site on 23 May 2001 (photo by S.E. Block).

Intermittent saturation and evapotranspiration

Although the water table in intermediate to regional groundwater flow systems changes slowly, the shallow alluvial aquifer is exceedingly dynamic. In the Rio Grande hyporheic corridor, the water table fluctuates on time scales ranging from hours to years as river stage changes (Figure 6). During the growing season, groundwater consumption by phreatophytes lowers the water table during daylight, which is recharged at night, producing a diel fluctuation. This evapotranspiration (ET)-derived fluctuation is largest in mid-summer (Dahm et al., 2002). ET-derived fluctuations concentrate salts in groundwater, and all of these discharge-recharge events produce redox cycling as oxygenated water enters the aquifer. This dynamic water table has been termed the zone of intermittent saturation (ZIS; Groffman et al., 1998) or the region of seasonal saturation (Baker et al., 2000b). Water table elevation data collected by the UNM Biology Department at 30-minute resolution (J.R. Thibault et al., unpub. data) allow statistical examination of the ZIS. For this discussion, I define the ZIS as the 10^{th}-90^{th} percentiles

of water table elevations. Outliers represent unusual events (such as floods, droughts, and large diversions) that occupy 20 percent of the time. Data collected during 1999-2002 reveal a ZIS approximately 45 cm in vertical extent in which the water table was located 80 percent of the time (Figure 9). For the 2001-2002 period documented in this research, the ZIS was approximately 35 cm in vertical extent (Figure 10). Previous research in low-order forested catchments has demonstrated that the ZIS contains a high level of biogeochemical activity (Groffman et al., 1998; Groffman and Crossey, 1999; Baker et al., 2000b).

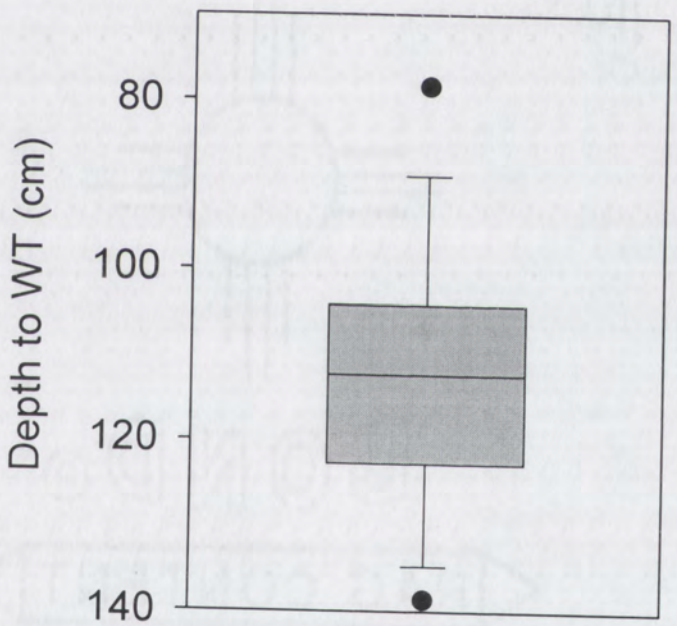

Figure 9. Box plot of measured water table elevations from 27 Apr 1999 to 6 May 2002. Box represents 25th-75th, whiskers 10th-90th, and dots 5th-95th percentiles (Thibault et al., unpub. data, $n = 45{,}509$).

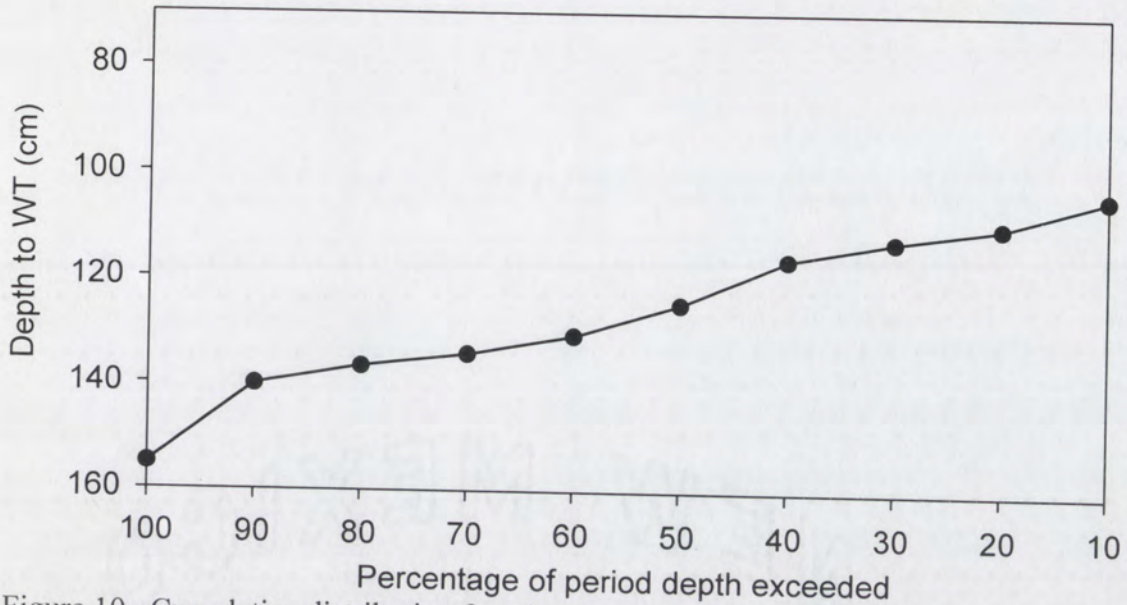

Figure 10. Cumulative distribution function of water table elevations from 1 May 2001 to 30 April 2002 (Thibault et al., unpub. data, n=16,100).

Biogeochemical processes in the ZIS

Many studies have documented a thermodynamically-predictable series of anaerobic organic carbon oxidation processes known as terminal electron-accepting processes (TEAPs). These processes occur along flowpaths at various scales (Champ et al., 1979; Matsunaga et al., 1991; Groffman and Crossey, 1999), as well as in vertical profiles below the sediment-water interface in lacustrine and marine sediments (Nealson and Stahl, 1997). Solid, gas, and aqueous phases are involved in many TEAPs (Table 2), making their study difficult by solute or sediment chemistry alone. Thus, both homogeneous (solute-solute) and heterogeneous (solute-solid and solute-gas) reactions must be considered. In a geological context, the insoluble materials are authigenic minerals, some of which accumulate through early diagenesis. Examining these processes at high resolution within the dynamic ZIS at Belén presents a challenge due to rapid groundwater exchange and perturbed hydrology.

Table 2. Redox processes among phases present in shallow groundwater. CH_2O denotes generic organic matter. Each group of reactions is arranged in usual order of descending thermodynamic favorability (shown by arrows), ambient temperature, and typical freshwater solute concentrations (modified from Baker et al., 2000a).

	Process	Equation	e^- acceptor	e^- donor
TEAPs (Heterotrophic) ↓	Respiration	$CH_2O + O_2 = CO_2 + H_2O$	O *(g)*	
	Denitrification	$CH_2O + (4/5)NO_3^- + (4/5)H^+ = (7/5)H_2O + (2/5)N_2 + CO_2$	N *(aq)*	
	$MnO_{2\ amorph}$ reduction	$CH_2O + 2MnO_2 + 4H^+ = 2Mn^{2+} + 3H_2O + CO_2$	Mn *(s)*	C_{org} *(s/aq)*
	$Fe(OH)_{3\ amorph}$ reduction	$CH_2O + 8H^+ + 4Fe(OH)_3 = 4Fe^{2+} + 11H_2O + CO_2$	Fe *(s)*	
	Sulfate reduction	$CH_2O + (1/2)SO_4^{2-} + (1/2)H^+ = (1/2)HS^- + H_2O + CO_2$	S *(aq)*	
	Methanogenesis	$CH_2O + (1/2)CO_2 = (1/2)CH_4 + CO_2$	C_{org} *(s/g/aq)*	
Lithoautotrophic ↓	Methane oxidation	$2O_2 + CH_4 = HCO_3^- + H_2O + H^+$		C_{org} *(g/aq)*
	Sulfide oxidation	$2O_2 + HS^- = SO_4^{2-} + H^+$		S *(aq/s*)*
	Fe^{2+} oxidation	$O_2 + 4Fe^{2+} + 10H_2O = 4Fe(OH)_3 + 8H^+$	O *(g)*	Fe *(aq/s*)*
	Nitrification	$2O_2 + NH_4^+ = NO_3^- + 2H^+ + H_2O$		N *(aq)*
	Mn^{2+} oxidation	$O_2 + 2Mn^{2+} + 2H_2O = 2MnOOH + 2H^+$		Mn *(aq)*

* - includes FeS *(s)* oxidation, equation not shown.
Abbreviations: *aq*:solute, *s*: solid, *g*: gas

Mineral-groundwater interactions can include precipitation, dissolution, adsorption, and coprecipitation (Drever, 1997). In shallow alluvial aquifers, the fate of abundant metals such as Fe, Mn, and Al is strongly affected by solid-phase interactions ranging from temporary sorption onto amorphous organic masses to nucleation of well-ordered crystals (Darke and Walbridge, 2000). These metals also remove substantial amounts of nonmetal ions such as H^+, O_2, HS^-, and PO_4^{3-} through precipitation or sorption, with varying degrees of permanence. Under anoxic conditions, these minerals form as a direct consequence of organic matter oxidation. Viewed this way, a traditional geological definition of a mineral as "a naturally occurring solid with a highly ordered atomic arrangement and a definite (but not fixed) chemical composition . . . usually formed by inorganic processes" (Klein, 2002) is complementary to a biological definition of mineralization, which involves the conversion of organic compounds to inorganic ones

(Fenchel et al., 1998; Molles, 1999). In this context, the two concepts of "minerals" are not easily distinguished.

Recent work has demonstrated that TEAPs are frequently associated with bacteria that may take advantage of exergonic reactions, catalyze slow processes, overcome activation energy barriers, and/or influence the thermodynamic favorability of a reaction. The usual objective of these processes is to supply the organism with metabolic energy (dissimilatory processes), but they may also provide nutrients to organisms (assimilatory processes) or immobilize harmful compounds (detoxification; Ehrlich, 1996).

Bacteria are highly specialized, made necessary by their small size (1.5-2.0 μm^3), which does not allow room for physiological complexity (Beveridge, 1989). This necessity, combined with rapid growth and short generation time, guarantees that bacterial species specialization is immense. Recently-developed molecular methods that do not require culturing have revealed much greater diversity in microbial communities than previously believed (Amann et al., 1996) because over 90% of microbes are thought to be unculturable (Banfield et al., 1998). Due to rapid advances in techniques for studying bacteria, numerous schemes have arisen for classifying the newly discovered bacteria. Microbiological processes of interest to geologists, including the oxidation and reduction of iron, manganese, and sulfur, are spread among several kingdoms within Domain Bacteria (Barns and Nierzwicki-Bauer, 1997).

Much of the research on TEAPs and groundwater biogeochemistry has focused on regional aquifer systems (Chapelle and Lovley, 1992; Chapelle et al., 1995), which have been extensively studied due to their value as public water supplies and irrigation waters. In these environments, flowpaths are kilometers long, hydraulic gradients are relatively

low, and diffusion to and from clay layers may be substantial. Less work has been done on sandy riparian aquifers, which exchange flow with river channels on the scale of hours to days along potentially reversible flowpaths and undergo complex interactions with mineral surfaces, microorganisms, and higher biota such as phreatophytes.

Microbial Fe/Mn respiration in sediments has been studied extensively in cultures and column experiments, especially by microbiologists. However, the overall geochemical significance of these processes is poorly understood, especially with regard to Fe/Mn interactions with other metals, sulfur, and phosphorous and *in situ* rates of microbial Fe/Mn oxidation and reduction at near-neutral pH (Emerson, 2000). This study evaluates field observations along the Rio Grande, a far more complex system than any laboratory culture. In this research, *in situ* mineral phases are examined in the context of their relationship to seasonal redox chemistry, aquifer hydraulics, and the microbial community.

Hypotheses

- Redox conditions in the aquifer shift at multiple time scales and are associated with water table fluctuations.
- The experimental design, which is based on published pore-size requirements of bacteria (Fredrickson et al., 1997), will reveal varying degrees of *in situ* Fe/Mn mineralization.

Methods

Most water samples were collected with the dialysis multi-level sampling (DMLS) system for continuously screened wells (Ronen et al., 1986a, 1986b; Magaritz et al., 1989; Freedman et al., 1994). This system collects samples passively with 30 dialysis cells distibuted along a 1.5 meter PVC rod (Figure 11). In this study, 14 sampling intervals were established at 9 cm resolution, providing a 30 mL sample per interval. Intervals were separated by rubber gaskets, which prevented vertical exchange within the well casing. The dialysis cells were fitted with membranes (0.2 μm, nylon) that passively filtered the sample. Dialysis cells were filled with deionized, distilled water (DDW) having a resistivity of at least 18 MΩ; the cells then equilibrated with their environment by diffusion across chemical gradients. The rod was left in the ground for three to four weeks, far in excess of the DMLS system equilibration time. Through tracer experiments, equilibration time was determined to be less than one day due to rapid solute transport in the aquifer.

Figure 11. The DMLS system. Cells are 3 cm in diameter.

Starting in November 2001, whole-well samples were collected from the existing well field to supplement the data set of Block (2002). These waters were collected with a peristaltic pump (Geotech) with in-line filters (0.45 μm, Millipore, except 11 Nov and 13 Dec 2001, when they were lab-filtered) into acid-washed plastic (ions) and glass (alkalinity) bottles after bailing one well volume. Large-volume (1 L) grab samples were taken from the Rio Grande and USJRD. For all samples, pH and temperature were recorded at the site. Surface water samples were filtered (0.45 μm, Millipore) and split into cation and anion subsamples in the lab (travel time = 1 hour).

In early 2002, a transect of porewater samplers was installed from the Rio Grande to the USJRD (Figure 12). These samplers consist of ¼" inside diameter plastic tubing inserted to a constant depth of 2 m below the non-surveyed floodplain surface. The samplers were installed by pounding a ½" steel pipe (with a loose-fitting metal bolt and washer in the bottom) into the ground with a fence-post driver. At 220 cm depth, the pipe was withdrawn 20 cm, allowing sand to collapse around and isolate the bolt and washer. The tube was then inserted in the pipe to 200 cm depth and the pipe was withdrawn. Each sampler was purged and sampled at a low flow rate (<10 mL min^{-1}) with a peristaltic pump (Geotech) into acid-washed plastic (ions) and glass (alkalinity, organic carbon) bottles. pH and Eh were determined by pumping through a sealed Teflon flow-through cell (Control Company).

Tracer experiment

DMLS cells were filled completely with a 100 mg L^{-1} bromide solution prepared from LiBr. Cells were installed into the DMLS system and incubated for three periods (approximately 1, 2, and 3 hours). The samples were then transferred to acid-washed

glass vials and analyzed by ion chromatography. This technique is used to estimate specific discharge, a rate of actual groundwater flow. The model used depicts water flowing through the well screen by advection into the narrow space between the screen and the DMLS cell, then diffusing across chemical gradients at the membrane via Fick's second law of diffusion (Crank et al., 1981). Ultimately, an equilibrium concentration is reached, which is the background Br^- concentration before the tracer was introduced (0.1 mg L^{-1}). This procedure is a variation of the point dilution technique; the calculations are described in Ronen et al. (1986b) and Groffman (2001).

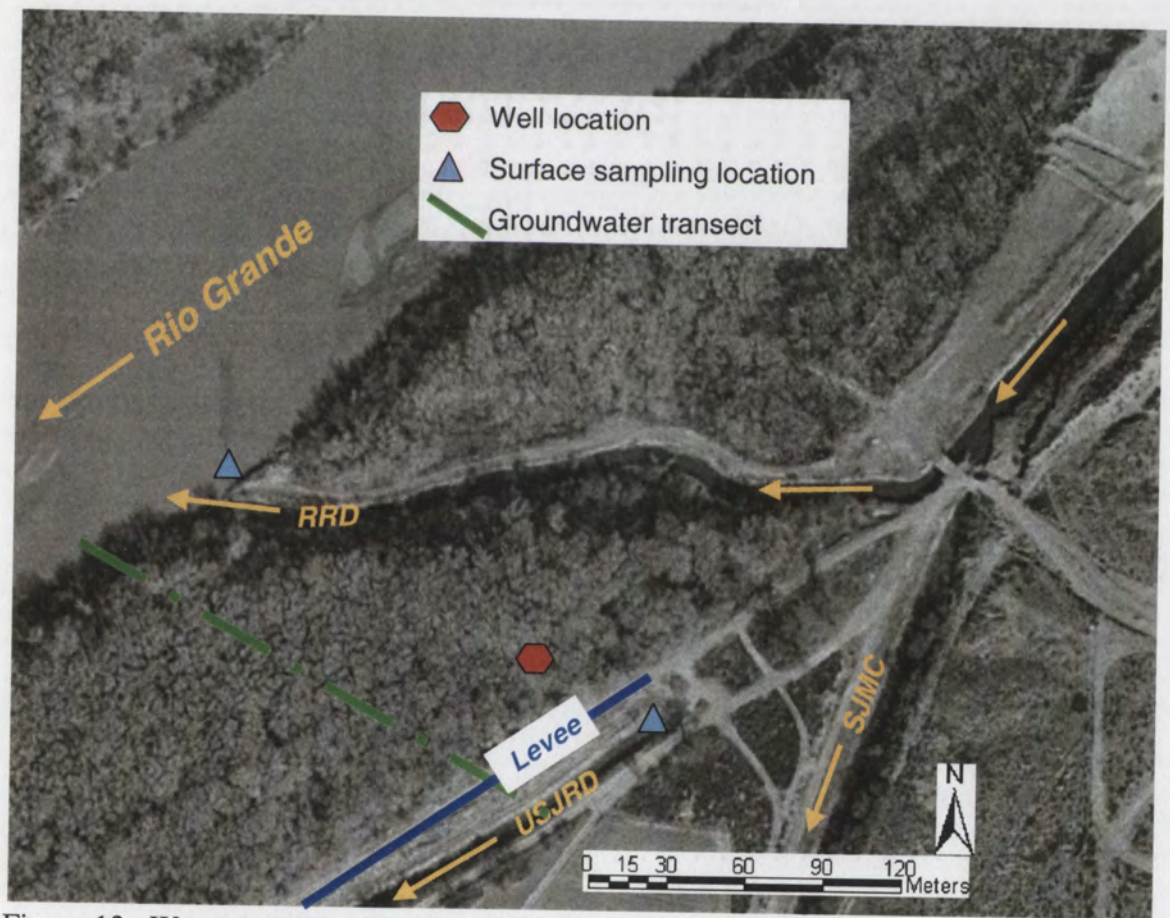

Figure 12. Water sampling locations at the Belén site.

Analytical methods: waters

Analytical methods conform with the standard methods of the American Public Health Association (APHA, 1995), except for adjustments necessitated by small sample volume. A 3 mL subsample was taken from the DMLS cells for immediate electrode analysis in the field. Oxidation-reduction potential (ORP) was determined using a redox electrode (Orion) with $Ag/AgCl_2$ reference (Bricker, 1982; APHA, 1995) and the Orion 290A meter in the millivolt mode. Calibration was provided by measurement in Zobell solution (0.003 M potassium ferrocyanide + 0.003 M potassium ferricyanide + 0.1 M potassium chloride) before, during, and after field work (APHA, 1995; Nordstrom and Wilde, 1998). ORP values were adjusted to the standard hydrogen electrode (Eh) and corrected for electrode drift. pH was analyzed on the same subsample using an Orion electrode with automatic temperature compensation. Dissolved oxygen (DO) and temperature were determined down-hole by the membrane electrode method (Baker et al., 2000a) with a YSI model 55 meter. Sulfide was determined colorimetrically by a modified methylene blue method using commercially prepared reagents (Hach) and fresh sodium sulfide standards (Cline, 1969; APHA, 1995). Samples were analyzed immediately upon return (travel time = 1 h) on a portable Hach DR-2000 spectrophotometer. Ferrous iron was determined colorimetrically at the same time using the 1,10 phenanthroline method and fresh ferrous ammonium sulfate standards (APHA, 1995), but was discontinued in fall 2001 due to poor data quality.

Major cations (Na^+, K^+, Ca^{2+}, Mg^{2+}) and other metals (Mn_T, Fe_T) were determined on acidified subsamples by flame atomic absorption spectrometry (AAS; APHA, 1995). The major elements were analyzed in a matrix of 1000 mg L^{-1} Cs + 10% HCl; the Fe/Mn

subsample was in a matrix of HNO_3 to a pH of below 2. On 11 Nov 2001, ammonia was determined by the ion-specific electrode method (APHA, 1995) on the 3 mL electrode subsample with pH adjusted to above 11 by 10 M NaOH, and using NH_4Cl standards. The electrode subsample was field-preserved with HCl and frozen upon return to the laboratory (APHA, 1995) and analyzed with a Fisher Accumet electrode and an Orion 290A meter in the millivolt mode.

Anions (F^-, Cl^-, NO_2^-, Br^-, NO_3^-, PO_4^{3-}, SO_4^{2-}, acetate, oxalate) were determined by ion chromatography (Dionex DX-500) with AS-14A exchange and AG-14A guard columns and carbonate-bicarbonate eluent (APHA, 1995; Dionex Corporation, 2000). Carbonate alkalinity subsamples (5 mL) were collected into acid-washed syringes stoppered with epoxy-filled pipet tips and analyzed within 24 h. Alkalinity was determined by a Gran titration on four of the fourteen DMLS intervals using a Hach digital titrator and 0.01639 N H_2SO_4. The per-digit interval was 1.25 µL, and calibrations revealed a titrant dispensing error of +0.12 %. For the remaining ten intervals, HCO_3^- was back-calculated by difference, based on the average charge balance error from the first four analyses.

Charge balance error was also used for quality control. Error averaged +2.9% (more cations recovered than anions) and exceeded 10 percent in only two out of 33 samples examined in this way. Because errors of opposite sign will cancel each other, the average of absolute values of charge balance error was also calculated, and was 4.0%. Non-purgeable (dissolved) organic carbon (NPOC) was determined on HCl-preserved samples by high-temperature oxidation (Shimadzu). The mean of three to five replicates plus or minus one standard deviation is presented.

Samples for dissolved gas concentrations were collected on 10 Oct 2001 by pumping into a clean glass vial with a Teflon seal using a peristaltic pump at a slow flow rate of ~100 mL min^{-1} (Jakobsen and Postma, 1999). This sample was rushed to the laboratory (travel time = 1 h), injected into an evacuated 250 mL Giggenbach bottle, and analyzed in the UNM Volcanology Laboratory on a gas chromatograph with thermal conductivity detector (TCD) for H_2 and flame ionization detector (FID) for CH_4.

Geochemical modeling

Water chemistry data for all DMLS samples were entered into PHREEQC software for Windows, version 1.5 (Post, 2001), a variation of PHREEQC, version 2 (Parkhurst and Appelo, 1999). Thermodynamic data for additional mineral phases were added from the WATEQ4F database (Ball and Nordstrom, 1991). PHREEQC output includes pe, speciation, and saturation indices. Stiff diagrams were created with RockWorks 99 software (RockWare, 1999). Eh-pH diagrams were created using The Geochemist's Workbench software (Bethke, 1998).

Sediment sampling

Nine monitoring wells were installed at the Belén site, with a variety of screened intervals. Sediments were collected from BLN2 and BLN9, two shallow wells immediately adjacent to one another (~1 meter apart). BLN2 was installed in January 2000 using a motorized drilling rig. BLN9 was installed in April 2001 by hand augering. Sediment samples were taken at 15 cm vertical resolution and oven-dried at 40 °C or 65 °C. Additional samples from the BLN9 sediments were collected using clean methods and frozen under sterile, anaerobic conditions in argon-purged, steam-autoclaved glass jars. BLN2 was completed at 549 cm depth, and BLN9 was pounded

slightly more than 168 cm depth, the deepest sample obtained. Saturated sand collapsed immediately into uncased holes, limiting the usefulness of hand augering. The BLN2 sediments have undergone more homogenization in the sampling process, especially in the upper 1.2 m (B.D. Allen, driller's note); BLN9 sediments were augered carefully and maintained their heterogeneity with depth. These adjacent wells were combined to make a single depth profile; BLN9 sediments were used for the upper part of the profile, and BLN2 sediments were used for the lower portion, to 550 cm depth. These sediments underwent particle size analysis by the methods of Day (1965) and Jackson (1969). BLN2 sediments were impregnated with blue epoxy resin and made into petrographic thin sections. These sections were randomly point counted (150 points per sample) using a Swift automated stage on an Olympus petrographic microscope.

Selective chemistry: extractions

Several extraction techniques were attempted on the samples from both wells. For all extractions, sediments were crushed to 100 mesh. The oxalate extraction technique (McKeague and Day, 1966) uses 0.2M ammonium oxalate buffered to pH 3 with oxalic acid. This technique is believed to dissolve amorphous iron(III) oxides plus magnetite. However, if the magnetic fraction is removed beforehand, which we did due to the presence of detrital magnetite, oxalate-extractable iron (Fe_{ox}) is a reasonable approximation of microbially reducible ferrihydrite (Lovley, 1987). After oxalate solution was added, the samples were extracted for 4 h on a shaker table in the dark, centrifuged for 10 min at 1500 rpm, and the supernatant was sampled for analysis by AAS. An additional technique with similar application to the oxalate extraction is the 0.5N HCl method (Roden and Edmonds, 1997), which also approximates amorphous

iron. Dried and crushed sediments were extracted in 0.5N HCl on a shaker table for 24 h, centrifuged, and the supernatant analyzed by AAS for Fe ($Fe_{0.5N}$) and Mn ($Mn_{0.5N}$). Because this method also dissoves phosphorous associated with metal oxyhydroxides (Roden and Edmonds, 1997), the 0.5N HCl extracts were also analyzed colorimetrically for phosphate ($P_{0.5N}$) by the ammonium molybdate – potassium antimonyl tartrate – ascorbic acid (AM) method (Murphy and Riley, 1962; APHA, 1995). Si concentrations in the acid extracts were determined by AAS, and Si-spiked blanks (bracketing actual Si concentrations, up to 100 mg L^{-1}) were run through the AM method to rule out the possibility of silica interference with the procedure (Brown et al., 1970).

Total non-silicate iron is estimated by the citrate – dithionite method (Mehra and Jackson, 1960; McKeague and Day, 1966), which employs sodium dithionite buffered by sodium bicarbonate to pH 7.3. Dithionite is used for two sequential 15-minute reaction periods at 77 °C, with centrifuging and sampling of the supernatant after each period, and analysis by AAS. The difference between Fe_{dith} and Fe_{ox} is crystalline, dehydrated iron(III) oxides, including goethite and hematite, but not ferrihydrite (McKeague and Day, 1966; Darke and Walbridge, 2000).

Bulk chemistry of size separates

BLN2 sediment samples were sieved into > 63 μm (sand) and < 63 μm (fine) splits. Sediments were analyzed for major elements (Si, Al, Fe, Mg, Ca, Na, K, Ti, and P) by X-ray fluorescence (XRF). In addition, loss on ignition (LOI) was determined in a furnace at 1000 °C (after removal of non-crystalline water at 110 °C) and reported as weight percent. LOI includes crystalline water, organic and inorganic carbon, and other volatiles. XRF data were reported as weight percent of oxides and normalized to

(100% - %LOI). In three fine samples, inadequate weight was available to determine LOI accurately, so the average of four fine LOI values was used to normalize those data.

Mineral growth incubations

Many researchers have explored microbial and abiotic redox mineral growth in laboratory media (Roden and Edmonds, 1997), but fewer experiments have attempted to isolate *in situ* authigenic minerals from natural sediments after their growth (Ferris et al., 1987) or through experimental design (Ferris et al., 1989a). For this study, experimental microcosms were created by placing glass microscope slides in the environment, an approach used previously to image iron-oxidizing (Hanert, 1974) and manganese-oxidizing bacteria (Robbins et al., 1999). The DMLS system has similarly been used to study mineral dissolution *in situ* (Freedman et al., 1994). In this research, varying the nominal pore size of the DMLS membranes allows the degree of particle and bacteria access to be manipulated (Table 3).

Glass microscope slides were frosted with silicon carbide to increase surface area, cut to fit the DMLS cells, sterilized in dilute sodium hypochlorite, rinsed in sterile DDW, and dried in a positive-pressure hood. The slides were inserted into the DMLS cells, which had been sterilized in the same manner. The cells were filled with sterile DDW and transported to the field site in sterile glass jars. Sterile gloves were worn at all times while handling these parts. After collection, cells were transported in a nitrogen-filled glove bag, stored frozen in nitrogen-purged jars, then dried at 35 °C in a nitrogen-filled glove box. Once dry, these samples were stored in an air-filled desiccator and sputter coated with carbon or noble metal prior to analysis. In addition, DMLS membranes from water sampling runs were air-dried and stored aerobically.

Table 3. Summary of mineral growth incubations.

Incubation period	Days in period	Types of samples
5 May 2001-27 Jun 2001	54	10 μm cells with large perforations, slides inside 0.2 μm cells, slides inside (abiotic control)
22 Aug 2001-19 Mar 2002	218	10 μm cells, slides inside 0.2 μm cells (abiotic control)

Scanning electron microscope (SEM) imaging was done on a JEOL 5800-LV instrument with low-vacuum capability. An Oxford Isis 300 energy dispersive x-ray spectroscopy (EDS) unit with an ultra-thin window detector provided qualitative chemical analysis for atomic numbers down to 5. Some preliminary work used uncoated, wet samples in low-vacuum (environmental) mode (ESEM). For most analyses, samples were Au-Pt coated and analyzed by conventional SEM for improved imaging and X-ray analysis. Under these conditions, the SEM is able to resolve structures well into the nanometer size range (Goldstein et al., 1992, Surman et al., 1996), although samples must undergo more disturbance during preparation (drying and coating). Conventional SEM/EDS analysis also included new (blank) 0.2 and 10 μm nylon DMLS membranes. Images were obtained in secondary electron (SE) mode for best imaging and backscatter electron mode (BSE) to rapidly locate metals while examining samples.

Results

Sedimentary petrology

In the phreatic zone and ZIS, sediments are sand-dominated (Figure 13). In the area between 100 and 200 cm depth, where this research was conducted, sediments are approximately 90% sand, with the remainder silt- and clay-sized. Vadose sediments exhibit particle-size reduction to silt and clay, characteristic of soil development. The data certainly underestimate gravel proportions due to the sampling methods used. Particle size data are tabulated in Appendix II. Point counting, done collaboratively with Block (2002), indicates a homogeneous detrital sand composition on the Q_M-F-L diagram (Figure 14). If polycrystalline quartz is counted as a lithic clast, most of the samples examined are classifed as sublitharenites by the system of McBride (1963). The most common lithic clasts are volcanic, which broadly agrees with the findings of Lozinsky (1994) for upper Santa Fe Group sediments.

Groundwater flow rates

No systematic trend across time or space could be seen in the tracer data. Based on the depth profile (Figure 15), groundwater flow rates are reasonably constant with depth. The average rate is 75 ± 8 m day^{-1}. The data are tabulated in Appendix I.

DMLS profiles

DMLS chemistry data are tabulated in Appendix IV and plotted beginning with Figure 48. Down-hole dissolved oxygen and temperature data (Figure 59-Figure 60) are tabulated in Appendix III. These data are presented in detail in the Discussion section.

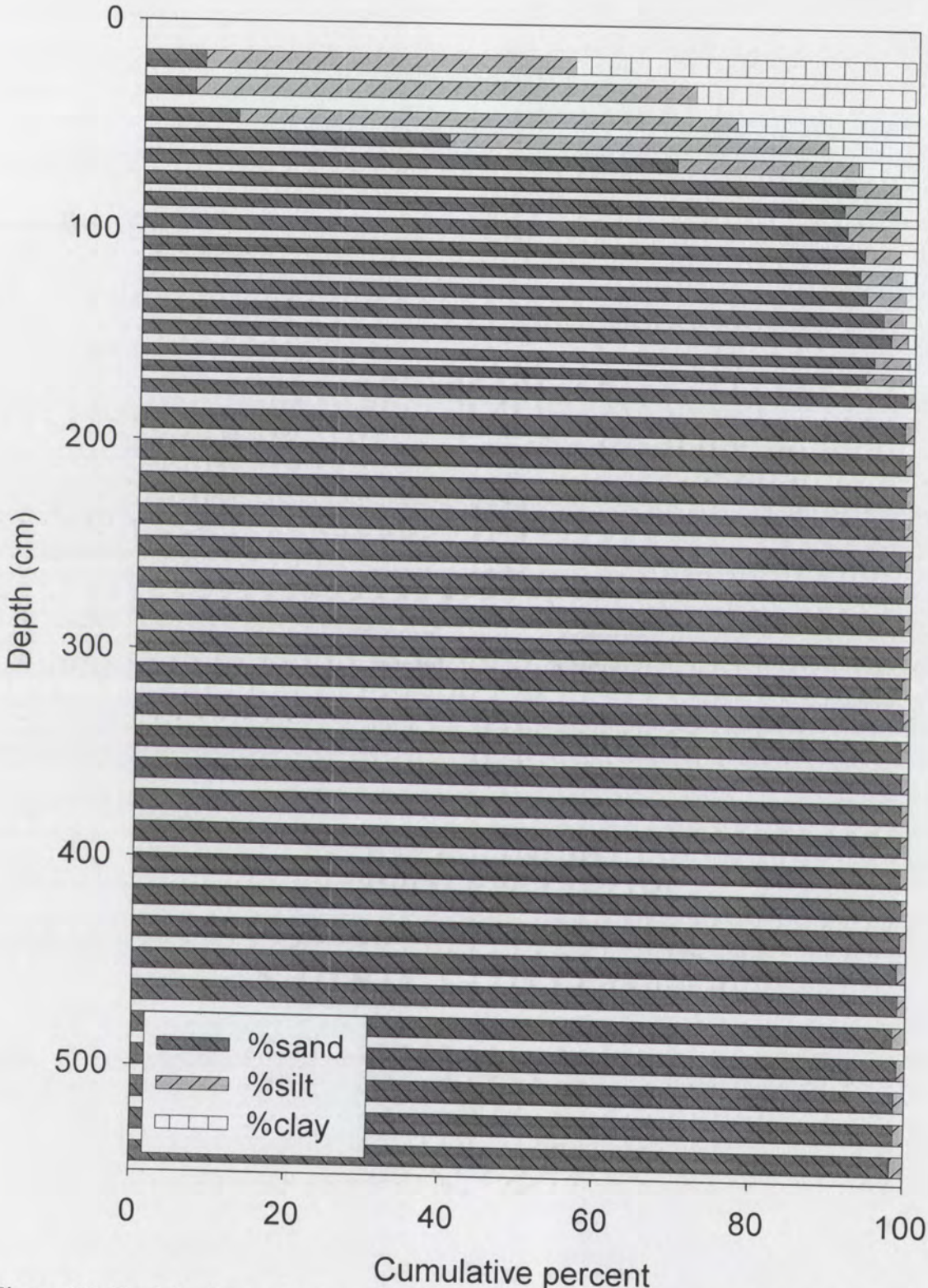

Figure 13. Particle size analysis results for the study site. Data above 168 cm depth are from BLN9; those below 168 cm depth are from Block (2002) for well BLN2. Gravel content is negligible.

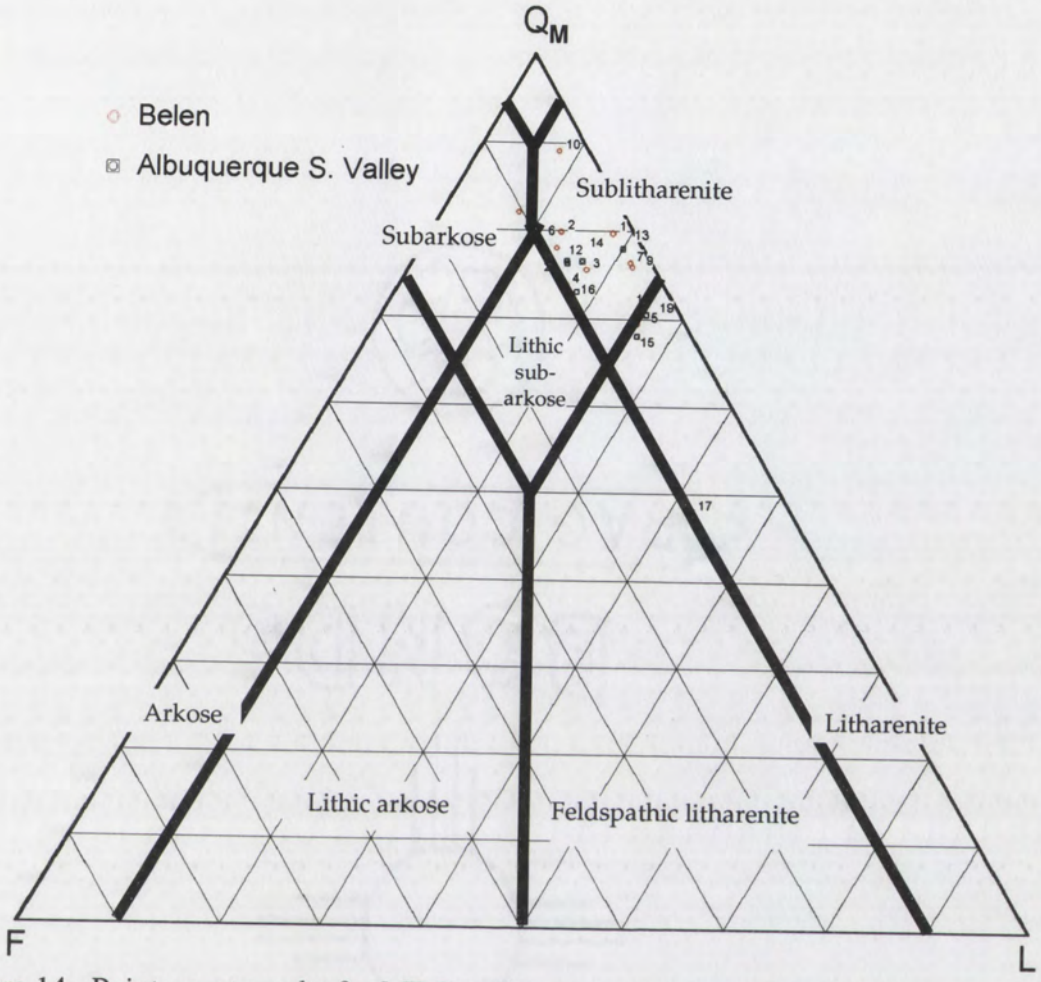

Figure 14. Point count results for MRG sediments superimposed on the sandstone classification of McBride (1963).

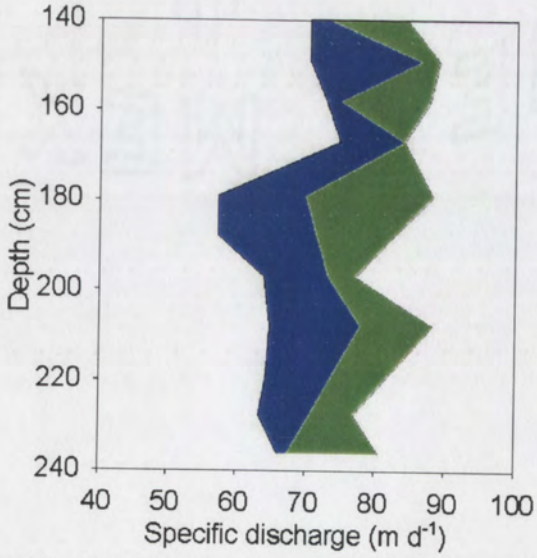

Figure 15. Range of specific discharge values with depth (3 values per depth interval). Blue region = minimum to median values; green region = median to maximum values.

Organic carbon

A preliminary data set of non-purgeable organic carbon (NPOC) characterizes dissolved organic carbon across the site (Table 4). The data indicate low to moderate NPOC concentrations.

Table 4. Non-purgeable organic carbon (NPOC) data for surface and ground water samples.

Type of sample	Sample ID	Pore size (μm)	Conc. ± std. dev. (mg L^{-1} as C)
Surface	BLN Rio 11/11/01	0.45	4.19 ± 0.39
	BLN Rio 01/27/02	0.45	3.02± 0.02
	BLN Rio 02/07/02	0.45	2.52± 0.40
	USJRD 11/11/01	0.45	4.22 ± 0.06
	USJRD 01/27/02	0.45	4.01 ± 0.39
	USJRD 02/07/02	0.45	4.73 ± 0.42
Conventional well	BLNC 01/27/02	0.45	2.34 ± 0.37
	BLN3 01/27/02	0.45	3.66 ± 0.34
	BLN4 01/27/02	0.45	3.47 ± 0.05
DMLS *BLNx: well ID* *mmddyy: date* *aaa-bbb: depth (cm)*	BLN2-111101-135-147	0.2	5.11 ± 0.08
	BLN2-111101-204-217	0.2	4.37 ± 0.05
	BLN9-031902-116-124	0.2	3.58 ± 0.31
	BLN9-031902-116-124	10	3.94 ± 0.34
	BLN9-031902-138-146	0.2	3.11 ± 0.20
	BLN9-031902-138-146	10	3.41 ± 0.36
	BLN9-031902-155-168	0.2	2.94 ± 0.35
	BLN9-031902-155-168	10	4.76 ± 0.71
	BLN9-031902-177-186	0.2	4.75 ± 0.19
	BLN9-031902-177-186	10	5.42 ± 0.26
Transect *TR-1: close to river* *TR-5: close to USJRD*	BLN TR-1 2/7/02	0.45	4.04 ± 0.35
	BLN TR-3 2/7/02	0.45	7.70 ± 0.32
	BLN TR-4 2/7/02	0.45	4.11 ± 0.37
	BLN TR-5 2/7/02	0.45	15.84 ± 0.18

On the three occasions sampled, NPOC was higher in the down-flow USJRD than in the river channel. NPOC was also enriched in each of four samples that were filtered to 10 μm rather than 0.2 μm on 19 Mar 2002. In addition, acetate and oxalate, two low-molecular-weight organic acids (LMWOAs), were analyzed by ion chromatography. In this study, acetate and oxalate are almost always below the instrumental detection limit

(~0.05 mg L^{-1}), but are occasionally quantified below 1 mg L^{-1}. Analysis of acetate was especially difficult because quantification depends on the adjacent fluoride peak, which was often large enough to interfere with the acetate peak. LMWOAs were rarely detected in adjacent DMLS intervals, nor were they consistently detected at specific depths. LMWOA data are tabulated in Appendix IV.

Dissolved gases

Gas chromatography data (Table 5) were obtained on 10 Oct 2001. Hydrogen is presented in the nanomolar units used by Chapelle et al. (1995) for TEAP diagnosis. The methane values, although quantifiable, are negligible.

Table 5. Dissolved gas data for whole-well samples.

Well	Screen (m)	H_2 (nM)	CH_4 (ng L^{-1})
BLN2	0.05-4.6	8.0	1.68 (TCD)
BLN3	4.5-6	8.3	0.64 (FID; TCD failure)

Groundwater transect

Chemical data of the groundwater transect from Rio Grande to USJRD are tabulated in Appendix V and presented graphically in Figure 63. The data reveal spatial trends in redox-sensitive solutes on two occasions in early 2002. Electrode Eh decreases by over 300 mV between the Rio Grande and the sulfidic TR-4 location, then increases by about 100 mV in USJRD, which is surface water. This represents a net decrease of over 200 mV from river to drain. Nitrate : chloride and sulfate : chloride ratios exhibit a net decrease, although one TR-3 sample contradicts the net trend. [Fe_T] and [Mn_T] increase along the transect, although Fe could not be detected in any of the samples on 7 Feb 2002. Alkalinity increases along the transect, and pH exhibits a net decrease between TR-3 and TR-4. NPOC is higher in USJRD than in the river, and temperature

undergoes a net increase from river to USJRD on 7 Feb 2002, when groundwater was warmer than surface water.

Sediment chemistry

The 0.5N HCl extracts were analyzed for Fe (Figure 16), Mn (Figure 17), and PO_4^{3-} (Figure 18). $Fe_{0.5N}$ and $P_{0.5N}$ are enriched in the zone of intermittent saturation (ZIS) at around 140 cm depth, but $Mn_{0.5N}$ is not noticeably higher at this depth. All three elements are highest in the fine-grained soil sediments located in the vadose zone at less than 100 cm depth. Oxalate-extractable Fe (Figure 19) is also substantially enriched in the ZIS. Dithionite-extractable Fe (Figure 20) has a more complicated profile, but may be enriched in the ZIS as well. Below the ZIS, extractable Fe and Mn reach a stable baseline level, and extractable Fe increases slightly at below 400 cm depth. In summary, oxalate extracted the least Fe, and dithionite dissolved the most Fe. These data are tabulated in Appendix VI.

Bulk chemical data reveal similar enrichments in redox-sensitive elements near the ZIS (Figure 21), although with poorer sampling resolution. In addition, these data were derived from BLN2 sediments, which were more disturbed and homogenized than hand-augered BLN9 sediments used for extractions. The fine fraction is much lower in Si than the sand fraction, but is enriched in all other major elements, including redox-sensitive metals. Fe, Mn, Ti, P, Na, K, Ca, and Mg are higher in the < 63 μm fraction. Undifferentiated volatiles (reported as loss on ignition) are also higher in the fine sediments than the sand. Fe, Mn, Ti, P, and volatiles are noticeably higher in ZIS and shallower sediments than in deeper, phreatic sediments. Si is lower in the ZIS but higher above and below. These data are tabulated in Appendix VII.

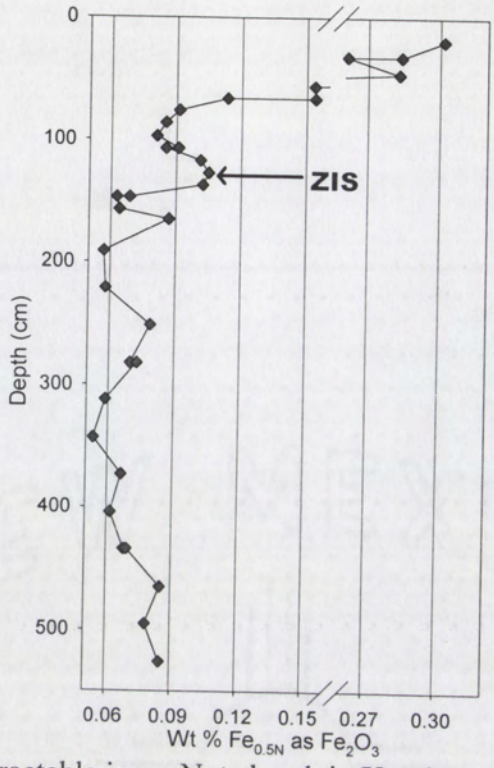

Figure 16. 0.5N HCl-extractable iron. Note break in X-axis to accommodate all data.

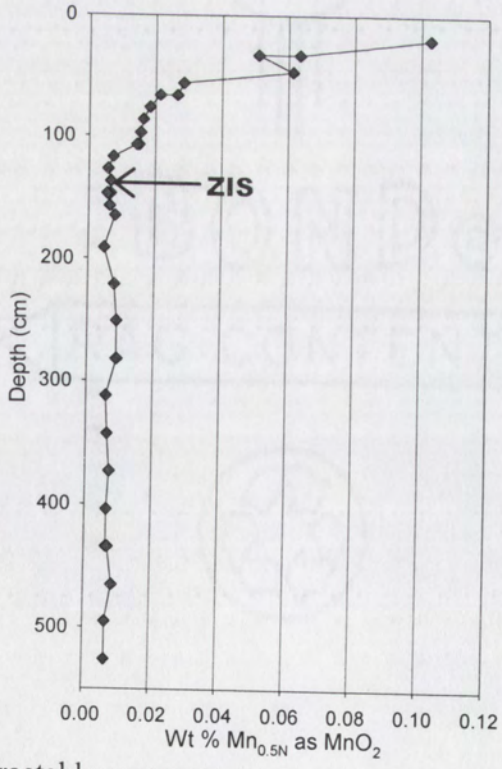

Figure 17. 0.5N HCl-extractable manganese.

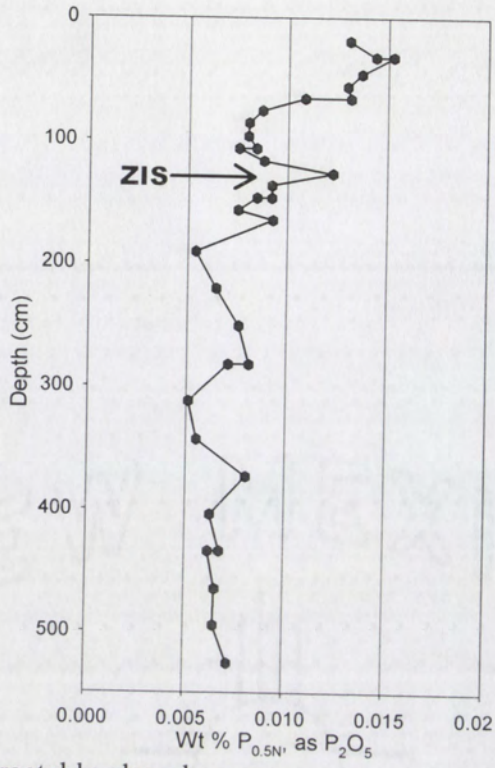

Figure 18. 0.5N HCl-extractable phosphorous.

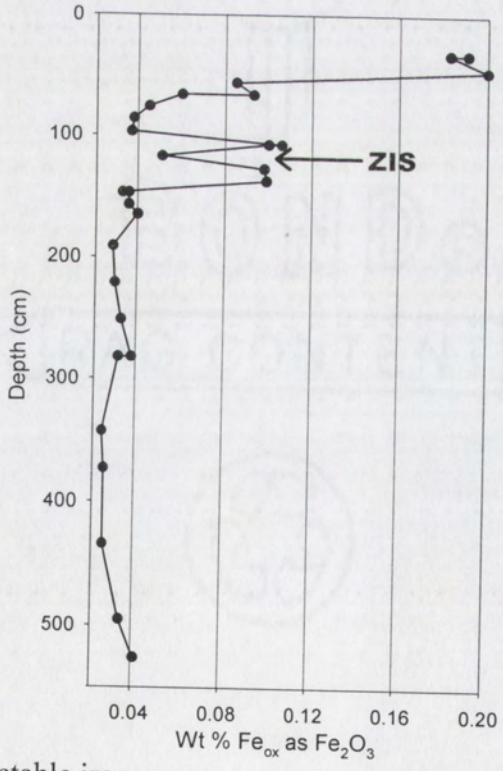

Figure 19. Oxalate-extractable iron.

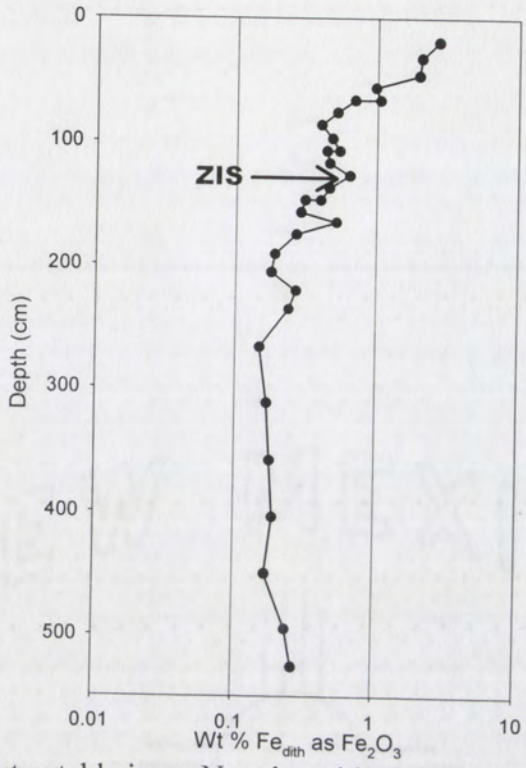

Figure 20. Dithionite-extractable iron. Note logarithmic scale on x-axis.

Iron(III) oxyhydroxides: morphologies

On the water sampling membranes, rich growths of Fe oxyhydroxides, ocher to brown in color, were observed after 3 to 4 weeks of incubation at a variety of depths in the meter below the water table. These growths were on the outsides of the 0.2 μm membranes used for water sampling; by contrast, the insides of these cells appeared to contain no such growths (Figure 22). A frequently seen morphology resembles single or bundled stalks, usually straight or sometimes curved (Figure 23-Figure 24). In many instances, these stalks contain, or are interconnected by, spherical Fe oxyhydroxide bumps about 0.5 μm in diameter (Figure 25). The stalks are associated with micron-scale silicate detrital material that was unable to pass through the 0.2 μm membranes.

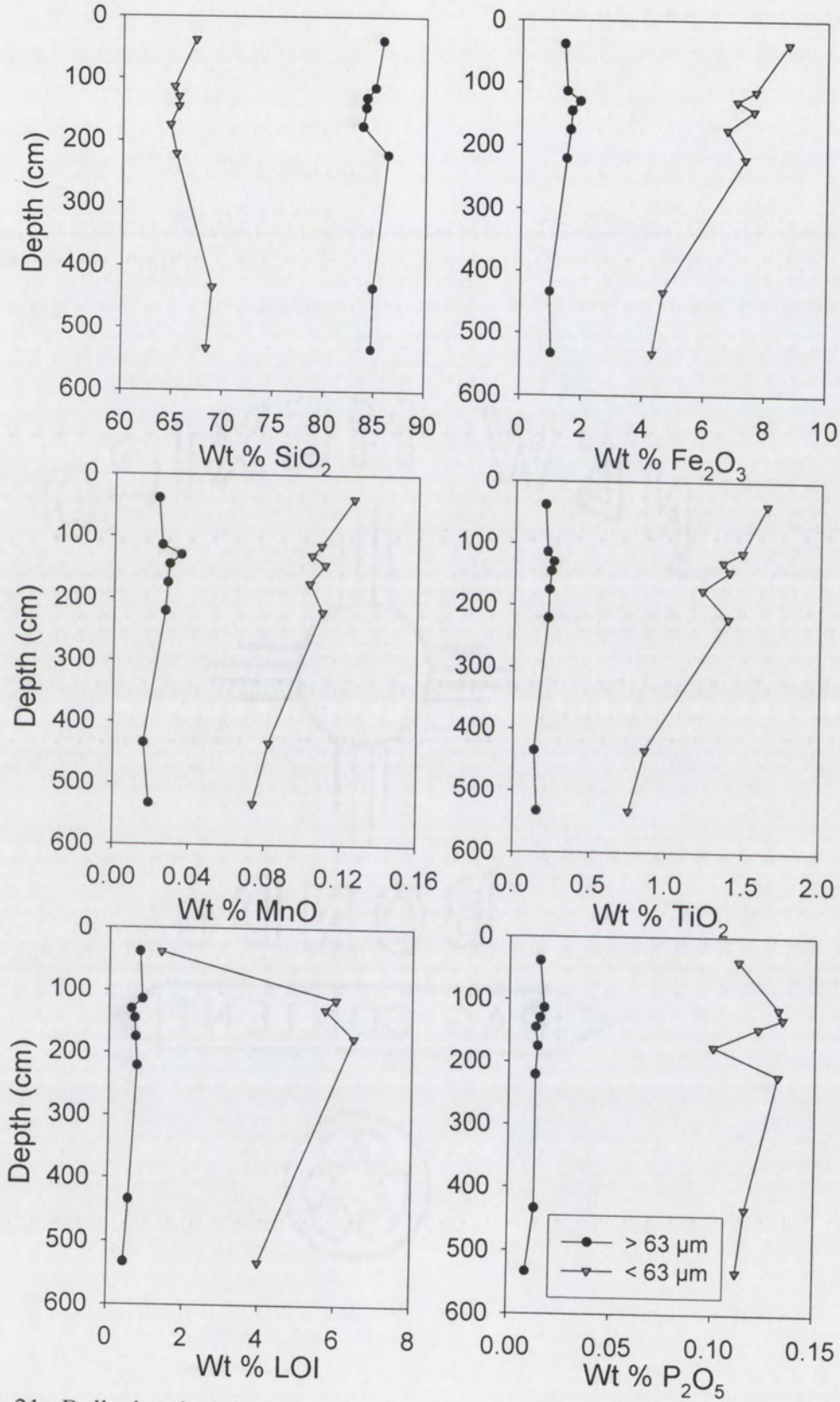

Figure 21. Bulk chemical data for size separates. Circles: sand; triangles: silt and clay.

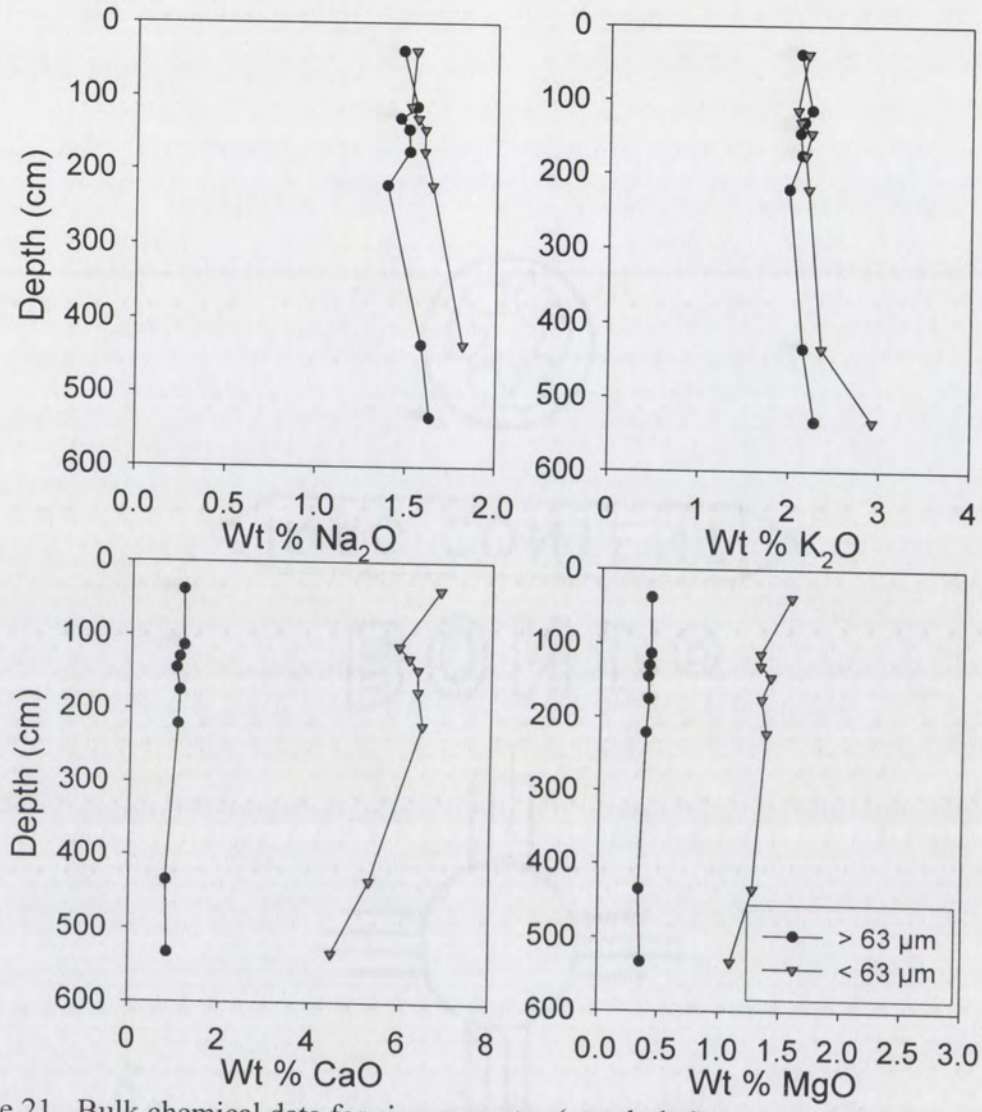

Figure 21. Bulk chemical data for size separates (concluded).

A second morphology had a helical appearance. This morphology was associated with clay-sized (Ca,Al) silicate particles and was frequently speckled with the spherical morphology (Figure 26-Figure 27). Growth directions are occasionally evident leading from detrital material (Figure 28). EDS analyses indicate that these helixes and bumps have strong Fe, O, and P peaks (Figure 29). This helical structure is widely identified as the stalk produced by the Fe(II)-oxidizing genus *Gallionella* (Tuhela et al., 1997; Emerson, 2000; Hanert, 2002). In published descriptions of pure cultures, bean-

shaped *Gallionella* cells have been seen near the stalks (Emerson, 2000), but such cells were not seen amid the detrital material cluttering the filters in this study.

A third notable morphology was clusters of spheres, appearing alone or with the other morphologies mentioned above. Individual spheres are approximately 0.5 μm in diameter (Figure 30-Figure 31). Their composition is iron oxide, often with significant phosphorous (Figure 32). These spheres appear in bunches with or without stalk morphologies. The chemistry of all three morphologies are not distinct at the accuracy provided by qualitative EDS.

Figure 22. Typical inner and outer surfaces of 0.2 μm cell filters from 10 October 2001 and 16 April 2002.

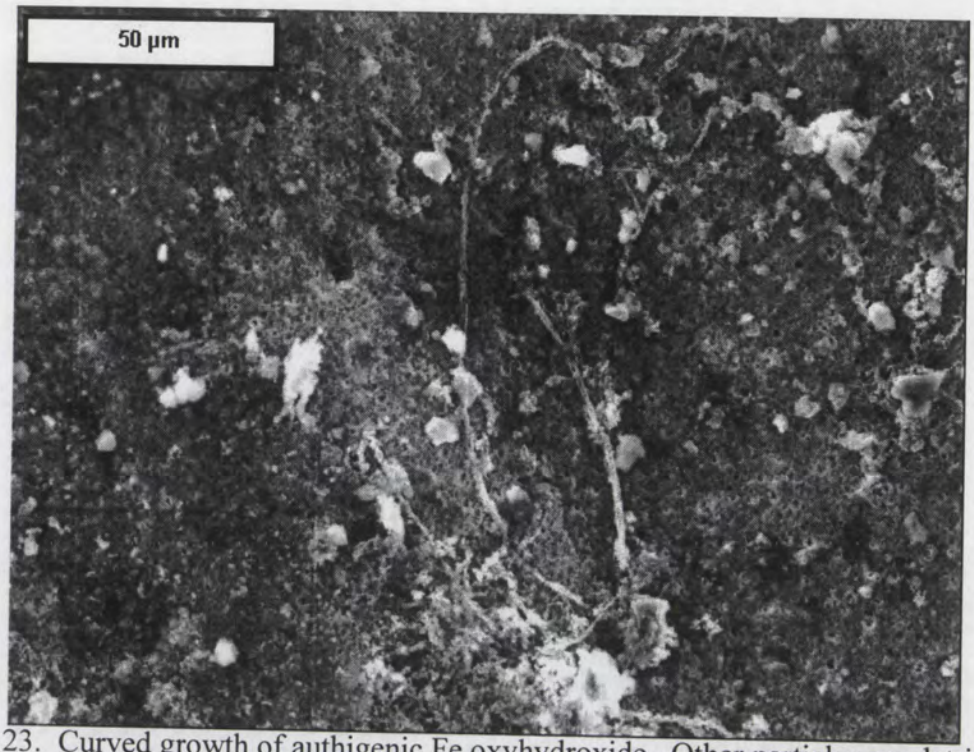

Figure 23. Curved growth of authigenic Fe oxyhydroxide. Other particles are detrital silicates – note their association with twig. SE mode, scale bar = 50 µm (sample BLN2-111101-147-156).

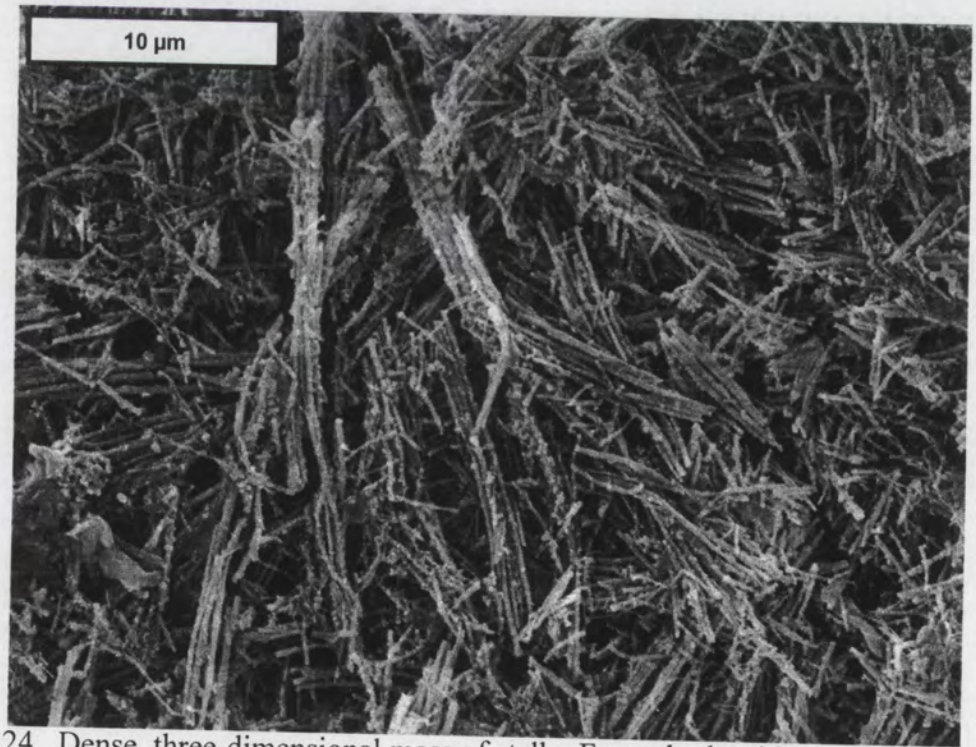

Figure 24. Dense, three-dimensional mass of stalky Fe oxyhydroxides. SE mode, scale bar = 10 µm (sample BLN2-072401-137-146).

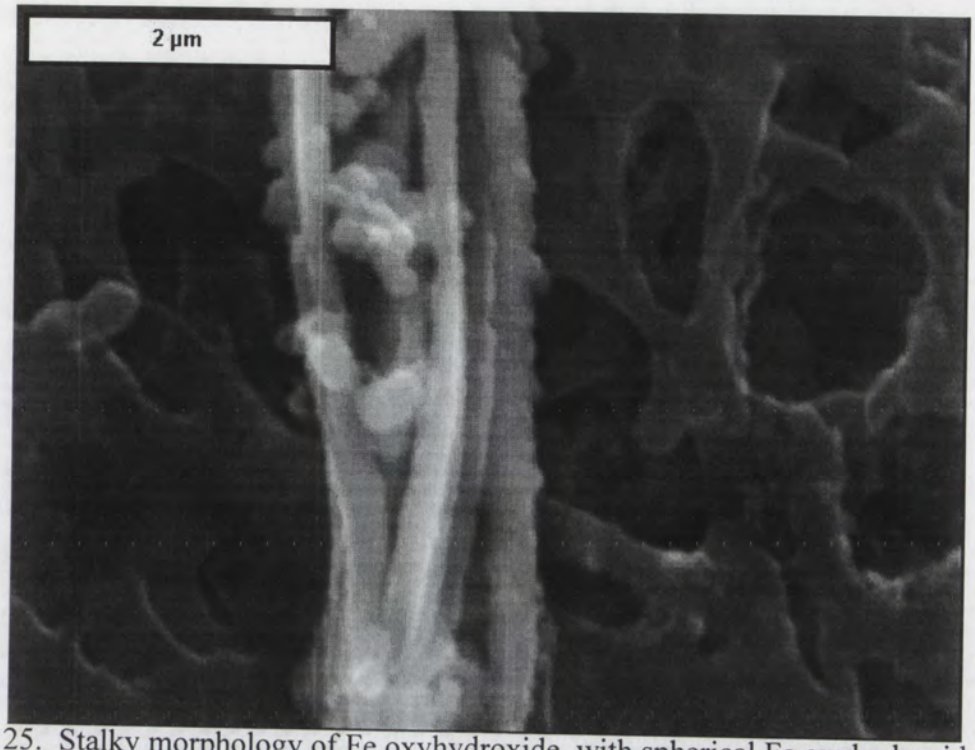

Figure 25. Stalky morphology of Fe oxyhydroxide, with spherical Fe oxyhydroxide between. SE mode, scale bar = 2 µm (sample BLN2-111101-147-156).

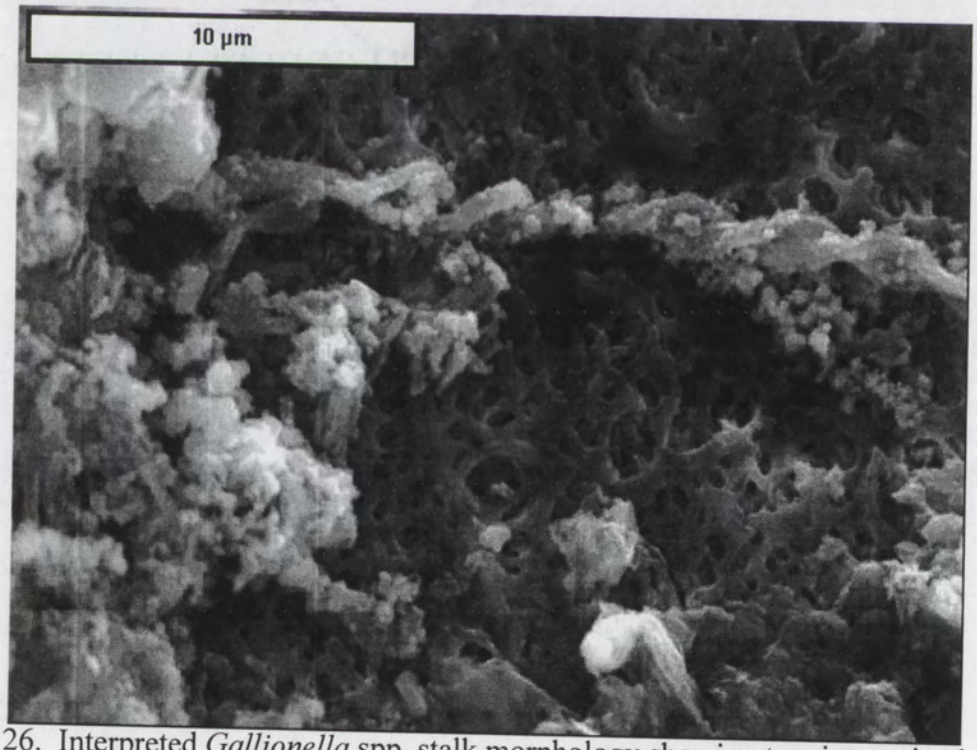

Figure 26. Interpreted *Gallionella* spp. stalk morphology showing two intertwined strands of Fe oxyhydroxide apparently growing from fine detrital material on the left. SE mode, scale bar = 10 µm (sample BLN2-111101-147-156).

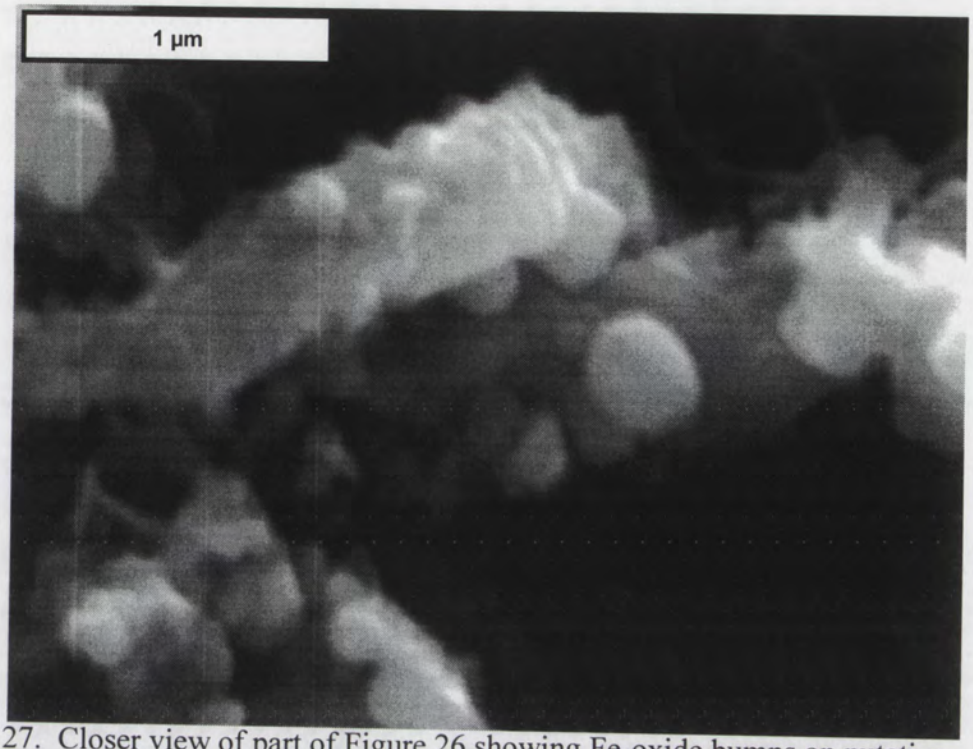

Figure 27. Closer view of part of Figure 26 showing Fe-oxide bumps on putative *Gallionella* stalk. SE mode, scale bar = 1 µm (sample BLN2-111101-147-156).

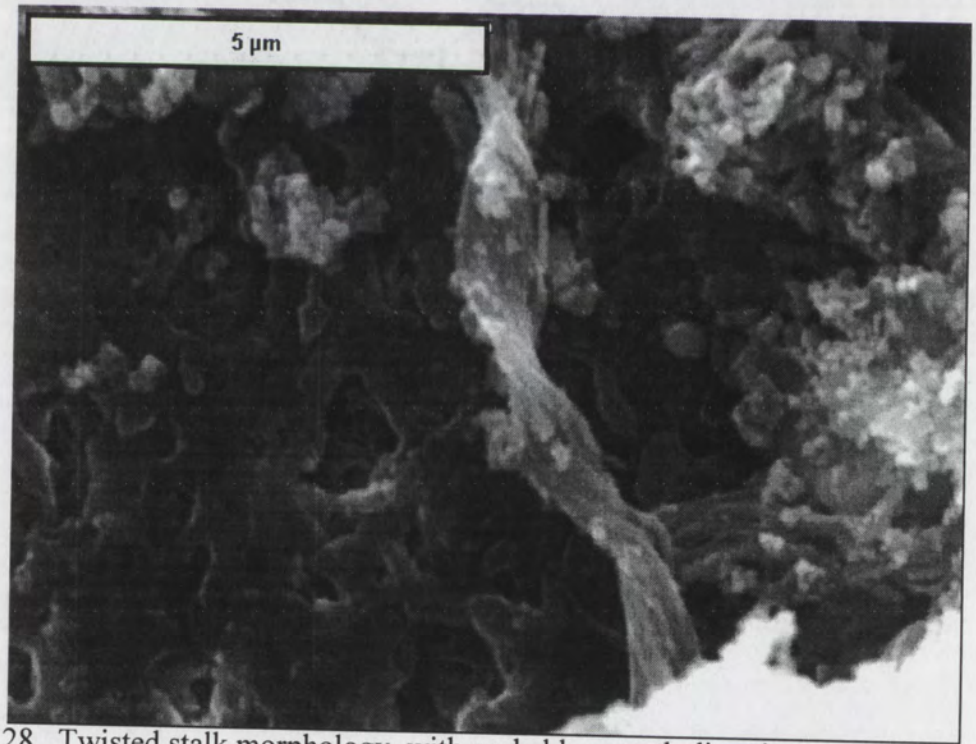

Figure 28. Twisted stalk morphology, with probable growth direction to top of image. SE mode, scale bar = 5 µm (sample BLN2-101001-145-154).

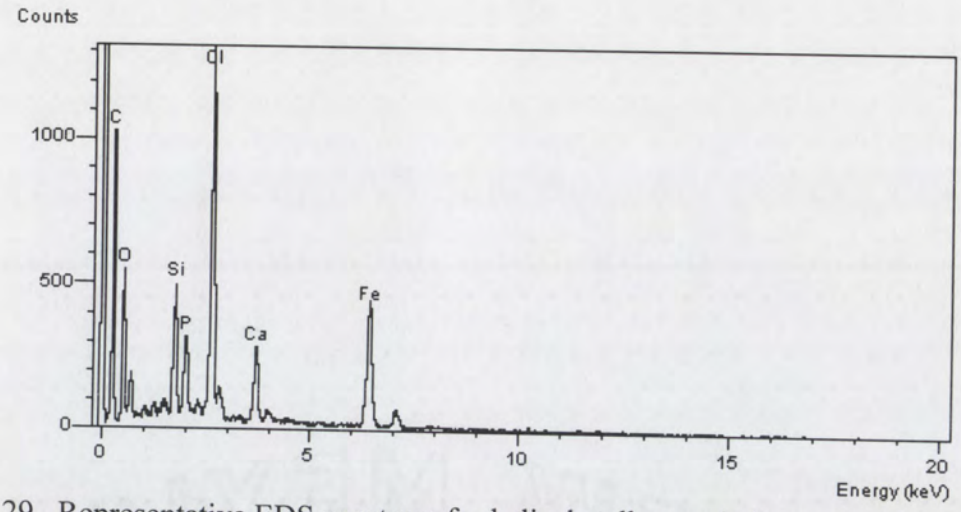

Figure 29. Representative EDS spectrum for helical stalk morphology. C and Cl are background signal from filter paper (sample BLN2-111101-147-156).

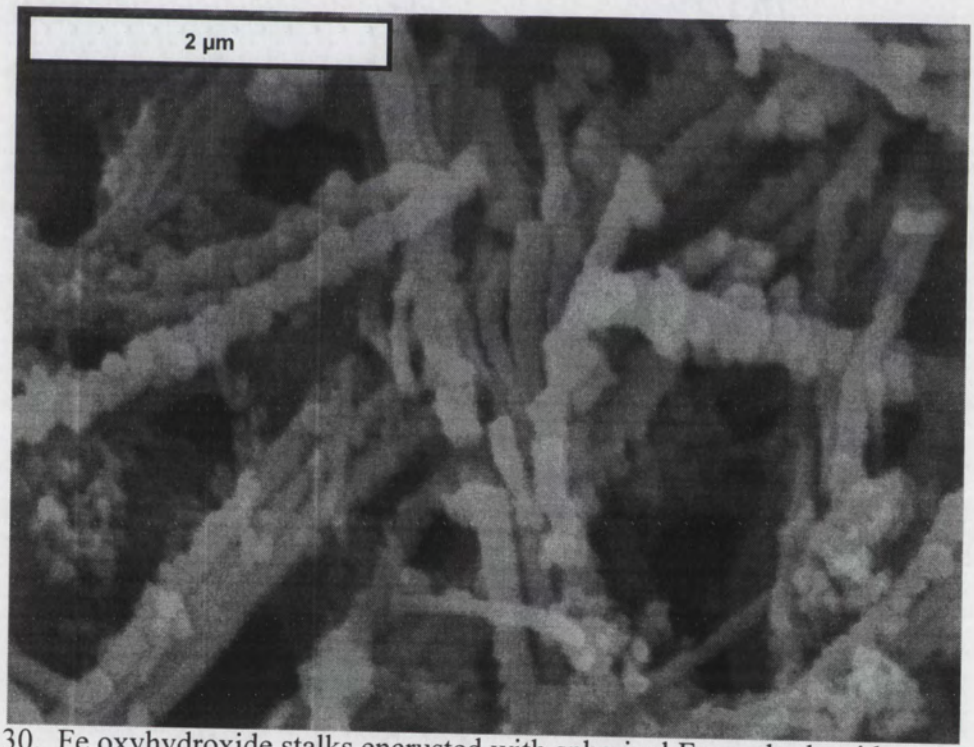

Figure 30. Fe oxyhydroxide stalks encrusted with spherical Fe oxyhydroxides. SE mode, scale bar = 2 µm (sample BLN2-072401-137-146).

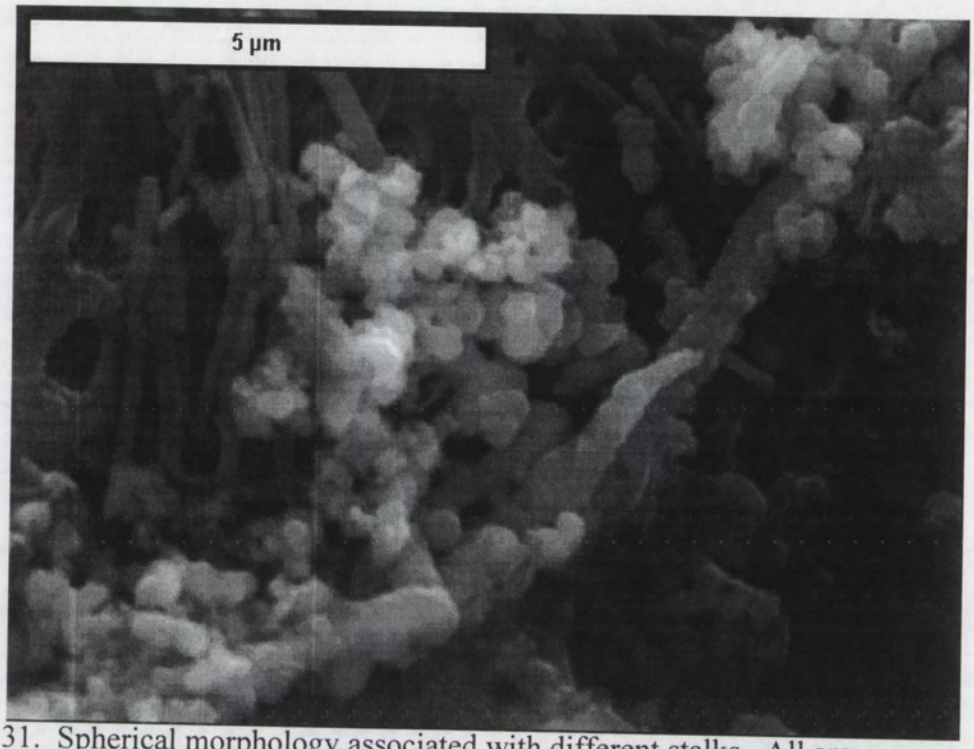

Figure 31. Spherical morphology associated with different stalks. All are Fe oxyhydroxides. SE mode, scale bar = 5 µm (sample BLN2-111101-147-156).

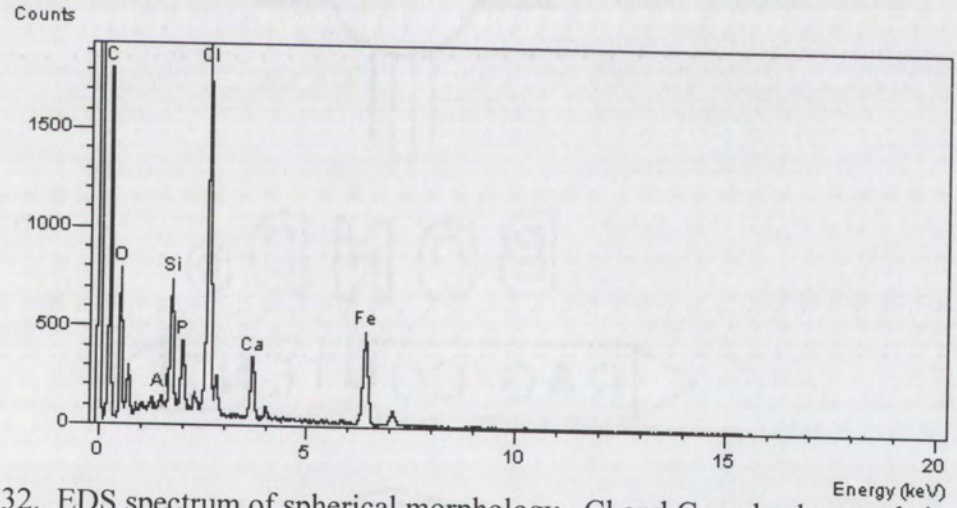

Figure 32. EDS spectrum of spherical morphology. Cl and C are background signal from filter (sample BLN2-111101-147-156).

Iron(II) sulfides

In addition to the iron oxides, small iron sulfides less than 1 μm in diameter were encountered. These particles are often square and sometimes circular in appearance. These sulfides occur alone or as small populations of identical grains within a few microns of one another. Figure 33 shows a pair of identical Fe sulfides attached to silicate detrital material, including presumptive clay-sized particles that entered the coarsely perforated microcosm and attached to the inner membrane. High-resolution imaging of a few Fe sulfides has revealed shapes that appear to be amorphous, tetragonal (Figure 35), or cubic (Figure 37). On several occasions, Fe sulfides were seen within a few microns of Fe oxyhydroxides (Figure 38).

Throughout the study, Fe sulfides were seen much less frequently than were Fe oxyhydroxides. In previous studies, however, FeS has been very difficult to locate by SEM, even in sediments where monosulfides were chemically extracted. This may be because amorphous FeS is often less than 35 nm in diameter, too small to resolve with SEM. In waters with strong sulfate-reducing bacterial populations, amorphous FeS may grow to the 100 nm size range (Herbert et al., 1998), a finding reasonably consistent with the ~500 nm diameters presented here. The fact that any Fe sulfides were seen at all can be credited to the large amount of sulfate reduction in the system and the use of DMLS to separate authigenic minerals from bulk sediments.

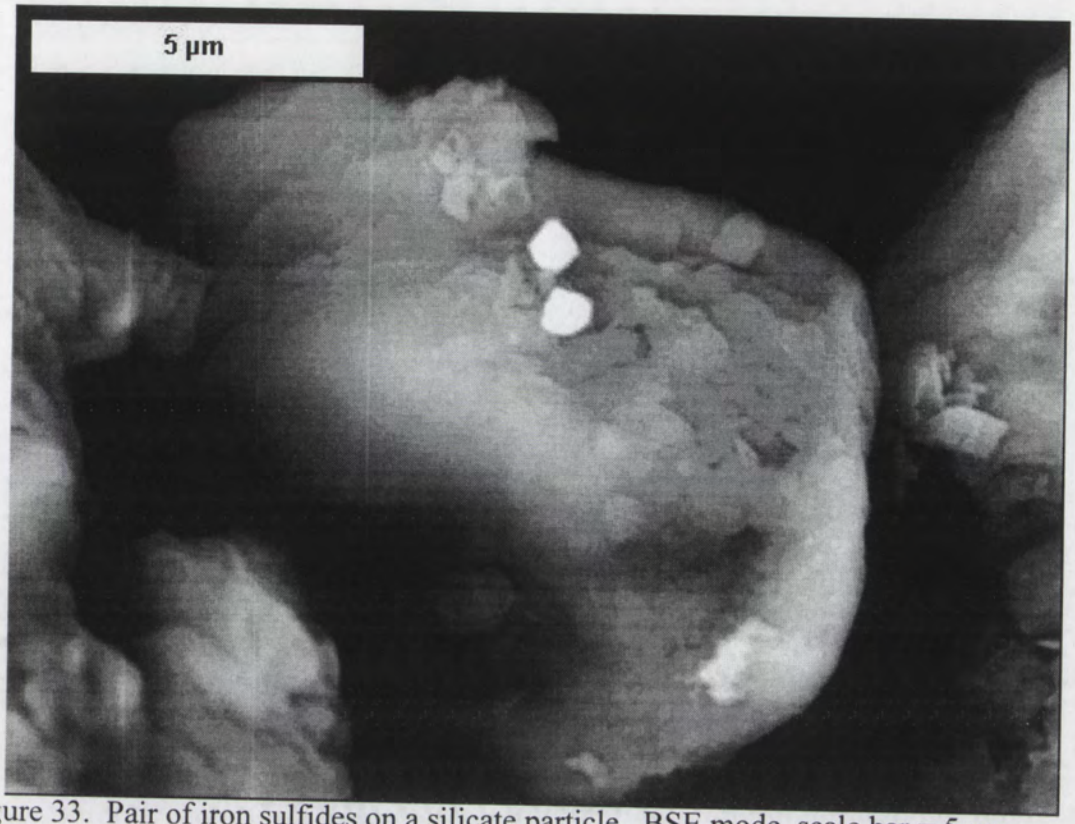

Figure 33. Pair of iron sulfides on a silicate particle. BSE mode, scale bar = 5 µm (sample BLN9-062701-169-182F).

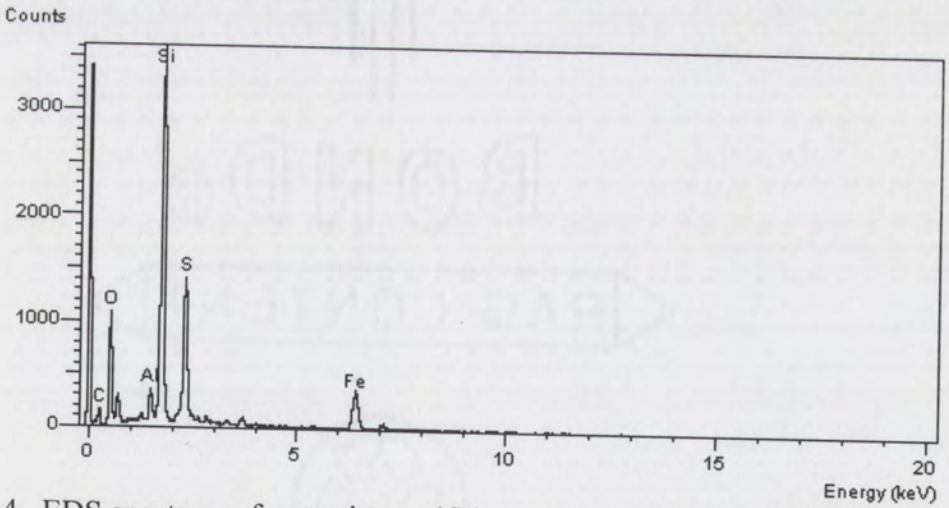

Figure 34. EDS spectrum of upper iron sulfide crystal in Figure 33. The analysis of the lower particle is virtually identical. Si, Al, and some O (?) are silicate background (sample BLN9-062701-169-182F).

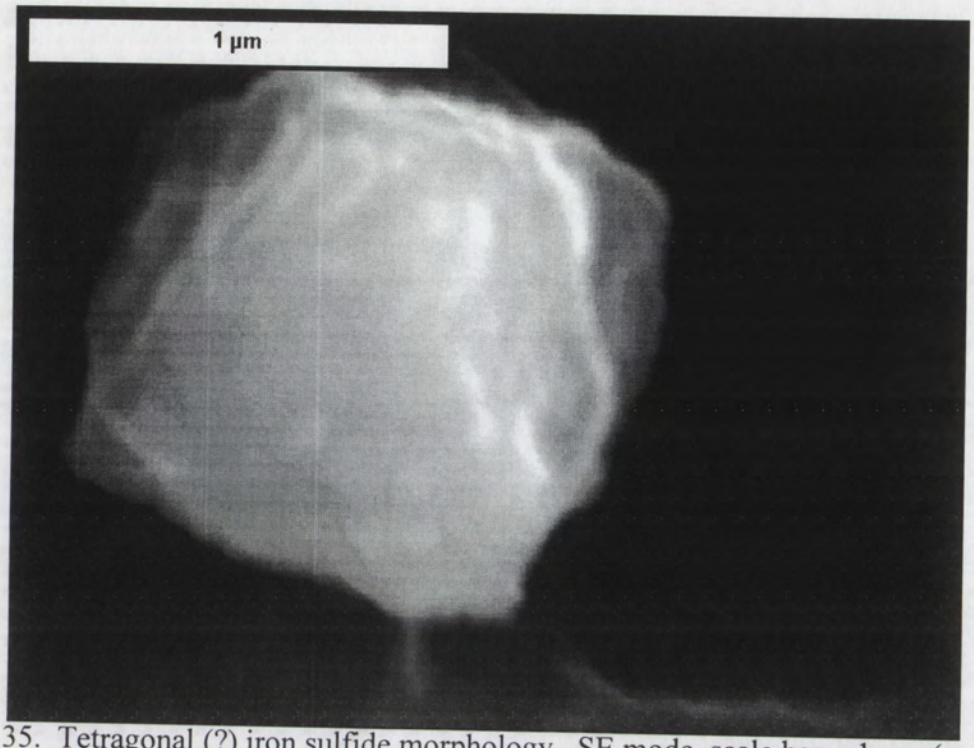

Figure 35. Tetragonal (?) iron sulfide morphology. SE mode, scale bar = 1 µm (sample BLN9-062701-169-182F).

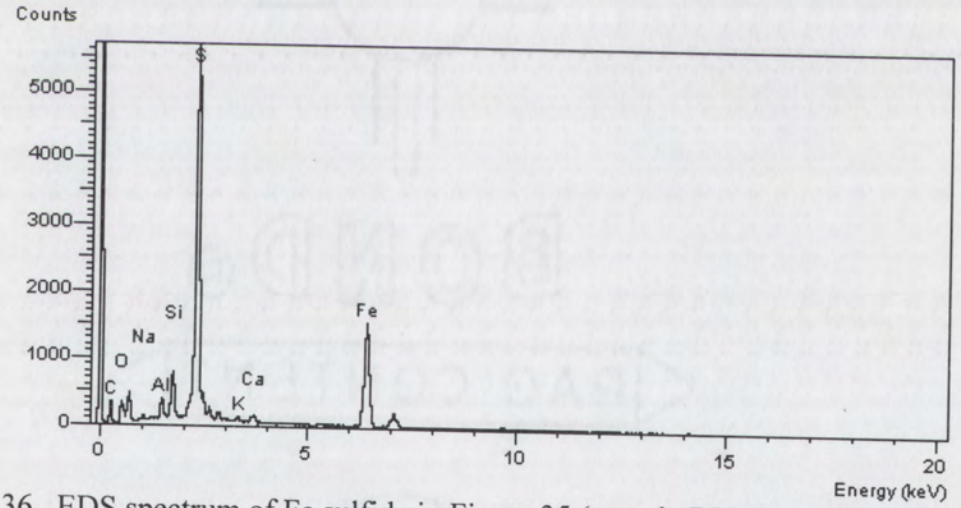

Figure 36. EDS spectrum of Fe sulfide in Figure 35 (sample BLN9-062701-169-182F).

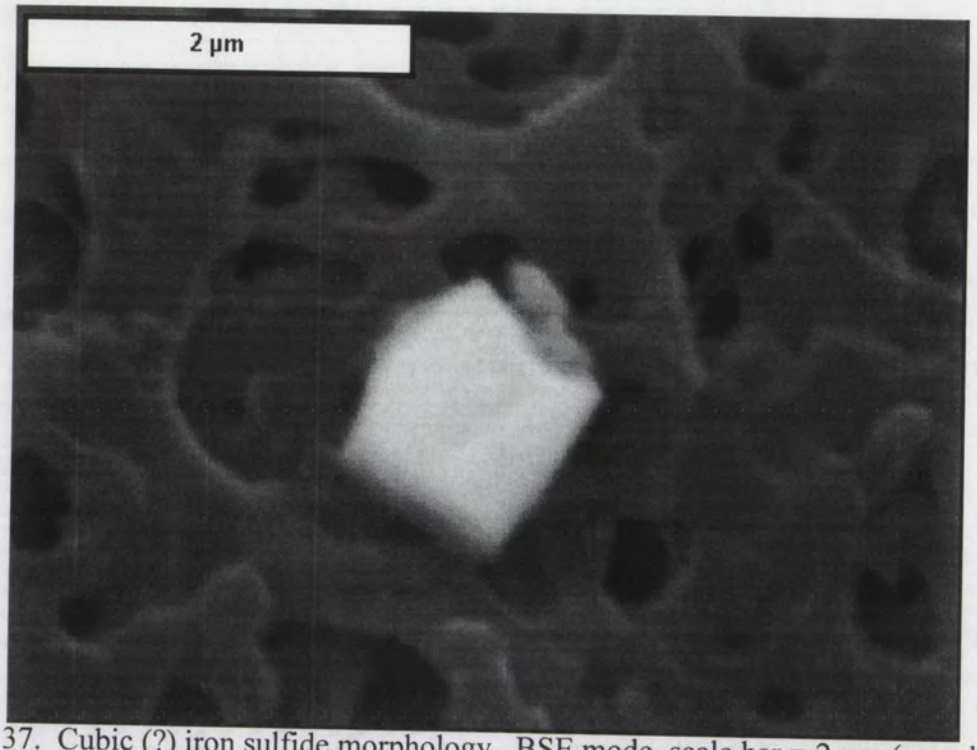

Figure 37. Cubic (?) iron sulfide morphology. BSE mode, scale bar = 2 µm (sample BLN2-072401-137-146).

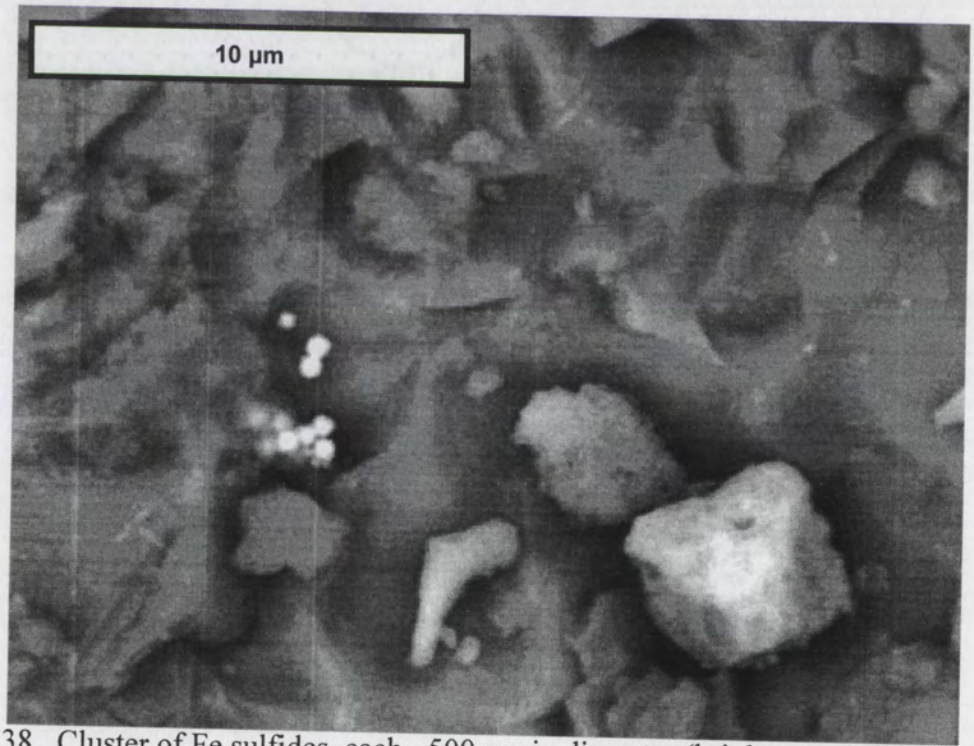

Figure 38. Cluster of Fe sulfides, each ~500 nm in diameter (bright spots left of center) and octahedral (?) Fe oxide, lower right. BSE mode, low vacuum (31 Pa), uncoated sample, scale bar = 10 µm (glass slide sample BLN9-062701-169-182G).

Phosphates

SEM work revealed occasional minerals which are tentatively identified as phosphates. An apatite crystal, 20 μm long, was observed on the outside of a 0.2 μm membrane not heavily coated with Fe-oxides (Figure 39-Figure 40). This particle could be detrital, but it is extremely unlikely. Other P-rich masses had more microbial-looking relationships, such as the large calcium phosphate masses covered with filaments (Figure 41). Finally, two amorphous rare earth phosphates were found on Spring 2001 incubation glass slides. One contained cerium as the dominant cation (Figure 42), and the other probably contained yttrium. These findings were not replicated at any other time during the study.

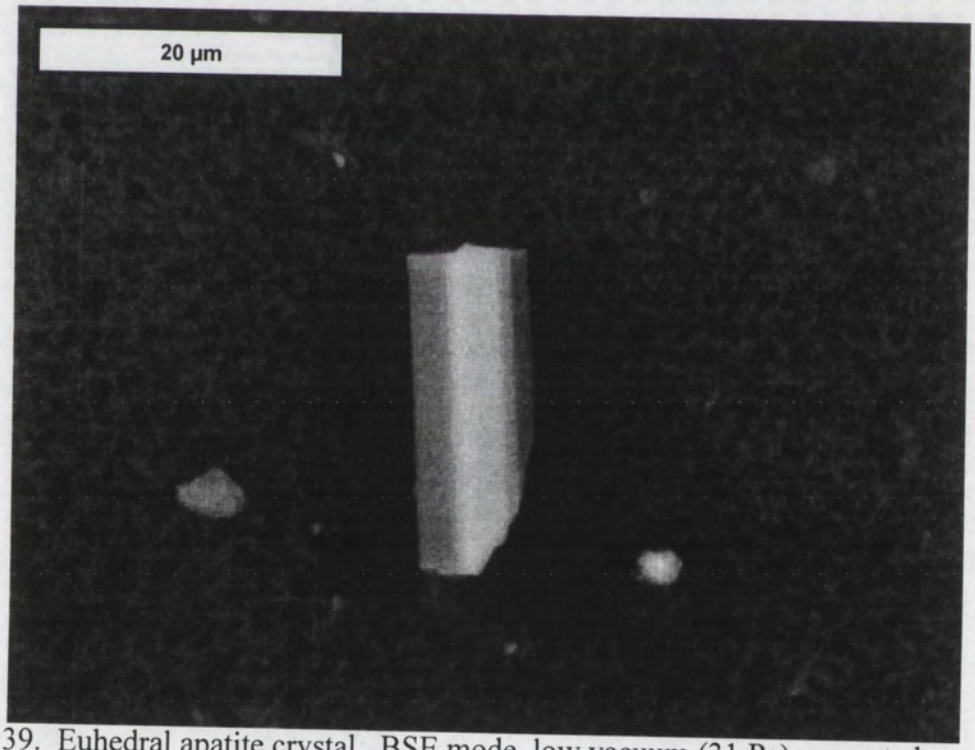

Figure 39. Euhedral apatite crystal. BSE mode, low vacuum (31 Pa), uncoated sample, scale bar = 20 μm (sample BLN2-072401-137-146).

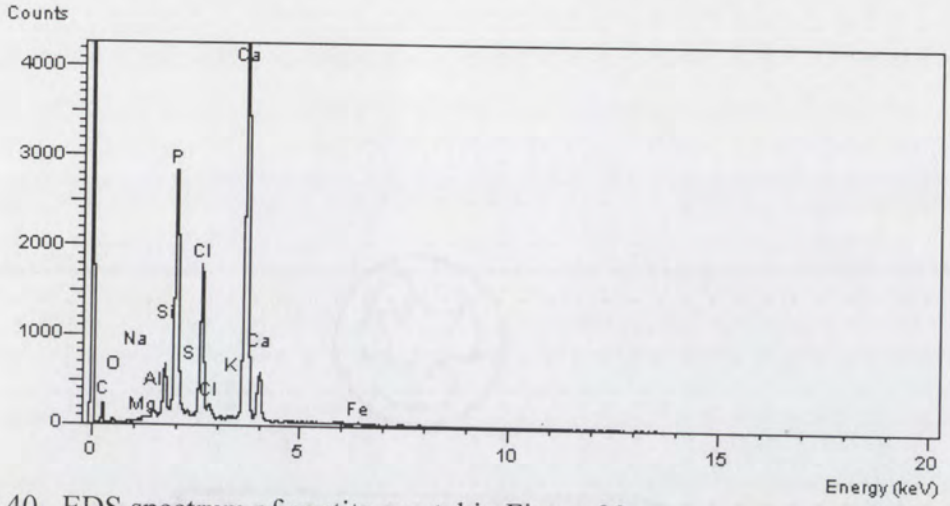

Figure 40. EDS spectrum of apatite crystal in Figure 39.

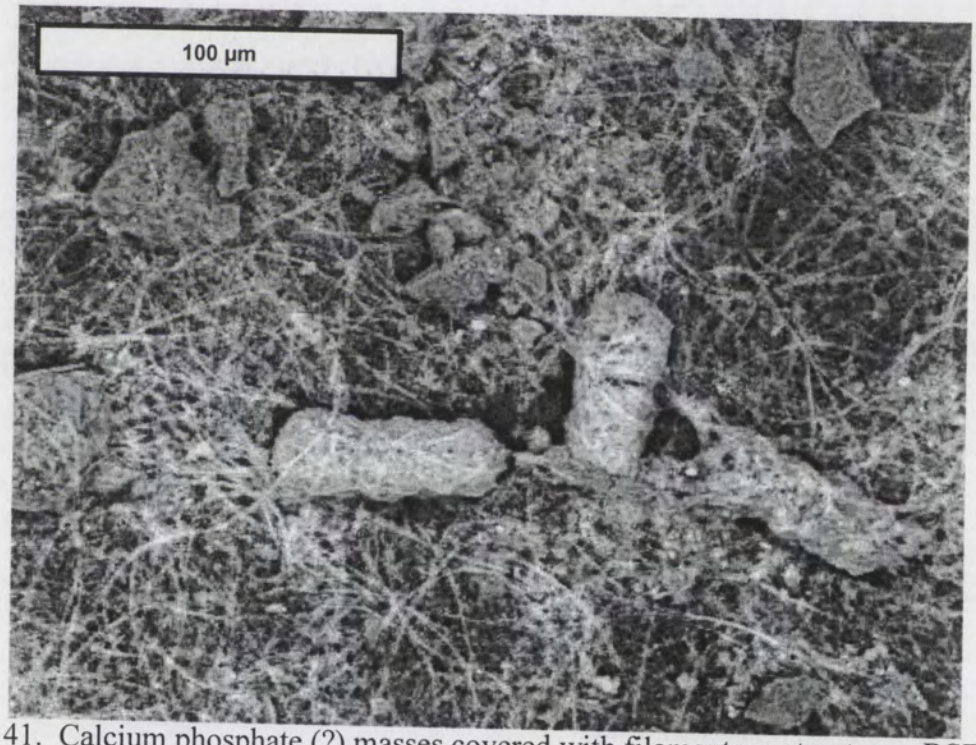

Figure 41. Calcium phosphate (?) masses covered with filamentous structures. BSE mode, low vacuum (31 Pa), uncoated sample, scale bar = 100 µm (sample BLN2-072401-137-146).

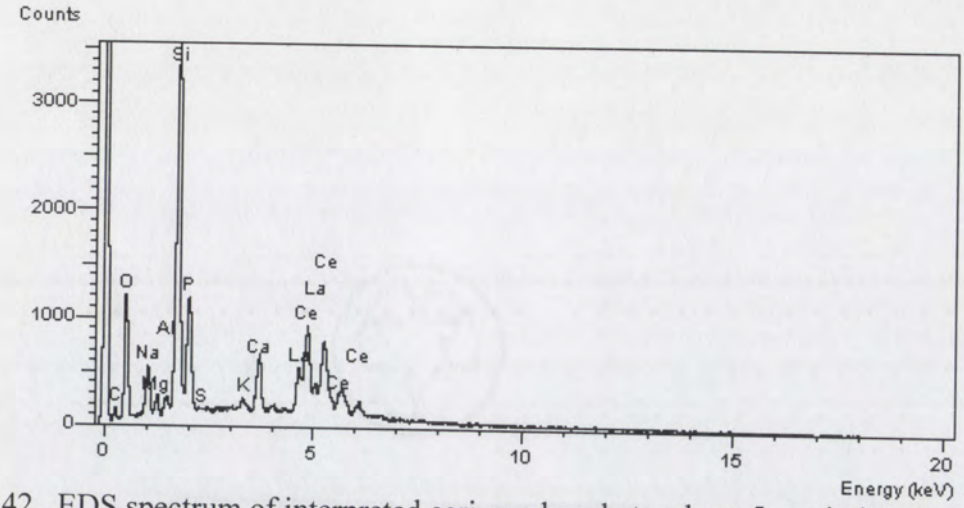

Figure 42. EDS spectrum of interpreted cerium phosphate, about 5 μm in length (glass slide sample BLN9-062701-169-182). Si and some O are background (uncoated sample).

Organic carbon

Another observed relationship is between apparent organic matter and metals (organo-metallic complexes). Organic material was identified on the filters by its appearance in backscatter mode; the organic filters were gray due to their Cl content, but purer C was much darker, even black, in appearance. These interactions appear as spots of Fe oxyhydroxide attached to large micron-scale pieces of apparent organic matter (Figure 43). On the insides of the 10 μm filters, metals were uncommon, but a widespread organic glaze was observed. These clustered masses of carbon-rich material were different to characterize because their chemistry differed little from the organic filter papers. These clusters of organic carbon usually appeared in clusters (Figure 44-Figure 45). A few disk-shaped organic masses also had slight chemical signatures over the organic background material (Figure 46). All SEM observations are summarized in Table 6.

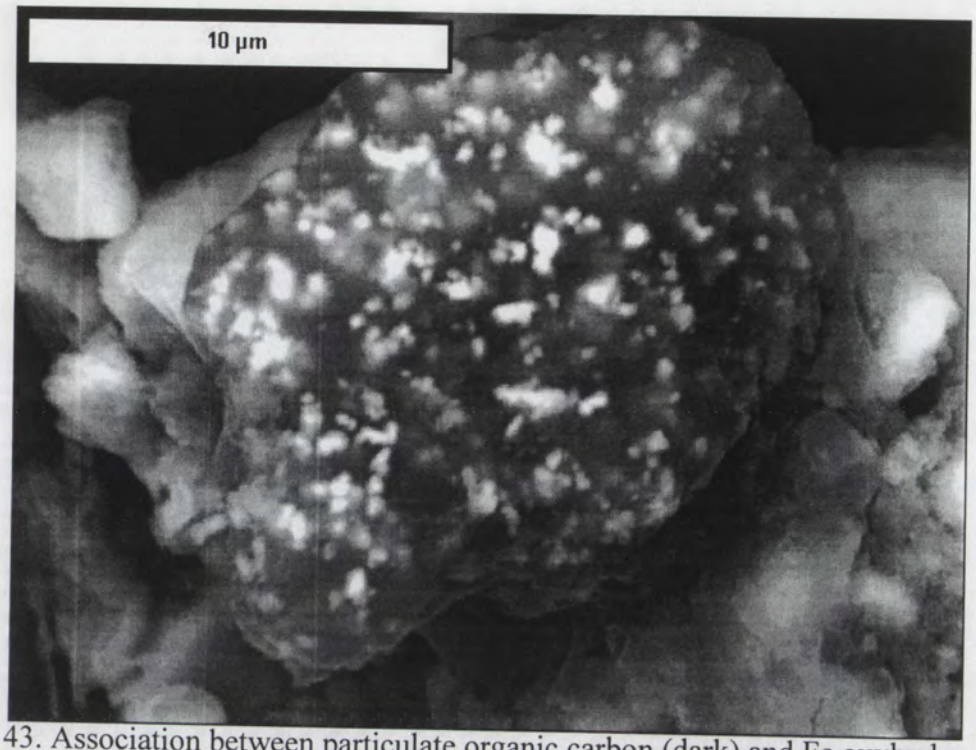

Figure 43. Association between particulate organic carbon (dark) and Fe oxyhydroxides (bright spots). BSE view, scale bar = 10 µm (sample BLN9-062701-169-182F).

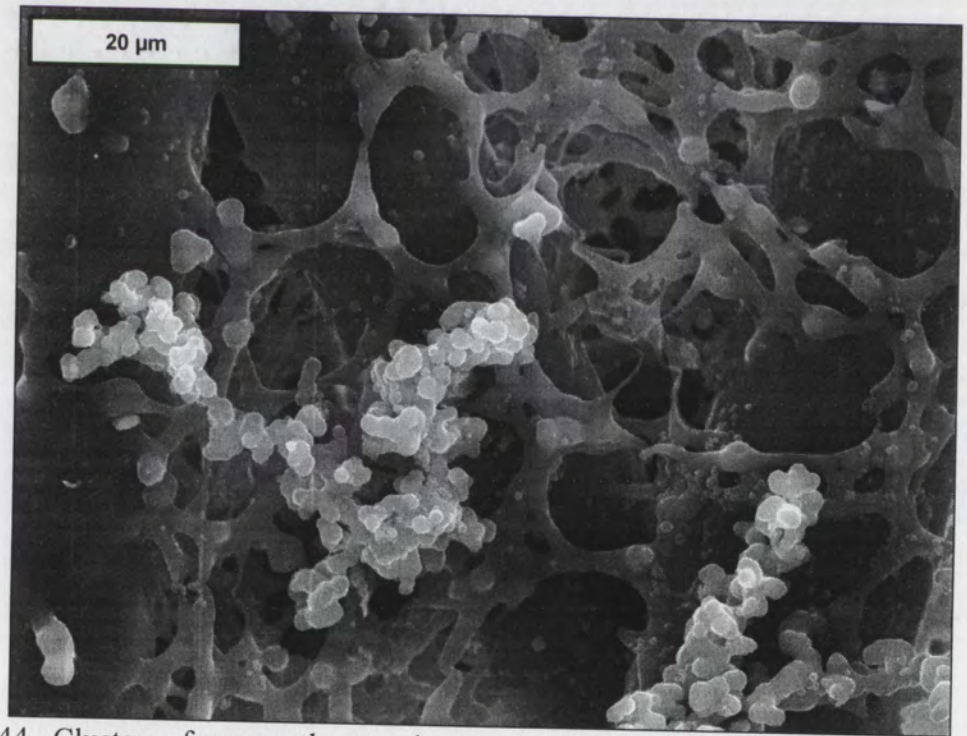

Figure 44. Clusters of apparently organic material glazing the inside of 10 µm filter paper. The large, dark structures are part of the filter, as is the small framework, but both are coated with organic material. SE mode, scale bar = 20 µm (sample BLN9-031902-177-186).

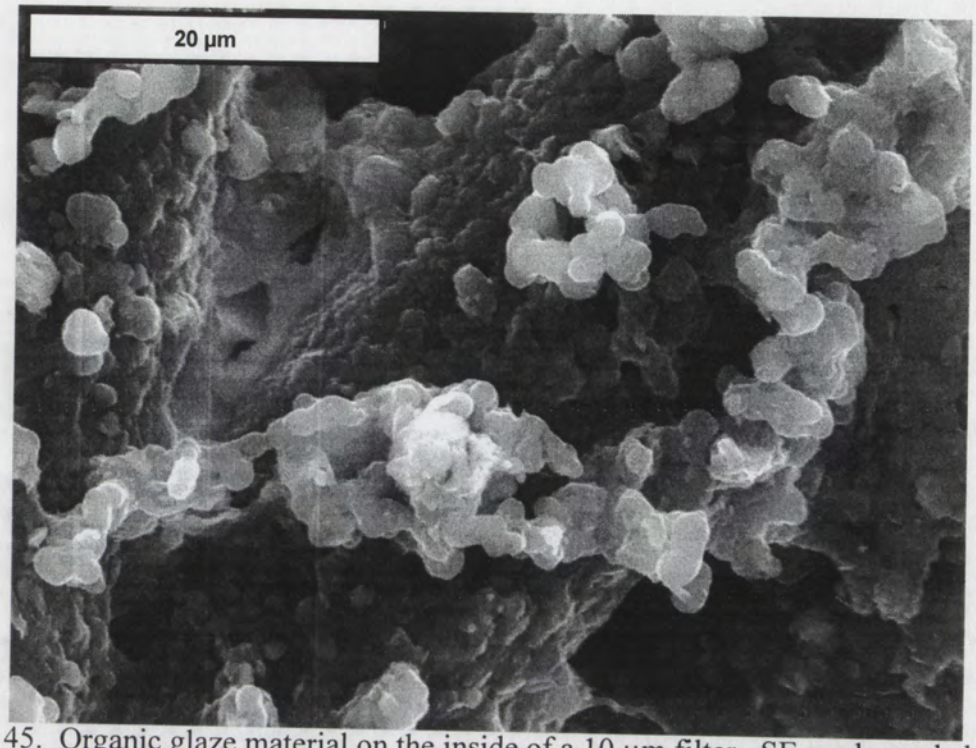

Figure 45. Organic glaze material on the inside of a 10 µm filter. SE mode, scale bar = 20 µm (sample BLN9-031902-138-146).

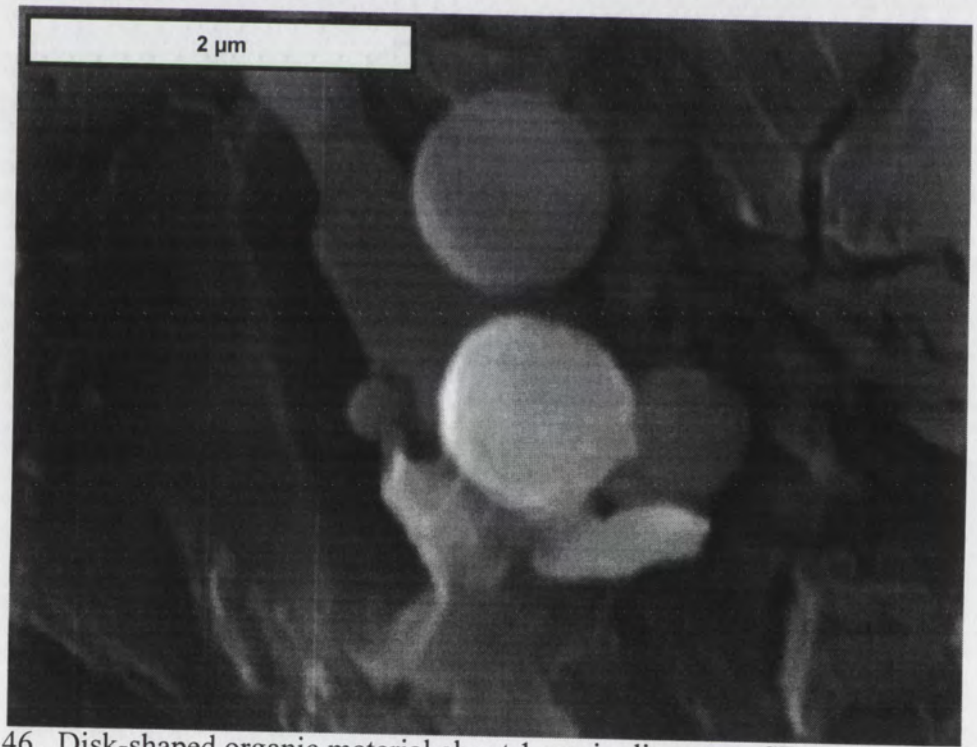

Figure 46. Disk-shaped organic material about 1 µm in diameter. SE mode, scale bar = 2 µm (glass slide sample BLN9-031902-116-125).

Table 6. Summary of SEM mineralogy results.

Size range	Description	Incu-bation (days)	Season	Fe-ox	P	Mn-ox	Fe-S	org. C	REE
<0.2 µm	Inside of "abiotic" control cells	54	Summer	rare				rare	
>0.2 µm	Outside of water sampling cells	~30	Varies	✓	✓	✓	✓	✓?	
<10 µm	Inside of microcosms	209	Winter	rare	rare		rare	✓	
coarse	Perforated 10 µm membranes	54	Summer	✓	✓		✓	✓	rare

Discussion

Variability in tracer estimates of specific discharge

When groundwater flow velocity (specific discharge) data are plotted on a probability-axis plot without regard to the depth or time of each observation (Figure 47), they appear in a straight line. Thus, data are normally distributed with a mean of 75 m day^{-1}, probably representing natural system variability, sample variance, and/or analytical error, rather than spatial variability in specific discharge within the upper 1.5 m of the aquifer. Specifically, each DMLS cell had a slightly different volume due to the soft membrane sides, and the cells were difficult to fill completely with tracer. Consequently, variability in the tracer experiment is likely.

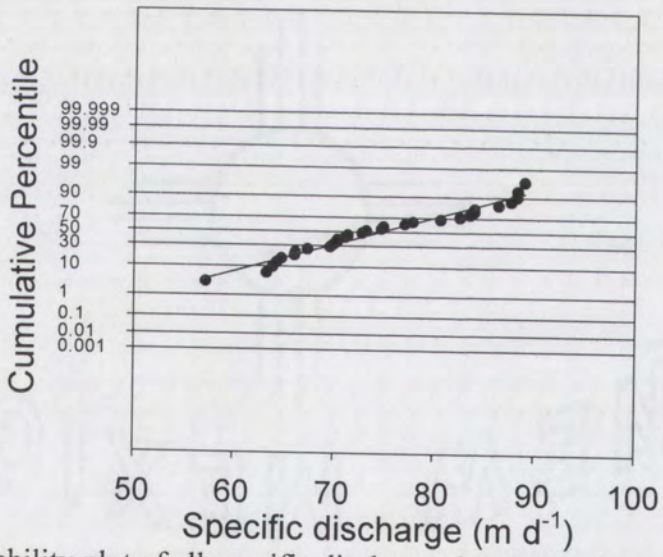

Figure 47. Probability plot of all specific discharge data indicating a normal distribution.

Groundwater flow directions and rates through hyporheic sediments

Because of the design of the drainage network, water travels from the channel (a groundwater ridge) to the riverside drains, after which it returns to the river via surface flow (Theis, 1938; Titus, 1963; Peter, 1987; Hansen and Gorbach, 1997). At the Belén site, this effect has been seen in the rapid response of hydraulic head in wells to changes

in river stage (Gilroy et al., 2001). Although hydraulic gradients have not yet been quantified at the Belén study site, groundwater flow directions have a strong component normal to the river. Paleochannel influences on flowpaths are also likely (Stanford and Ward, 1993). Before riverside drains were built in the 1920s and 1930s, groundwater flow was mostly underflow parallel to channel flow (Theis, 1938).

A few hydraulic parameters are available from the published literature (Table 7). Specific discharge can be estimated simply using Darcy's Law, an empirical relationship in which specific discharge is the product of hydraulic conductivity and hydraulic gradient (Freeze and Cherry, 1979). If the 30-300 m d^{-1} range of hydraulic conductivity from the Albuquerque South Valley (Peter, 1987) and the two calculated hydraulic gradients from Rio Grande to riverside ditch of 0.013 (Hansen and Gorbach, 1997) are used, a Darcian groundwater velocity estimate for horizontal flow normal to the Rio Grande is 0.4-4 m d^{-1}. If sandbox values of hydraulic conductivity (0.09-900 m d^{-1}; Freeze and Cherry, 1979) are used instead, Darcian velocities range from 0.002-10 m d^{-1}.

A third way of approximating specific discharge is to compare river and well hydrographs; this is possible because spikes in the discharge hydrograph are easily identifiable in the BLNc monitoring well, located about 125 m from the channel (Figure 6). Unfortunately, river discharge data are not available at less than day scale. Additionally, both gaging stations are kilometers away from the study site, with diversion structures that affect discharge situated along the reach. Thus, the time at which hydraulic pulses reach the Belén site can only be estimated at daily resolution. Locating the same hydraulic pulse on each of the three hydrographs on Figure 6 reveals rapid groundwater flow rates to the well. The Albuquerque gage is located 60 km upstream of

Table 7. Hydraulic parameters of the Middle Rio Grande valley-fill aquifer.

Parameter	Location	Value	Reference
Hydraulic conductivity	Clean sand (ideal)	0.09-900 m d^{-1}	Freeze and Cherry, 1979
	Gravel (ideal)	90-9000 m d^{-1}	
	Belén study site, mean of 3 tests, 2001	21.3 m d^{-1}	D.J. Gilroy and J.R. Thibault, unpub. data (falling-head slug tests)
	Throughout MRG bosque, mean of 16 tests, 2001	17.1 m d^{-1}	
	Albuquerque South Valley, valley-fill aquifer (sand/gravel)	30-300 m d^{-1} (estimated)	Peter, 1987
	Albuquerque reach valley-fill aquifer	up to 110 m d^{-1}	Cummins, 1993, as cited in Hansen and Gorbach, 1997
Horizontal hydraulic gradient	from Rio to riverside drain, Paseo del Norte, 1994, Albuquerque North Valley	0.013	Calculated from scaled cross-sections in Hansen and Gorbach, 1997
	from Rio to riverside drain, Rio Bravo Blvd., 1994, Albuquerque South Valley	0.013	
	from Rio to riverside drains, Albuquerque reach, mean of 7 transects, Oct. 1936	0.0105	Theis, 1938[1]
	from Rio to riverside drains, Albuquerque reach, mean of 7 transects, Jan. 1937	0.0086	
	Albuquerque South Valley, down-valley underflow (unperturbed)	0.001	Peter, 1987[2]
	Albuquerque South Valley, in local cones of depression	0.004	
Stream gradient (≈ hydraulic gradient of underflow)	Casa Colorada (immediately downstream from Belén site)	0.00082	Culbertson and Dawdy, 1964
Horizontal specific discharge	Belén study site	75 m d^{-1}	This study
Horizontal interstitial velocity[3]	Albuquerque South Valley, down-valley underflow (unperturbed)	0.1-3.1 m d^{-1}	Peter, 1987

[1] - "The gradients between river and riverside drain are much steeper than those on the inland side of the drain" (Theis, 1938).

[2] - "Steeper gradients near the drains, particularly during the irrigation season, are likely" (Peter, 1987).

[3] - Interstitial velocity is specific discharge divided by porosity (Peter, 1987).

the study site; hydraulic head pulses were seen at the study well 0 to 2 days after they were seen in the channel at Albuquerque (Table 8). The Bernardo gage is located 22 km downstream of the study site; pulses were seen at the study well 0 to 1 days after they were seen in the channel at Bernardo (although the only next-day measurement occurred at 2:30 AM, indicating that the well response at Belén is similar to the surface water response at Bernardo). This analysis suggests that changes in hydraulic head move from the Rio Grande channel to the monitoring well 125 m away in about one day. Thus, although the DMLS measurements in this study are at least an order of magnitude higher than Darcian calculations, the DMLS method appears to provide a flow rate consistent with other observations at the site.

Table 8. Analysis of dates on which selected hydrologic pulses were seen at Albuquerque and Bernardo surface water gaging stations and in water table data from the study site. See Figure 6 for data.

Pulse	1	2	3	4
Albuquerque (river)	4/6/01	5/23/01	8/14/01	8/30/01
Bernardo (river)	4/7/01	5/23/01	8/16/01	8/31/01
Belén (groundwater)	4/7/01	5/23/01	8/16/01	9/1/01

Static, one-way flowpaths fundamentally change the function of the hyporheic corridor, which normally hosts bidirectional flows driven by rising and falling river stage (Bencala, 1993) and underflow at other times. The conversion of groundwater flow from gradual underflow parallel to the Rio Grande to steeper river-ditch flow by the construction of riverside drains (Theis, 1938; Peter, 1987) could have increased hydraulic gradient, and thus Darcian velocity, by an order of magnitude, as well as changing the horizontal flow direction by up to 90 degrees. Such a change, caused by river regulation, would have increased fluxes of oxygen, nutrients, sulfate, and dissolved organic carbon though aquifer sediments. This could explain apparently higher biological activity seen

in the shallowest groundwater, in contrast to deeper water less connected to the Rio Grande (Block, 2002). Increased solute fluxes through the hyporheic zone potentially could have affected the rates of denitrification, sulfate reduction, metal oxyhydroxide reduction, and buried organic carbon oxidation. Much as the drainage system has affected recharge to the basin-fill aquifer (Hansen and Gorbach, 1997), these human modifications could have implications for water quality, such as nutrient processing and trace metal mobility, in ways not yet identified.

Diel water table fluctuation

Water table monitoring has revealed that the water table fluctuates up to several centimeters each day due to phreatophyte evapotranspiration (ET). This effect is greatest during the summer growing season and much less after leaf senescence in the fall (Gilroy et al., 2001; Dahm et al., 2002). ET may cause wetting – drying effects in the uppermost DMLS sampling interval on days that the diel fluctuation is large. This fluctuation has been calculated for each DMLS sampling date (Table 9).

DMLS profiles

Sodium and potassium profiles (Figure 48) are relatively constant with depth on most sampling dates, and [Na] is approximately an order of magnitude higher than [K] throughout the study. On several occasions, individual samples are substantially elevated in Na but not in K. In May and June 2001, increases in [Na] are paralleled by [K], however. Seasonal variability is clear in the Na data. [Na] is above 40 mg L^{-1} throughout the growing season, but below 40 mg L^{-1} during cooler periods. [K] is much less seasonally variable, and is anomalously higher in November.

Table 9. Diel water table fluctuations on DMLS sampling dates.

Date	Daily average depth to water table (cm)	Diel fluctuation (cm)
5/5/2001	115	2.6
5/30/2001	107	6.1
6/27/2001	131	3.2
7/24/2001	141	4.1
8/22/2001	136	5.0
9/19/2001	128	5.5
10/10/2001	134	2.1
11/11/2001	94	0.8
12/13/2001	113	1.7
1/27/2002	106	0.7
2/28/2002	109	1.6
3/19/2002	134	0.6
4/16/2002	123	0.7

Calcium and magnesium data (Figure 49) indicate that Ca is about one order of magnitude more concentrated than Mg. [Ca] is temporally and spatially variable. Throughout summer and fall 2001, except 22 Aug, [Ca] exhibits a fairly systematic decrease with depth. An increase with depth occurs on 22 Aug 2001, 28 Feb 2002, and 16 Apr 2002. Regardless of these trends, the uppermost cell of the DMLS column often has anomalous (very high or low) [Ca], up to 200 mg L^{-1} on one occasion. [Ca] is highest in the summer and fall of 2001 (> 50 mg L^{-1}), with modestly lower concentrations outside the growing season. However, seasonal variation is less evident in the Ca data than Na data. Seasonal variability is different for Mg, with lowest concentrations in the fall and winter (< 8 mg L^{-1}) and highest values in spring (> 10 mg L^{-1}).

Total iron and manganese profiles (Figure 50) document two companion redox-sensitive metals. In general, [Fe_T] has a more jagged vertical profile indicating spatial variability between sampling cells. Some periods, such as summer 2001, depict increasing [Fe_T] just below the water table, then decreasing with additional depth. On the

other hand, [Mn_T] usually appears to exhibit a gradual increase with depth, only occasionally tracking [Fe_T] (see 28 Feb 2002). Although temporal variation does exist in these data, concentrations alone do not indicate any identifiable pattern in [Fe_T] or [Mn_T].

Nitrate and phosphate data (Figure 51) are biologically active solutes with more variable profiles than conservative ions. [PO_4^{3-}] remains below 0.6 mg L^{-1} (as PO_4^{3-}) throughout the study period, but is always detectable. Nitrate concentrations vary from below detection to above 2 mg L^{-1} (as NO_3^-) and exhibit a higher degree of spatial variability. The highest nitrate concentrations are generally seen near the water table and, in general, nitrate concentrations decrease with depth. These values are low throughout the study period and do not exhibit noticeable seasonal variability. Nitrite was rarely detected in any samples analyzed (see Appendix IV). Phosphate concentrations are highest in winter 2001-02 and lowest in spring 2001.

Sulfate and chloride are the most prominent anions after bicarbonate. SO_4^{2-} is potentially biologically active and Cl^- is conservative; thus, these two anions can be compared as a ratio to evaluate the amount of biological sulfate reduction. The profiles (Figure 52) exhibit roughly parallel trends with depth, especially in summer and fall 2001. However, early and late in the study period, [SO_4^{2-}] increases with depth while [Cl^-] does not. Both anions have significantly higher concentrations in summer and early fall 2001, and lowest concentrations in winter 2002. Depth profiles of the sulfate-to-chloride ratio are presented in Figure 53. The profiles indicate that the ratio is often higher at depth than near the water table. In no cases is the ratio lowest at depth. This indicates the zone of intermittent saturation to be the area of most active biogeochemical activity, in this case sulfate reduction. This finding is consistent with the findings of

Block (2002) for the bosque and Groffman et al. (1998) and Baker et al. (2000b) for low-order forest streams in New Mexico. The sulfate-to-chloride ratio is usually depleted 10-20% below river values, except at depth, where it is equal to or above river values. Thus, up to 20% of the moles of sulfate entering the aquifer are reduced before reaching the sampling well.

Sulfide, a reduction product of sulfate, is reported as total sulfide because the method is not sensitive to speciation (Figure 54). Sulfide analyses tend to indicate peak concentrations near the middle of the profile (shallow phreatic zone), especially during summer 2001 when this spike was around 150 cm depth. No reliable seasonal variability was observed in the sulfide values, all of which are in the parts per billion range except for isolated data points on 30 May 2001. Sulfide concentrations are typically very low due to the low solubility of iron(II) sulfide. Sulfide data should be considered minimum values due to rapid oxidation before analysis. Fluoride and bromide are minor, conservative anions with concentrations below 1 mg L^{-1} throughout the study period (Figure 55). The profiles are spatially variable and exhibit no systematic changes with depth. Neither anion exhibits noticeable seasonal variability.

Bicarbonate (HCO_3^-) and pH are chemically related and their profiles are presented together (Figure 56). Bicarbonate concentrations are often, but not always, highest near the water table and frequently lowest at greatest depths; however, these trends are subtle. Bicarbonate concentrations also appear to decrease into summer and fall 2001 before increasing. pH is between 7.0 and 7.5 throughout the study period, except for winter 2001-02, when pH is elevated by up to 0.5 unit. No vertical trends were observed in pH.

Electrode Eh data were collected through the end of 2001. Except for the large (200 mV) decline in Eh a few centimeters below the water table with the depletion of oxygen input from the vadose zone, no temporal or spatial trends are evident from these data (Figure 57). A DMLS profile is available for ammonium on 11 Nov 2001 (Figure 58), indicating all concentrations below 1 mg L^{-1} and no noticeable trend with depth.

Down-hole dissolved oxygen data (Figure 59) indicate an oxic to suboxic zone in the upper 20-30 cm of groundwater, with this value being rapidly depleted with depth below the water table. Below this oxic zone, the aquifer is persistently anoxic to at least 250 cm depth. All of these reported values are at or below the instrumental quantification limit of about 0.4 mg L^{-1} and should be considered qualitatively anoxic (Baker et al., 2000a). Temperature profiles (Figure 60) reveal expected seasonal relationships for shallow groundwater. During warm periods of the year, groundwater temperature decreases with depth and is cooler than air. During cold periods, temperature increases with depth and is warmer than the atmosphere.

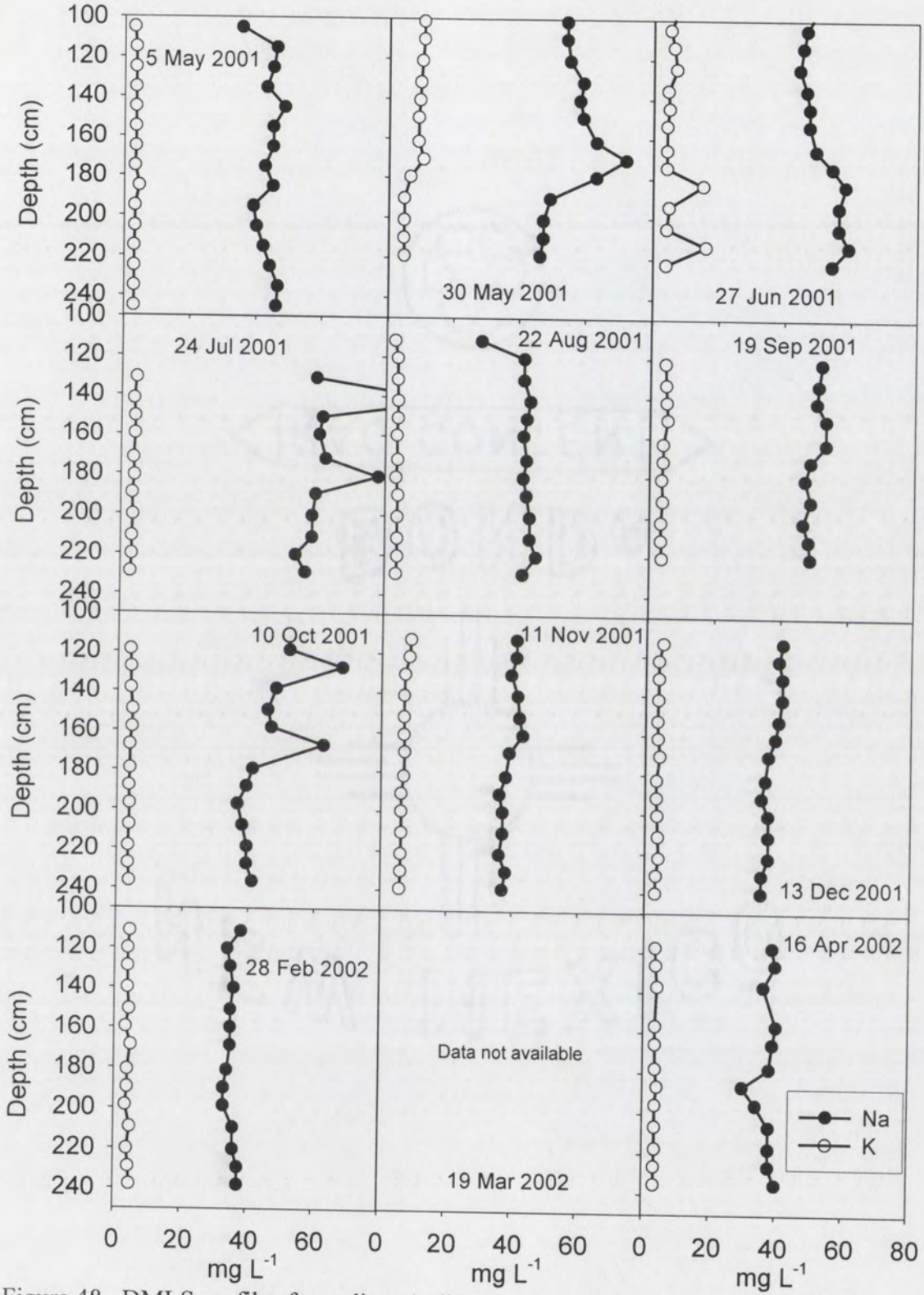

Figure 48. DMLS profiles for sodium (solid circles) and potassium (open circles).

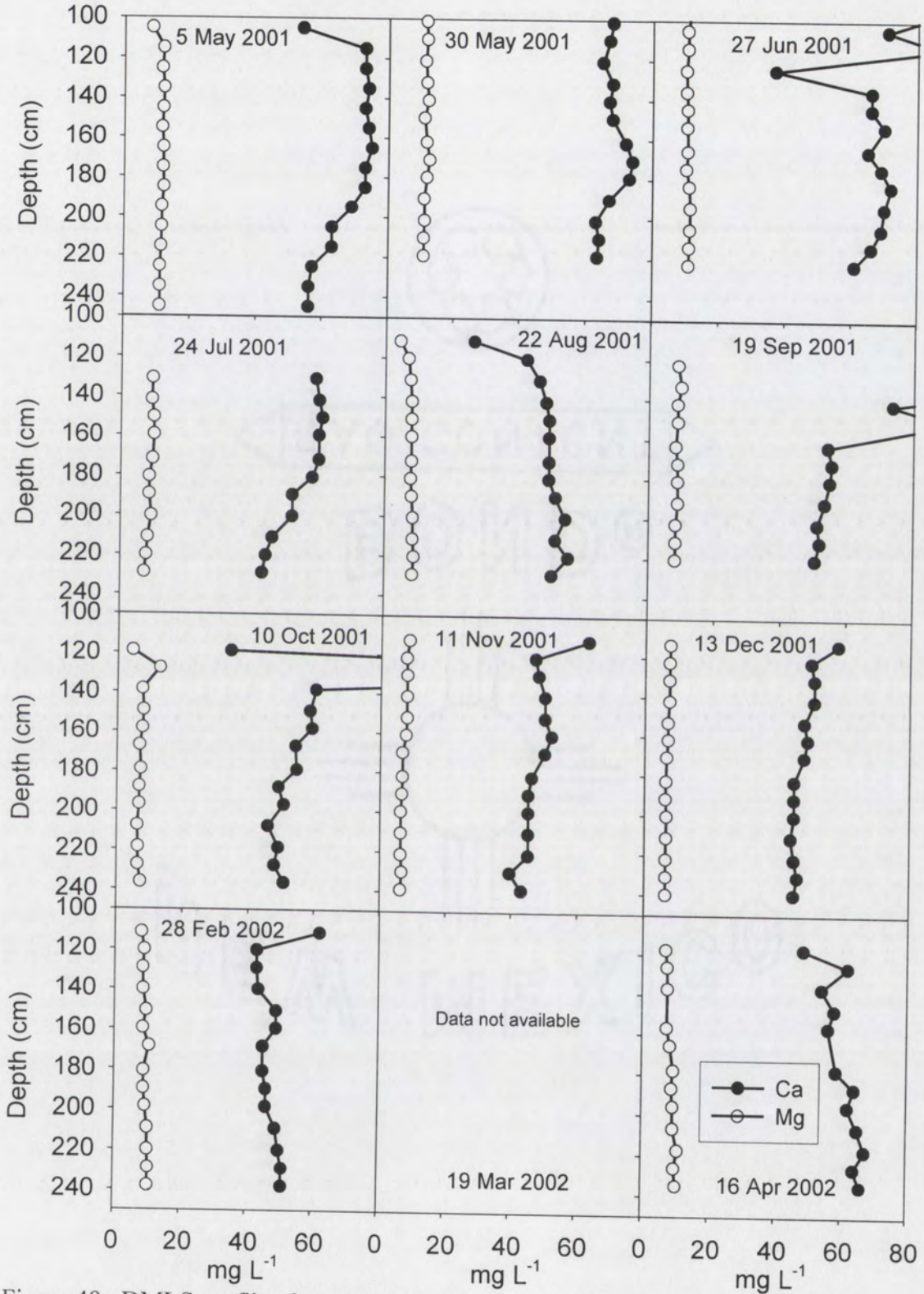

Figure 49. DMLS profiles for calcium (solid circles) and magnesium (open circles).

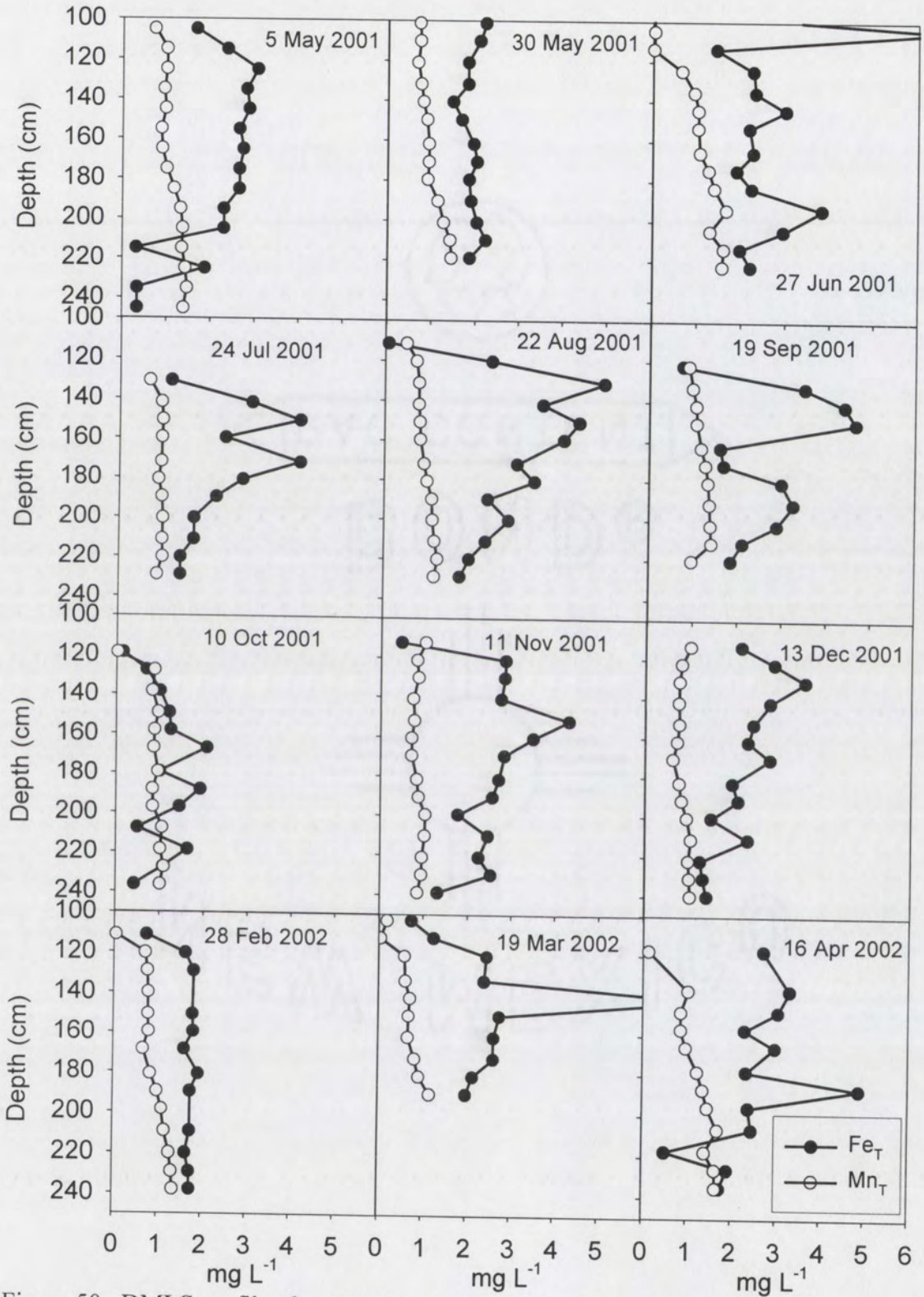

Figure 50. DMLS profiles for total iron (solid circles) and manganese (open circles).

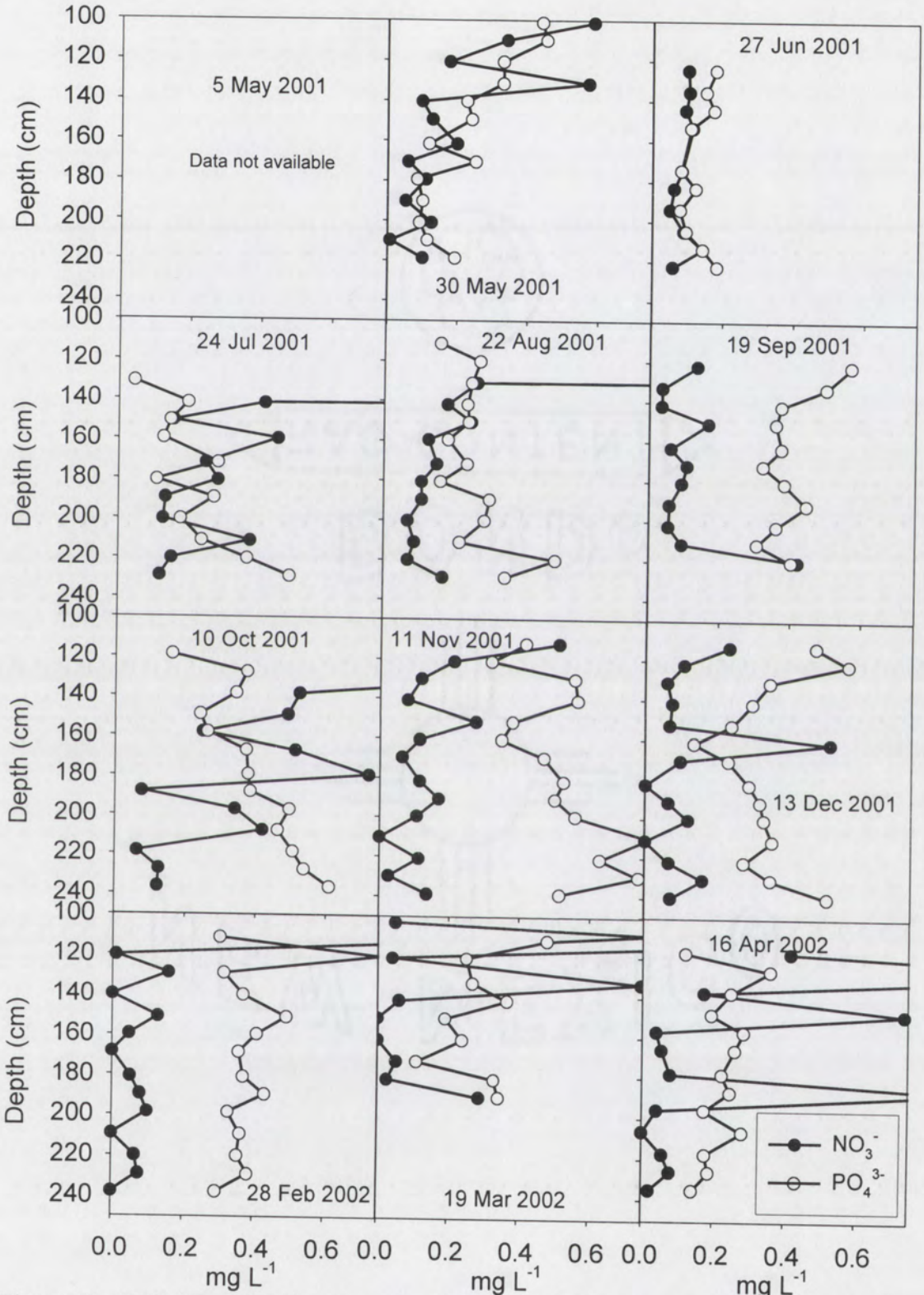

Figure 51. DMLS profiles for nitrate (as NO_3^-, solid circles) and phosphate (as PO_4^{3-}, open circles).

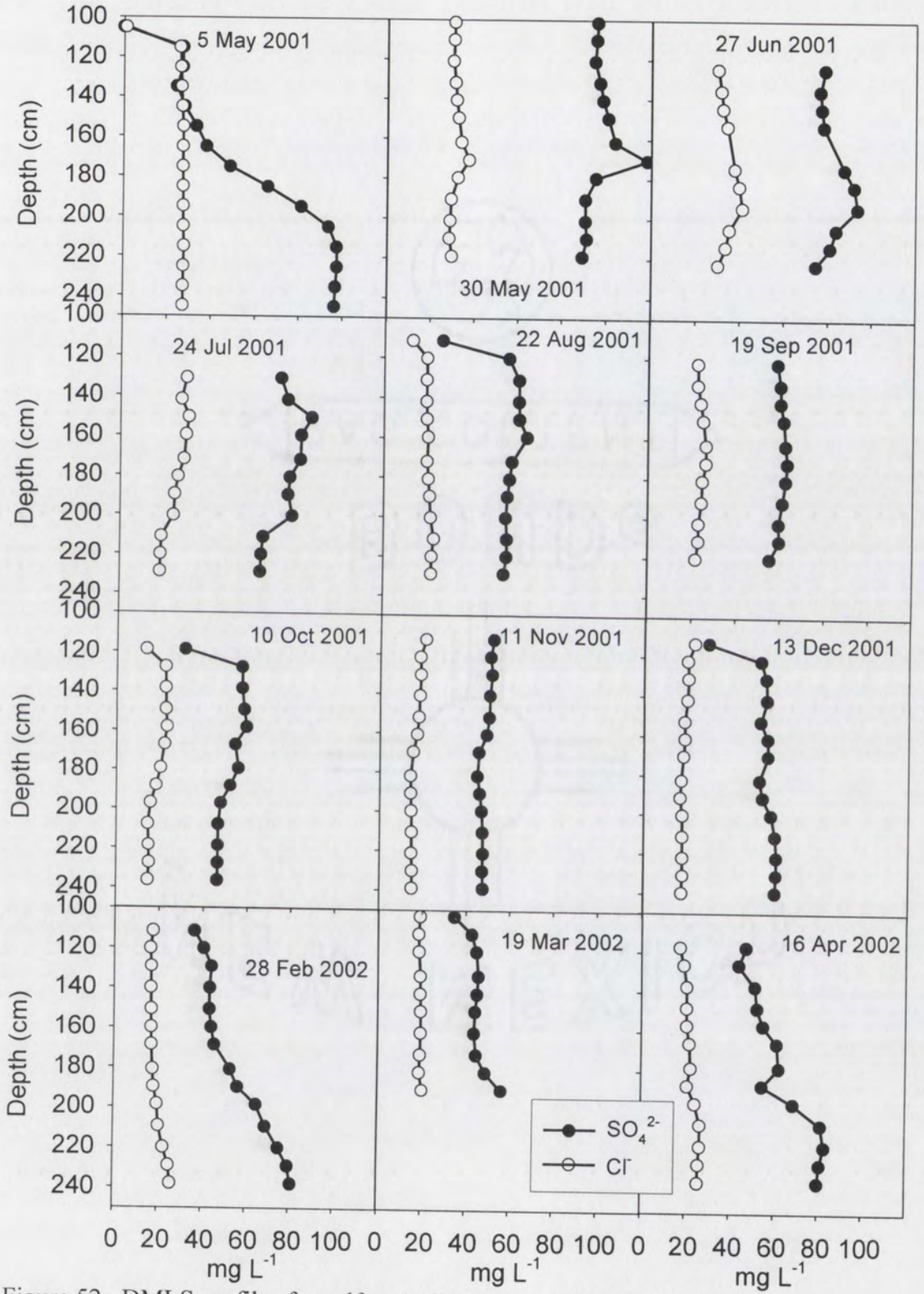

Figure 52. DMLS profiles for sulfate (solid circles) and chloride (open circles).

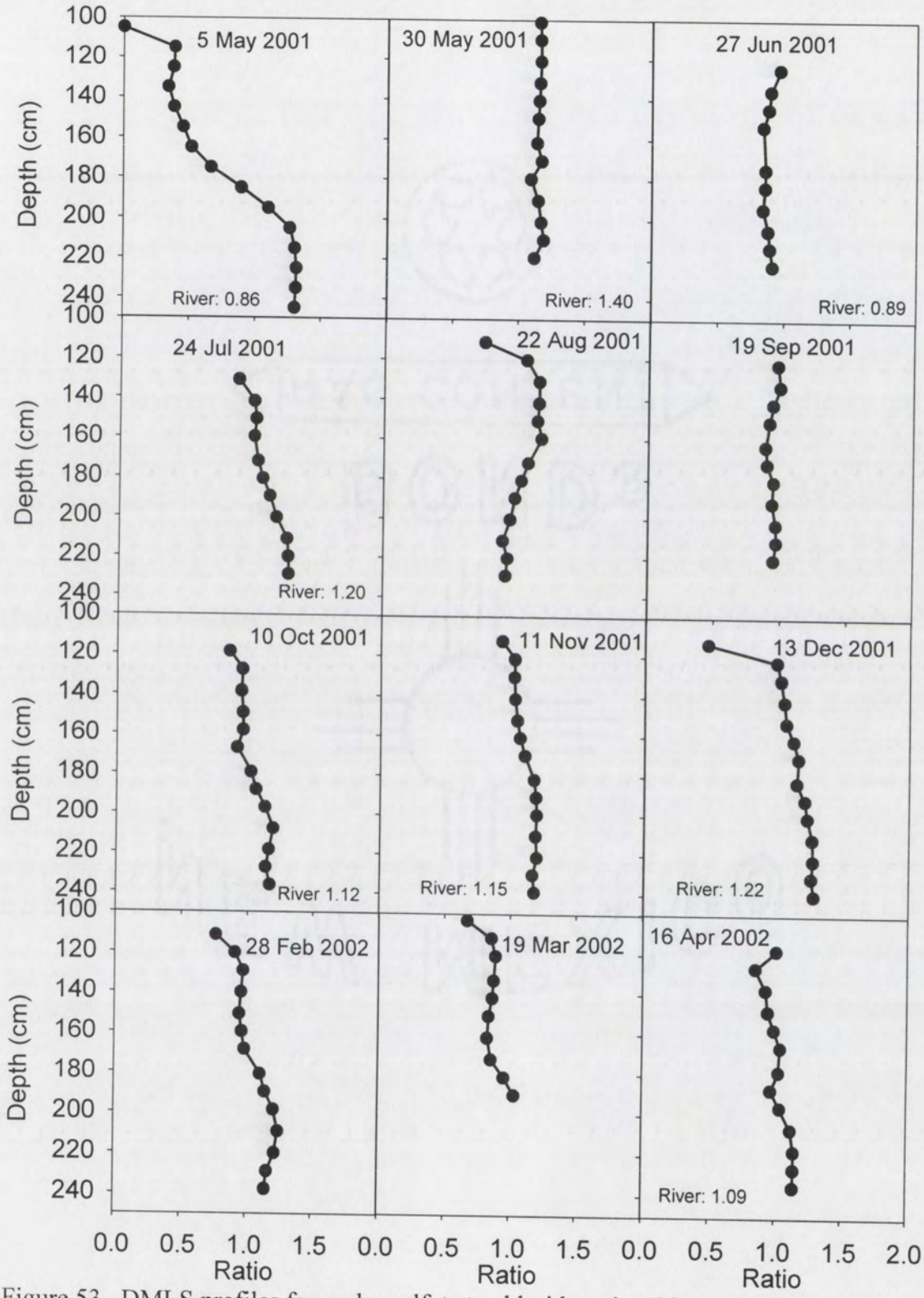

Figure 53. DMLS profiles for molar sulfate to chloride ratio. River values provided when available.

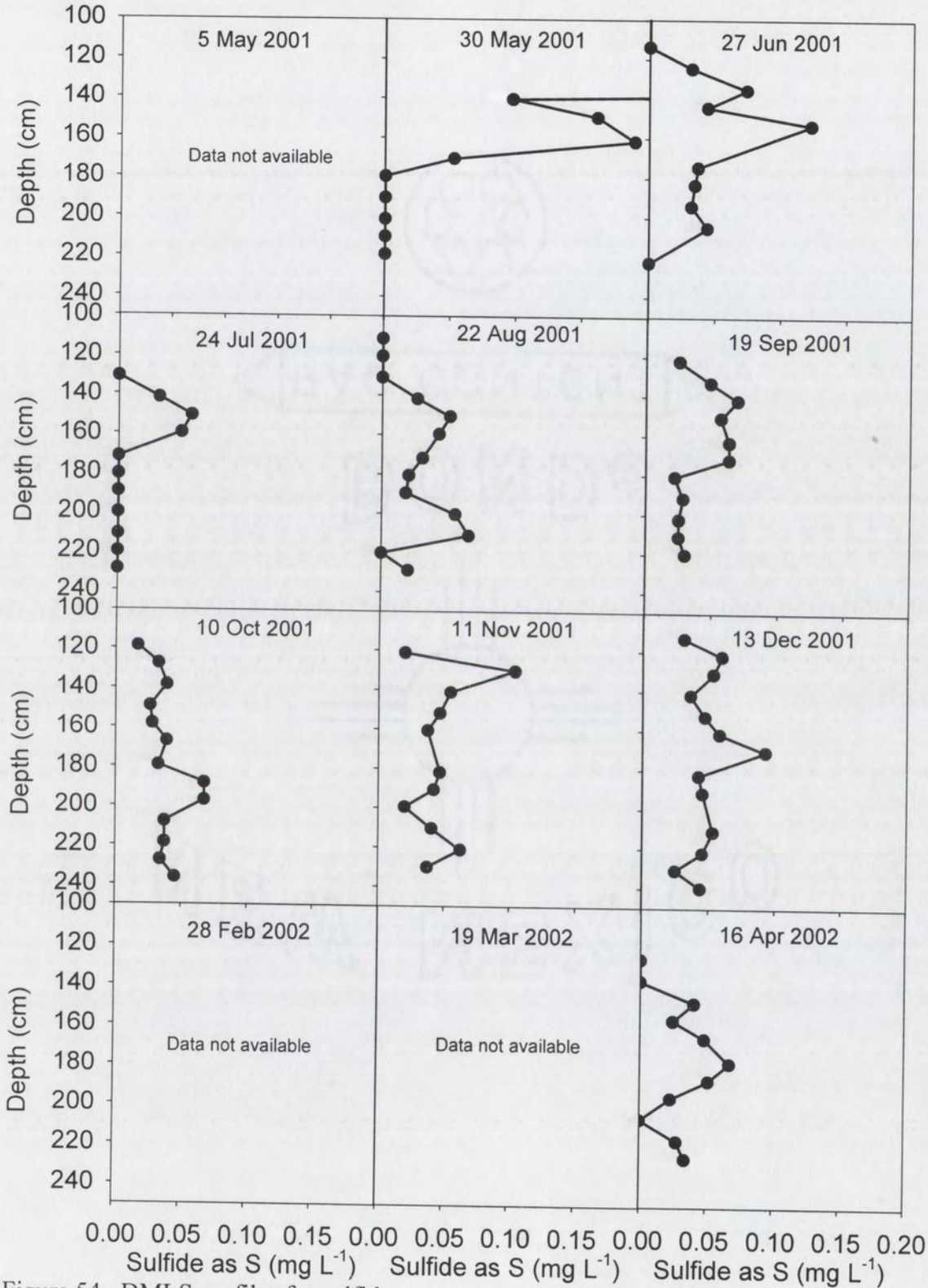

Figure 54. DMLS profiles for sulfide.

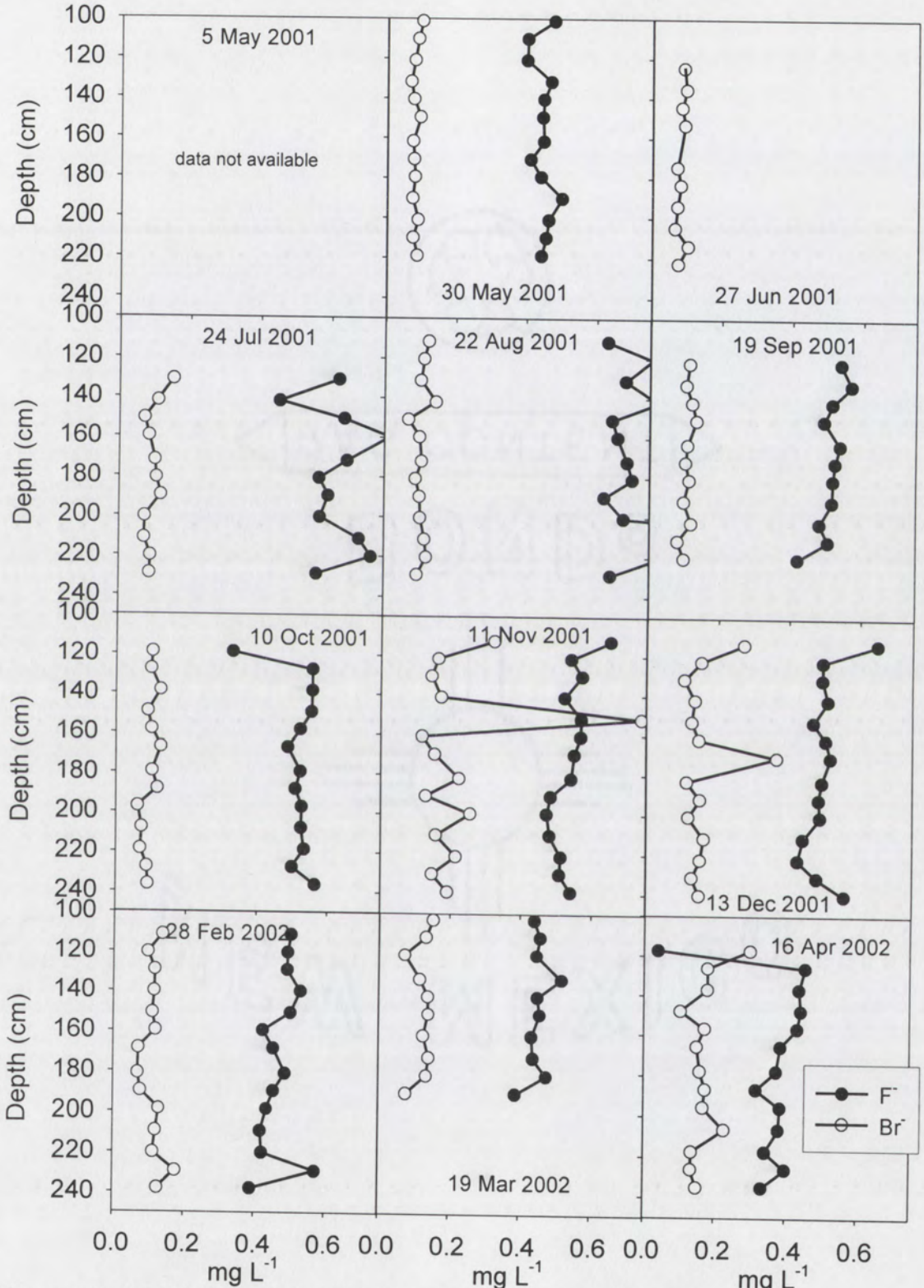

Figure 55. DMLS profiles for fluoride (solid circles) and bromide (open circles).

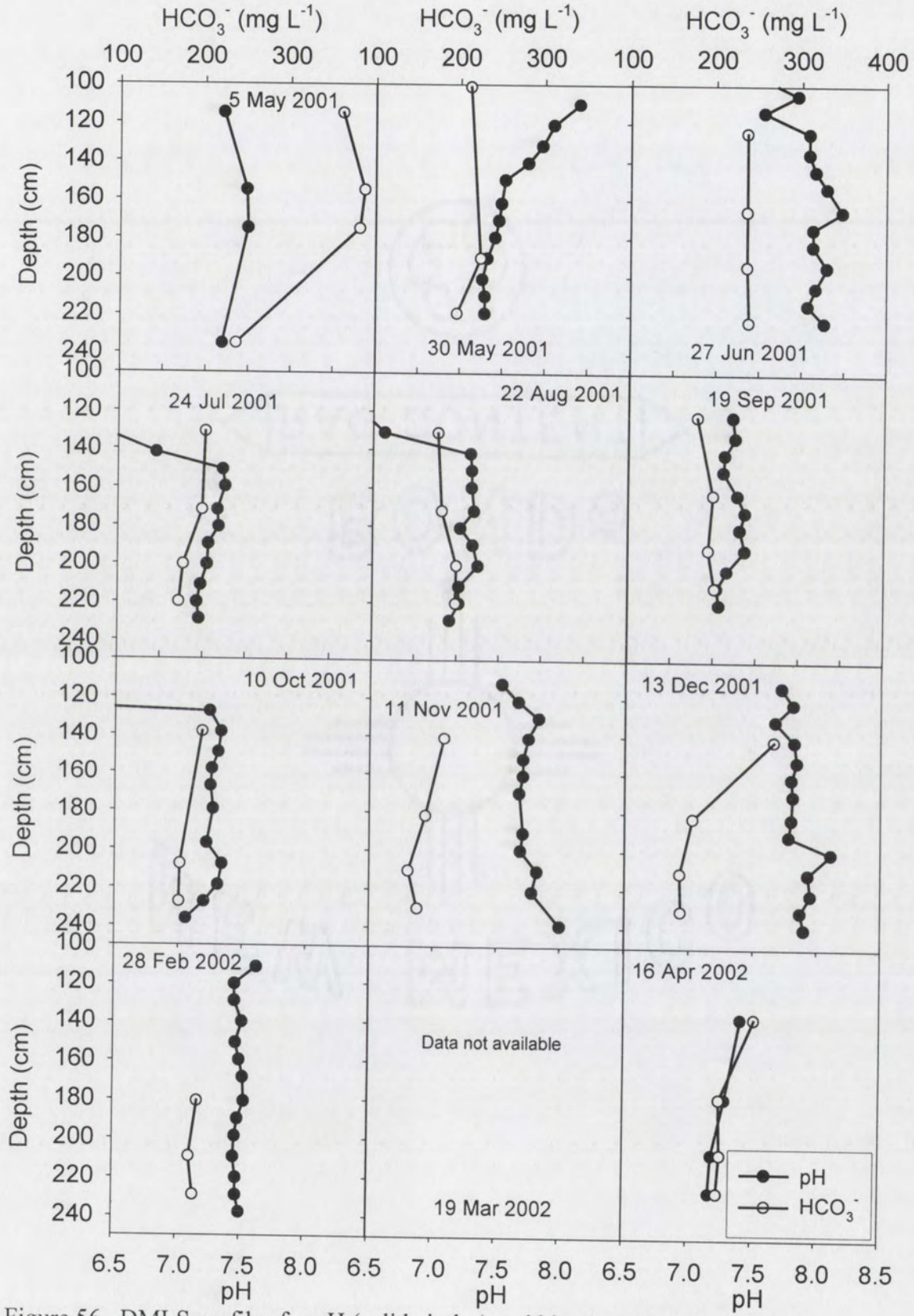

Figure 56. DMLS profiles for pH (solid circles) and bicarbonate (open circles).

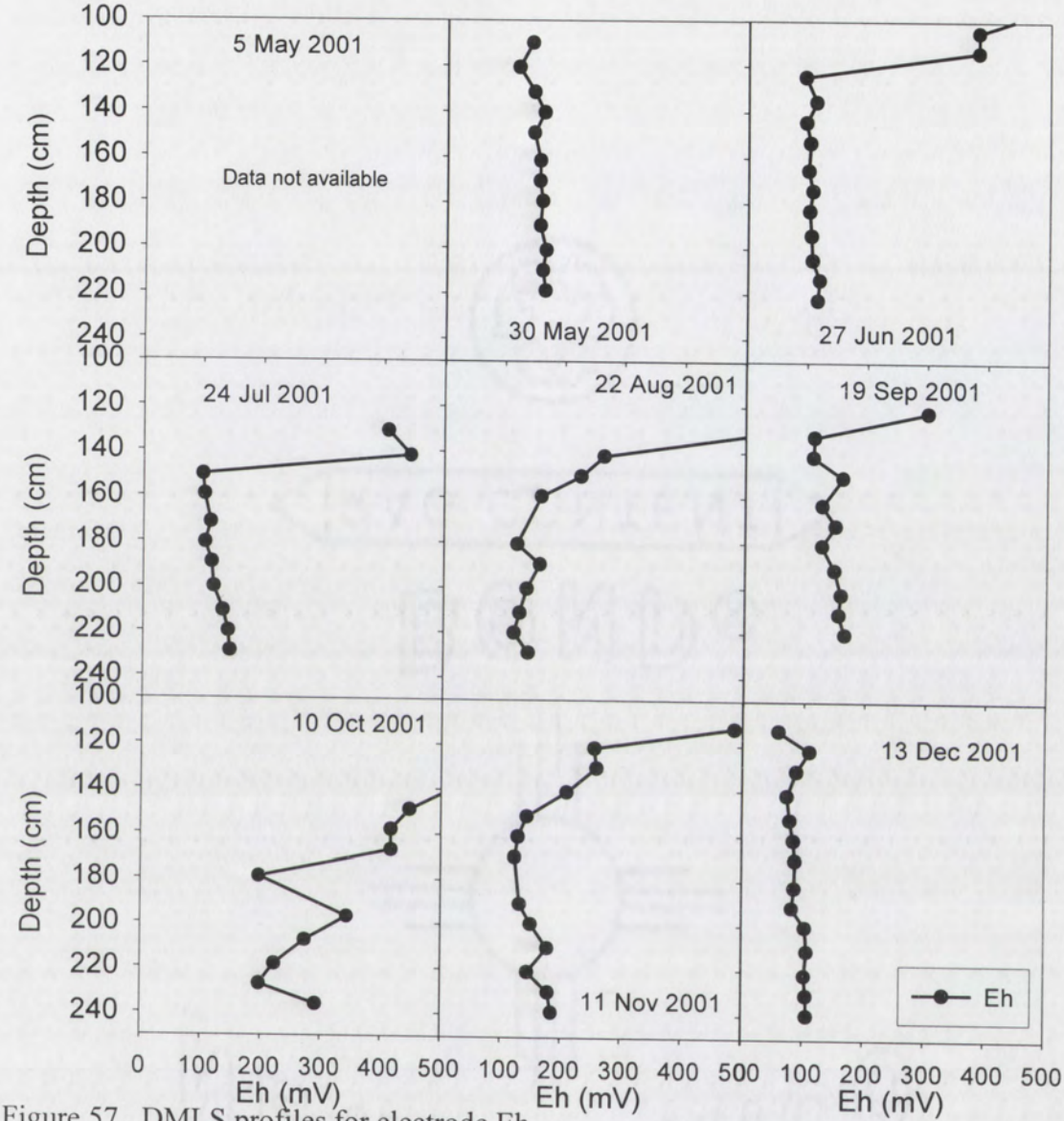

Figure 57. DMLS profiles for electrode Eh.

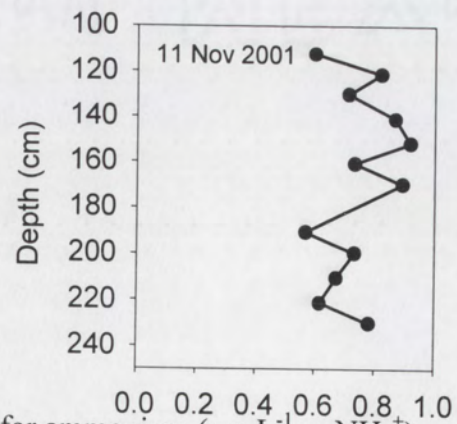

Figure 58. DMLS profile for ammonium (mg L^{-1} as NH_4^+).

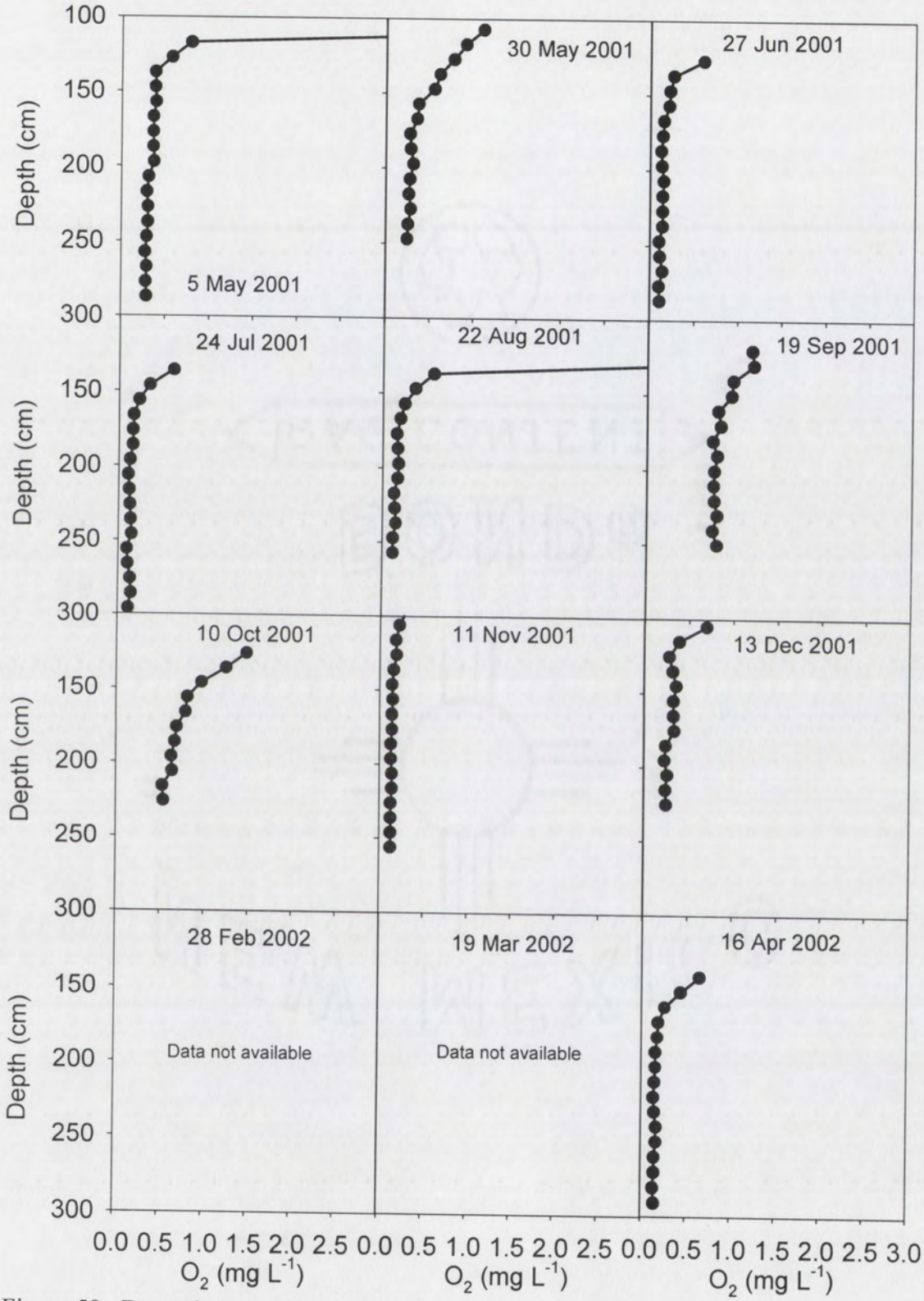

Figure 59. Down-hole dissolved oxygen profiles for BLN2.

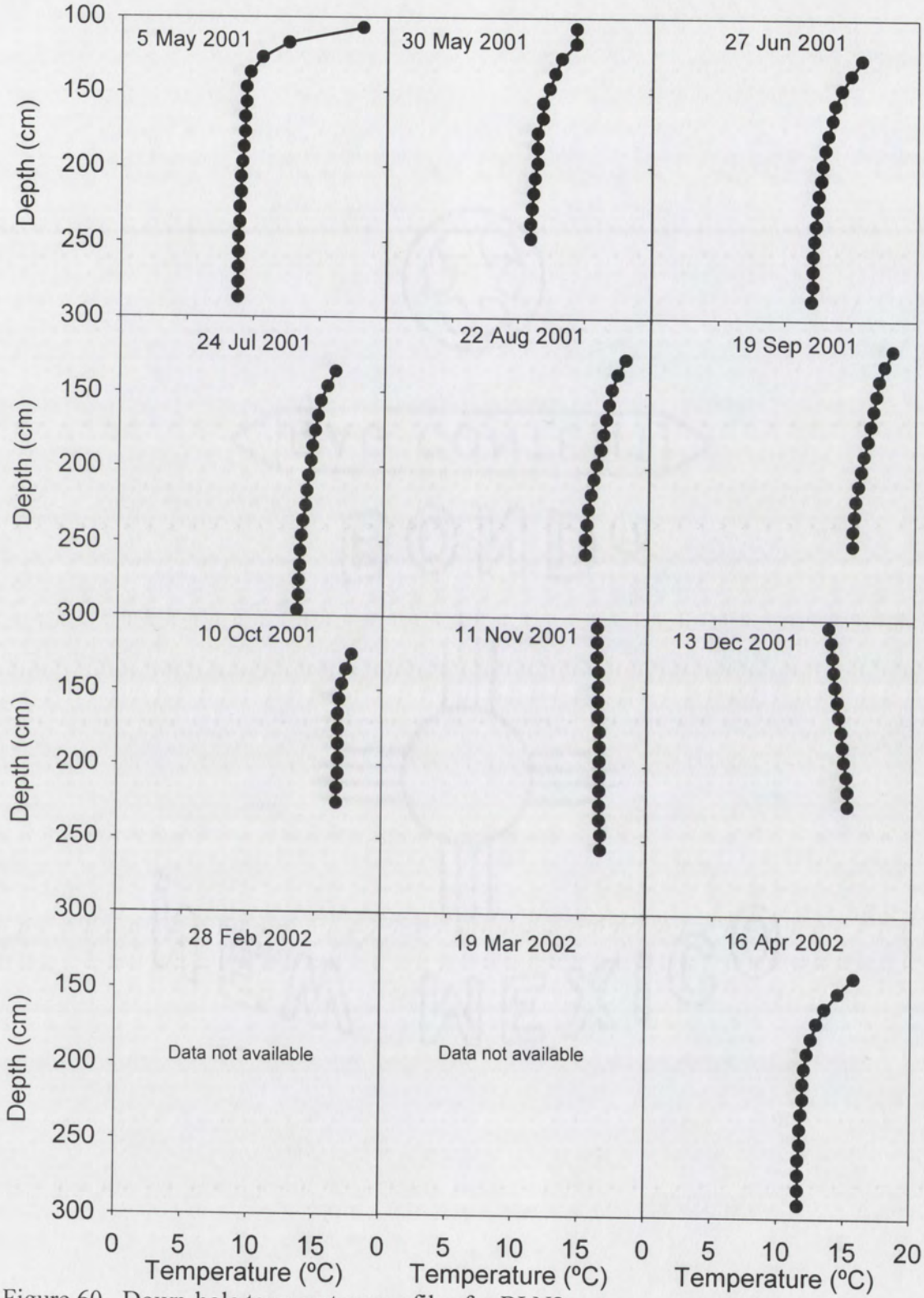

Figure 60. Down-hole temperature profiles for BLN2.

Evapoconcentration

Conservative ion concentrations provide information on water consumption by riparian zone vegatation via ET. This hydrologic flux has been quantified by micrometeorological methods in the MRG (Dahm et al., 2002). Its chemical effects are seen as enrichment of salts in the remaining groundwater. The extent of evapoconcentration can be determined by computing ion enrichment relative to the river in representative samples 1.5 m below the surface (Table 10). In July 2001, a period of peak ET, ion concentrations are concentrated over river values by 24-84%. In November 2001, the river sample was slightly more evapoconcentrated than groundwater. Tiered Stiff diagrams can be used to show varying degrees of evapoconcentration down a DMLS profile. The size of the polygons indicates the concentrations of major ions (Drever, 1997). The Stiff diagrams (Figure 61) suggest that water uptake by plants is spatially variable, perhaps caused by a non-uniform distribution of roots.

Table 10. Groundwater to river ratios (by weight) of ion concentrations in July and November 2001. *- July river data from Block (2002).

BLN2 Sample	Ca^{2+}	Mg^{2+}	$Na^{+} + K^{+}$	Cl^{-}	SO_4^{2-}
072401-146-155*	1.39	1.24	1.55	1.84	1.58
111101-147-156	0.91	0.85	0.91	0.66	0.60

Redox along flowpaths: Terminal electron accepting processes

Although field investigations have long identified anoxic organic carbon oxidation processes such as sulfate reduction in marine sediments, more recent work has unified these investigations into the concept of terminal electron accepting processes (TEAPs; Chapelle, 2001). The cascading processes are driven by thermodynamic control of Gibbs free energy (Jackson and Patterson, 1982; Postma and Jakobsen, 1996) and/or competitive exclusion among microbes (Berner, 1981b; Chapelle, 2001). The TEAP

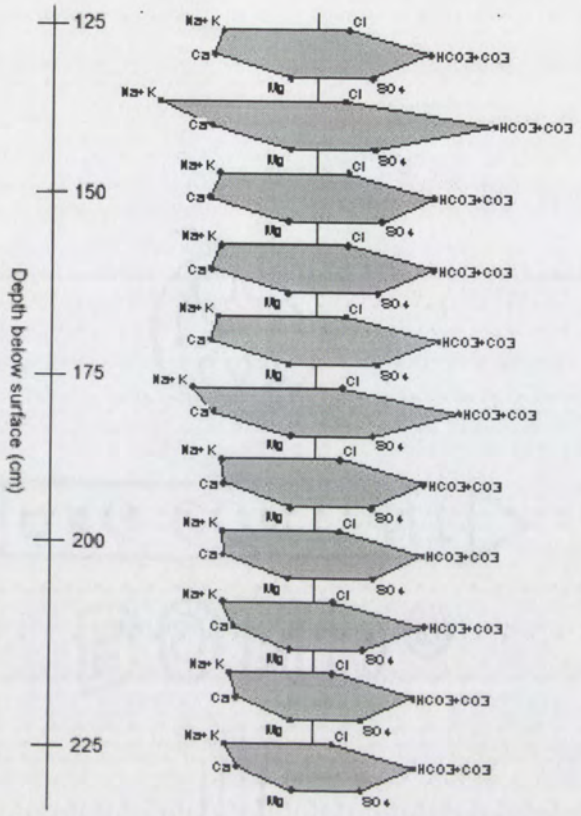

Figure 61. Tiered Stiff diagrams of a DMLS profile from 24 Jul 2001, indicating evapoconcentration of major ions. The size of the polygon indicates total dissolved solids.

concept depicts organic carbon being oxidized by transferring electrons to redox-sensitive inorganic compounds. Along a flowpath, TEAPs occur in a thermodynamically predictable order: aerobic respiration, denitrification, Mn oxyhydroxide reduction, Fe oxyhydroxide reduction, sulfate reduction, and methanogenesis. In each case, carbon dioxide (carbonate alkalinity) is produced as a microbial respiration product; thus, organic C oxidizes to inorganic C (Table 2).

Thermodynamic relationships become more complicated when alternative end products are considered, incorporating solids, dissolved gases, and ions. For example, NO_3^- can reduce to NO_2^-, N_2 *(aq/g)*, or NH_4^+, and SO_4^{2-} can reduce to H_2S *(aq/g)*, HS^-, or FeS *(s)*, all of which affect thermodynamic predictability. Minor changes in pH drive the

partitioning between ionic and gas solutes (*e.g.* HS^- / H_2S and NH_4^+/NH_3). Furthermore, TEAPs occur at widely varying rates that are controlled by production of electron donors via fermentation (Jakobsen and Postma, 1999). Labile electron donors such as low-molecular weight organic acids (fermentation products) are rapidly scavenged by microbes, so their concentrations are usually very low.

The first TEAP, oxygen consumption, is aerobic respiration that takes place in aerobic surface water, oxic groundwater, or oxic microenvironments. Oxygen may be consumed by facultative or obligate aerobic bacteria, or by higher organisms (hyporheos). Once oxygen is substantially reduced, microbial competitive relationships cause redox zones to emerge. Nitrate is quickly reduced, either to N_2 via denitrification, a dissimilatory process, or incorporated into cells via nitrate reduction to NH_4^+, an assimilatory process. Once nitrate has been depleted (usually rapid in unpolluted waters), metal reduction begins. Solid-phase Fe and Mn oxyhydroxides reduce to soluble divalent metal cations. Facultative metal-reducing bacteria may also reduce trace metals during this phase; however, this depends on redox-solubility relationships specific to each metal (Chapelle, 2001).

Metal reduction is succeeded by sulfate reduction. Evidence for sulfate reduction at Belén includes depleted SO_4^{2-} : Cl^- ratios, detectable sulfide, the odor of H_2S gas, and observed Fe sulfide minerals. The abundance of sulfate reduction is made possible by high sulfate concentrations in the MRG system. This condition is due to large exposures of gypsum in the basin, desert dust processes, and evaporation that exceeds precipitation. Many studies of the TEAP concept have been conducted in temperate or mountain settings, particularly low-order forested catchments, where sulfate is not a major ion. A

major sulfate reduction pathway is usually associated with marine sediments in the literature (Nealson and Stahl, 1997; Straub et al., 2001; Roden et al., in press), but sulfate reduction is clearly important in high-sulfate desert river systems such as the Rio Grande.

To assess which TEAPs are most significant, approximate organic carbon oxidation amounts were calculated using the reaction stoichiometry of Baker et al. (2000a; Table 2). Using year-round average river concentrations (including data from Block, 2002), oxygen and nitrate were assumed to be reduced completely down-flow from the Rio Grande to the well. Iron and manganese were assumed to increase from non-detectable in the river to 5 mg L^{-1} (Fe_T) and 2 mg L^{-1} (Mn_T) at the well, simulating actual down-flow evolution. Sulfate was assumed to decrease from an annual average river concentration. Since sulfate is not reduced to completion across the floodplain, organic carbon oxidation was calculated for varying degrees of sulfate reduction. Based on changes in the sulfate to chloride ratio (Figure 53), up to 20% of sulfate undergoes reduction between the river and the well. The results of this analysis (Figure 62) suggest that 20% sulfate reduction oxidizes more moles of organic carbon than the next largest TEAP, oxygen reduction. Thus, sulfate reduction has the potential to oxidize at least as much organic carbon as other TEAPs, depending on the actual degree of sulfate reduction.

Because the average river concentration of NPOC is 27 μM (as C), dissolved organic carbon from the Rio Grande should be completely oxidized within the oxygen reduction zone. Thus, at least 250 μmol (as C) of buried, labile organic carbon must be available per liter of groundwater to explain the extensive TEAP sequence observed throughout the study. Organic carbon content of sediments was not measured for this

study; however, the fine fraction of ZIS sediments has about 5% loss on ignition at 1000 °C (Figure 21). Much of the loss on ignition is probably organic carbon, although some may be calcite.

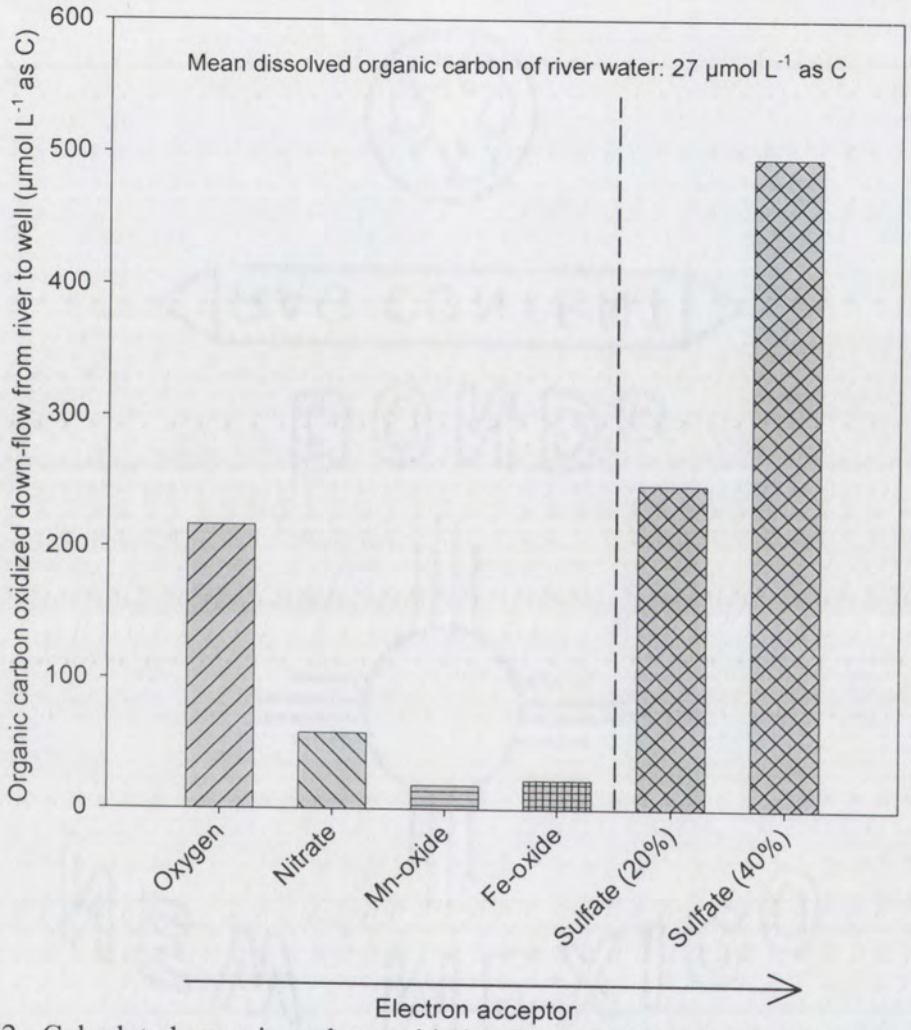

Figure 62. Calculated organic carbon oxidation for each TEAP in the alluvial aquifer.

Sulfate reduction has several important geochemical implications. Fe(II) mobility is controlled by sulfate reduction because iron(II) sulfides are insoluble under reduced conditions. Since metal reduction occurs at higher Eh than sulfate reduction, Fe^{2+} concentrations may be counter-intuitively higher under less reducing conditions because subsequent sulfate reduction at lower Eh would immobilize Fe(II) (Chapelle and Lovley, 1992). Sulfate reduction does not control Mn mobility because no Mn(II)

sulfides are plausible in freshwater sediments (Berner, 1981a; Matsunaga et al., 1991). In summary, Fe and Mn mobility cannot be viewed the same way, and the two metals may behave alike or differently based on the extent of sulfate reduction and/or differences in oxide stability.

The final major TEAP is methanogenesis, in which organic carbon is converted CH_4 and CO_2, either with acetate as the substrate, or in which H_2 and CO_2 are converted to CH_4. Significant methane has not yet been detected in MRG sediments (Table 5; C.N. Dahm, pers. commun.), which strongly suggests that competitive exclusion by sulfate-reducing bacteria prevents methanogenesis from occurring in significant amounts (Lovley and Klug, 1983).

Relating redox chemistry to flowpaths at Belén

Two sources of oxygen are available to shallow groundwater. Proximity to the water table supplies oxic soil water and vadose zone oxygen, producing a small oxic zone immediately below the water table. This oxygen is rapidly depleted within a few centimeters depth below the water table (Figure 59), leading to competition for alternative electron acceptors at greater depth. These electron acceptors (nitrate, manganese(IV), iron(III), and sulfate) are reduced to create a persistently stratified TEAP regime in the shallow saturated zone.

More important in most phreatic systems is the depletion of oxygen down-flow from recharge areas, stimulating competition for alternative electron acceptors and producing horizontal redox zones along flowpaths (Champ et al., 1979). At the small scale used in this study, however, both TEAP-stimulating mechanisms must be considered. A single DMLS profile is most useful for illustrating cycling associated with

the water table. However, a transect across the floodplain is needed to describe a flowpath.

Depth profiles alone are of limited utility in a dynamic environment, such as the bosque, where transport may exceed reaction rates. Thus, the presence of a reduced solute is not evidence of *in situ* reduction, nor is its absence a sign that the process is not occurring. The problem of transported solutes is not unique to the bosque aquifer. A recently developed technique uses hydrogen gas (H_2) concentration to diagnose which TEAP is dominant in a groundwater environment. H_2 is a fermentation product that is rapidly used by anaerobic microbial respiration and inefficiently transported. TEAPs vary in their efficiency of H_2 consumption, permitting H_2 concentrations to indicate the prevalent TEAP. H_2 concentrations at Belén (Table 5) are high enough to diagnose methanogenesis (Chapelle et al., 1995), but the continued presence of sulfate and sulfide and the absence of significant methane cause me to conclude otherwise. Furthermore, Jakobsen and Postma (1999) illustrate that the H_2 method works best for steady-state sediments with stable microbial competitive relationships. In sum, the best evidence indicates that electron acceptors through sulfate are reduced in the short (hours to days) trip through the aquifer from river to USJRD.

Transect interpretation

The porewater sampling transect was a useful approach for delineating TEAPs. Because the bed level of the USJRD is lower than any corresponding point on the Rio Grande bed, groundwater flows from the river to the ditch. While the transect is unlikely to represent a true flowpath, it contains a substantial down-flow component. Redox fronts have been interpreted for denitrification, Mn oxide reduction, Fe oxide

reduction, and sulfate reduction (Figure 63). For nitrate and sulfate, concentrations were normalized to chloride, which is not biologically active and provides an indication of biological reduction.

Nitrate trends are equivocal; however, the highest NO_3^- concentrations at the site are in the river, suggesting that the aquifer is a net sink for nitrate. With the exception of one TR-3 point that may represent perched or evaporated water, the nitrate : chloride ratio decreases from river to USJRD. [Mn_T] increases along the transect and, in general, USJRD Mn_T concentrations are the highest at the site. Along this transect, Fe_T concentrations are very low, probably made low by removal as sulfides, but [Fe_T] increases down-flow on 16 April. A large sulfate reduction front is interpreted down-flow from the metal reduction front and may account for the large drop in electrode Eh. In Figure 63, this is seen in the decrease in sulfate : chloride ratio, made uncertain due only to the anomalous TR-3 point mentioned above.

The increase in bicarbonate along the path is consistent with TEAPs increasing down-flow because CO_2 is a microbial respiration product. The decrease in pH occurs where Fe/Mn oxyhydroxide reduction is also evident; a decrease in pH from river to wells was observed on almost every sampling date. Metal hydroxide reduction is the only TEAP that produces protons at near-neutral pH (Table 2), although all TEAPs and fermentation influence pH by producing carbon dioxide. The non-purgeable organic carbon (NPOC) data do not indicate net depletion of dissolved organic carbon down-flow, as the TEAP concept suggests. The USJRD, despite being surface water, is substantially (200 mV) more reduced than the Rio Grande, indicating that it receives large volumes of reduced groundwater at a rate that exceeds full aerobic reoxidation. The

USJRD is also down-gradient of floodplain agricultural areas and basin-fill sediments beyond to the east, which provide an influx of groundwater not characterized in this study. However, the riverside drains contain water mostly from the river rather than inland (Theis, 1938; Peter, 1987).

Mineral interpretations and spatial patterns

The ZIS sediments are alternatively oxic near the water table and anoxic-sulfidic below according to the classification scheme of Berner (1981b). However, Fe and Mn oxyhydroxides persist with depth, even under anoxic-sulfidic conditions (Lovley, 1987; Wersin et al., 1991; Postma, 1993; Lovley, 2000). This emphasizes the importance of crystallographic control on solubility and microbial reducibility. Specifically, sulfate reducers can outcompete Fe(III) reducers forced to use crystalline Fe oxides as electron acceptors (Lovley, 2000). In a floodplain in Georgia, Darke and Walbridge (2000) found that repeated flooding promoted amorphous Fe oxides, and non-flooding periods enabled Fe oxides to age into crystalline forms.

Any microbial role in Fe^{2+} and Mn^{2+} oxidation is difficult to discern because abiotic Fe^{2+} oxidation occurs rapidly in the presence of molecular oxygen (Nealson, 1983), although Mn^{2+} does not rapidly oxidize abiotically at pH below 8 (Bartlett, 1988). Enzymatic Fe^{2+} oxidation allows Fe-oxidizers to harvest the energy of this spontaneous process by performing it faster than would occur abiotically (Fortin et al., 1997). Fe^{2+} oxidation may also detoxify the environment for obligate anaerobes. Fe/Mn oxyhydroxides may precipitate on mineral surfaces or coat bacterial cells (Nealson, 1983).

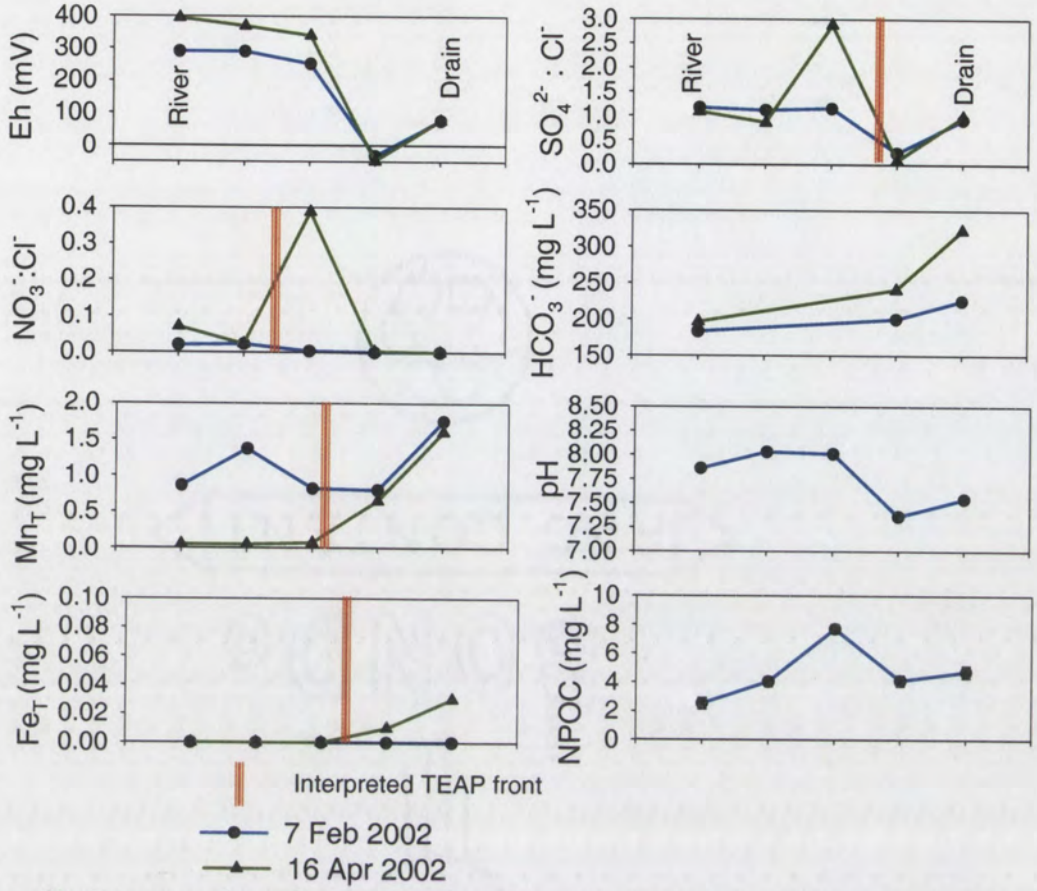

Figure 63. Interpretation of transect redox chemistry from spring 2002. Vertical lines are interpreted TEAP fronts. Transect was not surveyed, so X-axis does not represent distance across floodplain.

Once formed, amorphous Fe and Mn oxyhydroxides are geochemically reactive, attracting trace metals and nutrients such as phosphate and incorporating them via coprecipitation and sorption. These solutes are released when metal oxyhydroxides undergo reductive dissolution (Ferris, 2000). Metal oxide reduction may control phosphate concentrations in aquatic sediments (Boulton et al., 1998), although the overall biogeochemical significance of these processes is "barely recognized" (Emerson, 2000). Furthermore, Fe/Mn redox processes influence the carbon cycle, trace metal mobility, and physical sedimentology, because oxides may clog pores (Lovley, 2000). Reducibility

of metal oxides depends on crystal structure, surface area, and particle size, and often varies within sediments.

The most plausible iron(III) oxide on the time scale of weeks is ferrihydrite, $Fe(OH)_3$ (Matsunaga et al., 1991). Ferrihydrite may be crystalline or amorphous; bioavailability increases with surface area (Zachara et al. 2002), which ranges from 159 to 720 $m^2\ g^{-1}$ (Tebo and He, 1998). Ferrihydrite may coat detrital Fe minerals, precipitate at the oxic-anoxic interface, or form colloidal suspensions in groundwater (Zachara et al., 2002). Another ferric hydroxide, lepidocrocite, has a more organized crystal structure than ferrihydrite. Hematite, a non-microbially reducible iron oxide, is dehydrated ferrihydrite with lower surface area and strong crystallographic order (Tebo and He, 1998). The most likely Mn oxyhydroxides are amorphous MnO_2, birnessite, or perhaps vernadite or todorokite. Birnessite can incorporate Na^+, Ca^{2+}, and OH^- (Gilkes and McKenzie, 1988). Mn-oxides are assumed to be mostly Mn(IV), rather than Mn(III), because microbes tend to oxidze Mn(II) fully to Mn(IV) (Emerson, 2000). Fe oxides may oxidize Mn^{2+}, creating mixed Fe/Mn oxides (Gilkes and McKenzie, 1988).

In this study, Mn was usually seen as a lesser constituent of mixed oxides, rather than as pure Mn oxides (although smaller SEM spot sizes might reveal more Mn-pure areas). Many Fe oxyhydroxides contain no detectable Mn. Comparing Mn : Fe ratios of mineral and aqueous phases (Table 11) reveals that Mn is more mobile than Fe because Mn^{2+} is more prevalent in the aqueous phase relative to Fe^{2+}. This suggests that Eh is possibly high enough for abiotic Fe^{2+} oxidation but rarely high enough to cause much abiotic Mn^{2+} oxidation. Further evidence for this is the lack of a spike of amorphous Mn oxyhydroxides in the ZIS (Figure 17).

Table 11. Fe:Mn weight ratio statistics.

	Mean Fe:Mn	Std. Deviation	*n*
0.5N HCl extracts	9.56	3.81	33
Water samples	2.30	1.37	77

Amorphous extractable Fe, Mn, and P are correlated, suggesting that these oxides are mixed, intergrown masses, rather than discrete, stoichiometric Fe and Mn minerals. When Fe, Mn, and P are plotted against each other (Figure 64), the best fit for these data is an exponential increase to a maximum value. This trend resembles surface area-dominated processes, in which sites become less available as concentrations increase (Drever, 1997). The R^2 value indicates how much variation in y is explained by variability in x. The *P*-value is the probability that the correlation occurred randomly; thus, a low *P*-value indicates a statistically significant correlation. Ferrihydrite has a zero point of charge of 7.9-8.2 and would sorb anions such as PO_4^{3-} below that pH (Tebo and He, 1998), a range of values seen throughout this study. It is unclear whether this relationship is sorption of PO_4^{3-} to charged oxyhydroxides of high surface area (Borggaard, 1983) or microbial nutrient scavenging. In the case of microbial Fe oxyhydroxides, these two processes may be indistinguishable.

The formation of Fe sulfides requires the presence of sulfate reduction and organo-metallic complexes. The complexes are important to increase the reactivity of metal cations toward sulfide and can form when acidic groups exposed on the edges of bacterial cells (*e.g.* carboxyls, phosporyls) exchange a proton for a metal cation. As a result, Fe sulfides are associated with organic matter in sediments (Ferris et al., 1989b; Fortin et al., 1997; Ferris, 2000). Interpreted interactions between particulate organic matter and Fe have been seen occasionally in bosque samples (Figure 43).

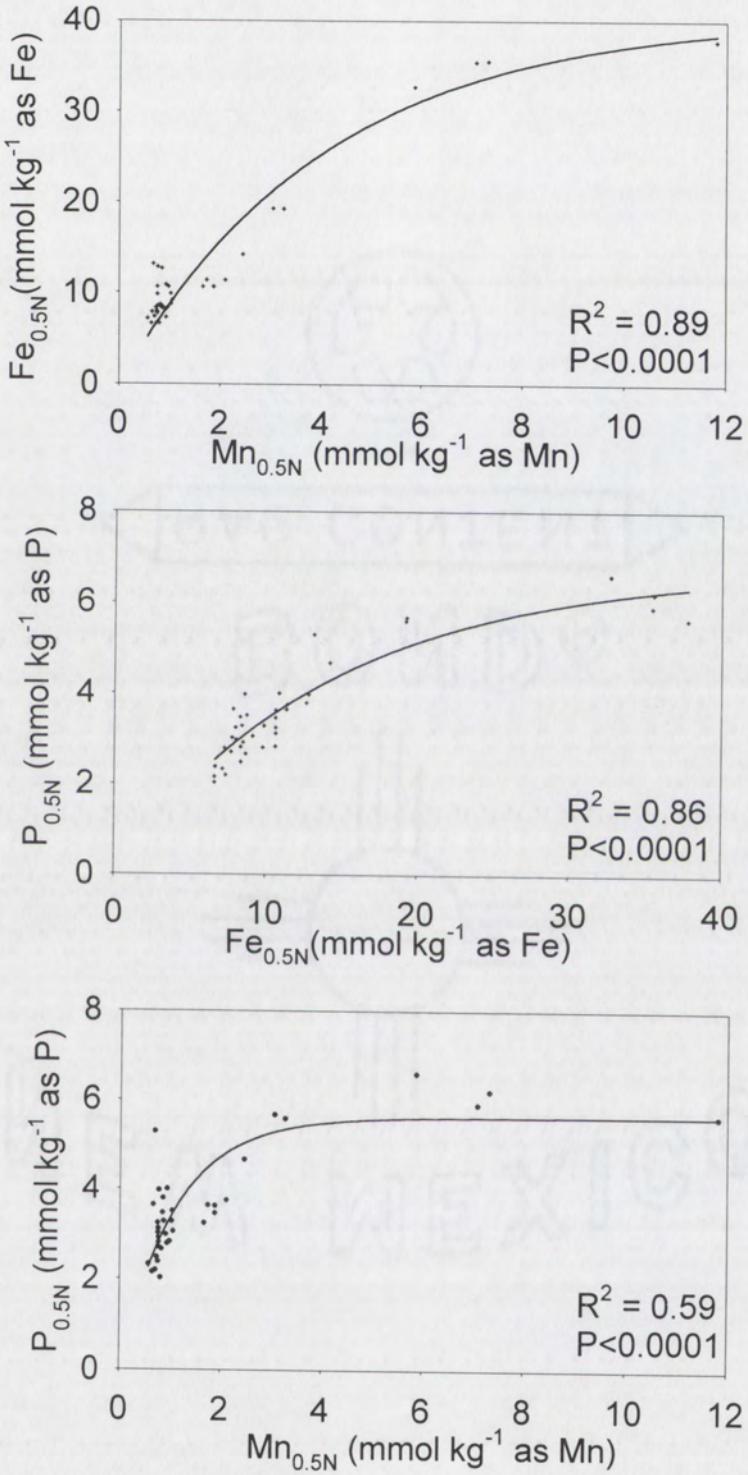

Figure 64. Correlations between 0.5N HCl-extractable Fe, Mn, and P.

The most easily formed crystalline Fe sulfide is mackinawite ($Fe_{1+x}S$, $x \approx 0.05$), an early diagenetic phase that forms black, fine-grained "slime" in reduced sediments

(Berner, 1970). However, crystalline forms are usually preceded by amorphous FeS (Davison, 1991; Matsunaga et al., 1991). Because mackinawite cannot form abiotically, its presence is considered evidence of bacterial sulfate reduction (Little et al., 1997). Under these conditions, amorphous FeS ages to mackinawite within days (Mullet et al., 2002). The most common long-lived Fe sulfide is pyrite, FeS_2, formed by the reaction of Fe monosulfides with elemental sulfur (Berner, 1970; Little et al., 1997). This process occurs most prolifically in fine-grained marine sediments. Most, if not all, of the Fe sulfides observed in this study are probably amorphous or crystalline monosulfides. These minerals are short-lived unless subjected to continuing sulfate reduction, in which case they may mature to mackinawite, greigite, smythite, and eventually pyrrhotite (Little et al., 1997). In the presence of small amounts of oxygen, however, mackinawite and other iron(II) monosulfides may rapidly undergo solid-phase oxidation to become iron(III) oxyhydroxides (Mullet et al., 2002). Thus, in an opposing-gradient system of molecular oxygen and hydrogen sulfide, iron may rapidly cycle back and forth between ferrous and ferric species, an idea described for nonsulfidic systems by Sobolev and Roden (2001) and Roden et al. (in press).

A possibly crystalline Fe sulfide (Figure 35) appears tetragonal. If so, this mineral may be mackinawaite. Other iron sulfides look cubic (Figure 37). If so, these minerals could be greigite (Fe_3S_4), another early-stage sulfide, or possibly pyrite. Additionally, a rare, metastable, cubic form of FeS has been described in laboratory experiments that precedes mackinawite but has the same X-ray diffraction pattern as pyrite (Pósfai et al., 1998). The geochemical mechanisms of pyrite formation (Berner, 1970) are not evident in the MRG sediments, nor are accumulations of stable

sulfides observed in the field. Probably, all of the iron(II) sulfides observed in the study are monosulfides that exist on a seasonal time scale.

Seasonal iron variability

Along a DMLS profile, the variation between each cell was used to compute percent relative standard deviation (%RSD), here an expression of vertical spatial variability at a given time:

$$\%RSD = 100 \times \frac{\text{std. deviation}}{\text{mean}} \qquad (1)$$

In summer and fall 2001, dissolved Fe and Mn experienced opposite trends in spatial variability. In spring 2002, Fe_T and Mn_T experienced similar trends in spatial variability (Figure 65). These periods can be compared statistically (Table 12). Note the difference in sign of the covariance of the two populations.

Table 12. Statistical relationships between %RSD of Fe_T and Mn_T for two seasons during the study period.

Inclusive dates	Covariance	Correlation	R^2	*P*
5/5/01-12/13/01	-51.3	-0.85	0.71	0.004
12/13/01-4/16/02	471.7	0.82	0.67	0.092

Increased spatial variability in Mn_T or Fe_T should be caused by increased solid phase interactions (precipitation / dissolution of a heterogeneous distribution of labile minerals) or times of hydrologic transition (rising or falling limbs of the hydrograph). Times that Fe_T and Mn_T exhibit opposing amounts of spatial variability may indicate that iron(II) was insoluble due to the presence of HS^-, and thus behaving differently than manganese(II). Alternatively, it may indicate that that Eh was high enough to oxidize Fe^{2+} but not high enough to oxidize Mn^{2+}. At times that Fe_T and Mn_T exhibit similar spatial variability, Fe^{2+} and Mn^{2+} are similarly soluble. None of these trends are apparent when absolute Fe_T and Mn_T concentrations are compared to the hydrograph, due to the

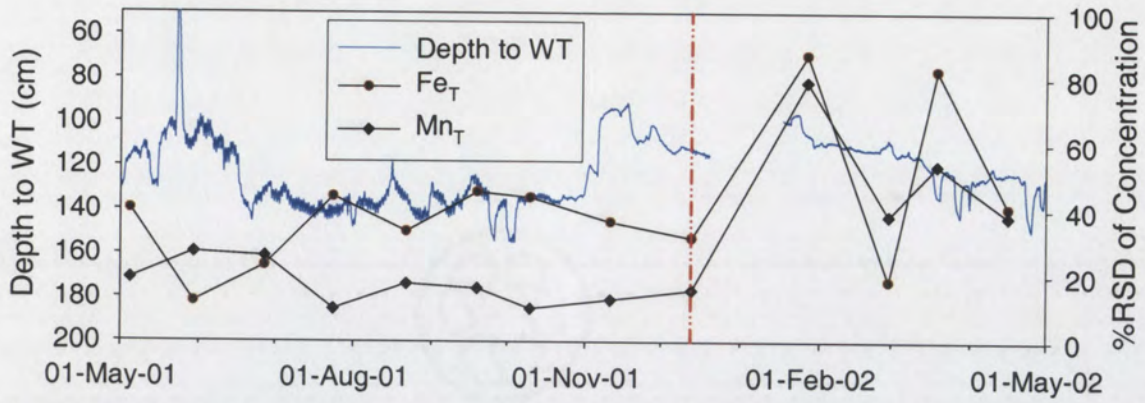

Figure 65. Spatial variability of Fe_T and Mn_T on each sampling date. %RSD = percent relative standard deviation. Each point represents a DMLS sampling trip, except 27 Jan 2002, which is from conventional wells. Water table elevations provided by J.R. Thibault (unpub. data).

"buffering" effect of heterogeneous reaction kinetics controlling concentrations. Some authors (Matsunaga et al., 1991; Bourg and Bertin, 1994) have suggested that seasonal temperature variability can increase overall biological activity and drive metal mobility, but metal concentrations in this study do not appear to be related to temperature.

Thermodynamic modeling of heterogeneous reactions

Comparing observed chemistry with published mineral solubility can provide valuable information on plausible phases in groundwater systems. Demonstrating supersaturation and actually observing the mineral are mutually reinforcing lines of evidence in geochemical studies (Davison, 1991). PHREEQC calculates the saturation index (SI) for a large database of mineral phases based on equilibrium thermodynamics (Table 13). It uses equilibrium constants (K) for the relevant reactions. The equilibrium constant for mineral solubility in water is known as the solubility product (K_{sp}). For the simple mineral dissolution – precipitation reaction:

$$X \Leftrightarrow aY + bZ$$

where X is a mineral, Y and Z are ions, and a and b are their coefficients, the saturation index would be

$$SI = \log \frac{\alpha_Y{}^a \alpha_Z{}^b}{K_{sp}(of\ phase\ X)} \qquad (2)$$

The SI indicates a solution's degree of saturation with respect to a mineral. If SI = 0, the solution is saturated. Positive SI values indicate supersaturation, and negative SI values indicate undersaturation (Drever, 1997). A small positive SI (slight supersaturation) may indicate tendency to precipitate. Similarly, a small negative SI (slight undersaturation) may indicate tendency to dissolve and/or sensitivity to concentrating processes such as ET and drying.

Large differences in computed and measured pe have long been known (Lindberg and Runnels, 1984) and are attributed to redox disequilibrium, slow reactions, analytical difficulties for redox-sensitive solutes, and the difficult nature of the electron activity concept itself (Thorstenstein, 1984). Because thermodynamic models assume equilibrium, PHREEQC requires the user to designate how pe is to be calculated for speciation modeling. Attempts were made in the first several months of collection to separately analyze ferrous and total iron, then reconcile differential method recoveries and compute pe via $[Fe^{3+}] : [Fe^{2+}]$ (Barcelona et al., 1989). This approach offered many problems, including poor precision and calibration lines. If they are to be believed, the Fe^{2+} data indicate that calculated $[Fe^{3+}]$ often exceeds $[Fe^{2+}]$, an impossibility at circumneutral pH. The most likely explanation is that ferrous complexes were not recovered by the 1,10 phenanthroline method at neutral pH, but total iron determination on acidified samples by AAS included all ferrous and ferric species. Although the

Table 13. Selected minerals modeled by PHREEQC. Minerals in italics were excluded from consideration for geologic reasons (see text).

Mineral	Formula	log K_{sp} at 25°C	Database used
	Ferric minerals		
Ferrihydrite or $Fe(OH)_3$*(a)*	$Fe(OH)_3$	4.891	WATEQ4F OR PHREEQC (same values)
Lepidocrocite	FeOOH	1.371	WATEQ4F
Hematite	*Fe_2O_3*	*-4.008*	*PHREEQC*
Goethite	*FeOOH*	*-1.000*	*PHREEQC*
Magnetite	*Fe_3O_4*	*3.737*	*WATEQ4F*
	Manganic minerals		
Birnessite	MnO_2	18.091	WATEQ4F
Pyrolusite	*MnO_2*	*41.380*	*PHREEQC*
Manganite	*MnO_2*	*25.340*	*PHREEQC*
	Ferrous minerals		
FeS*(ppt)*	FeS	-3.915	PHREEQC
Mackinawite	FeS	-4.648	PHREEQC
Greigite	Fe_3S_4	-45.035	WATEQ4F
Pyrite	*FeS_2*	*-18.479*	*PHREEQC*
Vivianite	*$Fe_3(PO_4)_2 \cdot 8H_2O$*	*-36.000*	*PHREEQC*
	Carbonates		
Calcite	$CaCO_3$	-8.480	PHREEQC
Rhodochrosite	$MnCO_3$	-11.130	PHREEQC
Siderite	*$FeCO_3$*	*-10.980*	*PHREEQC*
	Salts		
Gypsum	*$CaSO_4 \cdot 2H_2O$*	*-4.580*	*PHREEQC*
Anhydrite	*$CaSO_4$*	*-4.360*	*PHREEQC*
Halite	*NaCl*	*1.582*	*PHREEQC*
Hydroxyapatite	$Ca_5(PO_4)_3OH$	-3.421	PHREEQC
Fluorite	*CaF_2*	*-10.600*	*PHREEQC*

ferrous : ferric ratio would be useful, analytical uncertainties limit its utility in quantitative geochemical modeling.

On the few occasions that nitrite was detected, pe from electrode Eh closely matches that calculated from the N(V) : N(III) redox couple. However, electrode Eh matched none of the other redox couples and can best be described as a compromise between widely divergent pe values of the O(0) : O(-II) and S(VI) : S(-II) couples. Whenever sulfide was quantified, the model was directed to use the S(VI) : S(-II) couple. This was for three reasons:

1.) When electrode Eh, N(V) : N(III), or O(0) : O(-II) were used for speciation in PHREEQC, unrealistic ferrous : ferric ratios were inevitably obtained. For example, using electrode Eh usually produced a molal $[Fe^{3+}] : [Fe^{2+}]$ of at least 100. When using the sulfur redox couple to calculate iron speciation, molal $[Fe^{3+}] : [Fe^{2+}]$ became a far more realistic $\sim 10^{-8}$, with $[Fe^{3+}]$ on the order of 10^{-13} M, a reasonable value at near-neutral pH (Drever, 1997). This discussion of ferrous : ferric ratios requires the assumption that minimal colloidal iron(III) was digested into the acidified Fe_T samples. The electrode is unresponsive to the sulfur redox couple (Jackson and Patterson, 1982; Barcelona et al., 1989), so a large difference in pe between the electrode and the S(VI) : S(-II) ratio should be expected.

2.) The redox electrode is notoriously unreliable as a quantitative tool. In order to be incorporated into the electrode value, reactions must be swift and reversible, and both solutes in the redox couple must be above trace levels ($>10^{-5}$ M), suggesting that insoluble species such as Fe^{3+} are unable to influence the electrode

value. Finally, the electrode must be free of sorbed redox-sensitive ions (Jackson and Patterson, 1982).

3.) Independent evidence confirms that sulfate reduction and Fe(II) sulfide formation are important redox processes; thus, low pe values calculated from sulfate : sulfide ratios are appropriate. In a study of shallow groundwater, Jackson and Patterson (1982) provide four criteria to prefer the sulfate : sulfide ratio over electrode Eh as the best determinant of overall redox state: a.) Loss of Fe^{2+} and SO_4^{2-} along the flowpath; b.) Only the sulfur couple produces calculated supersaturation with respect to observed iron sulfides; c.) Detection of sulfate-reducing bacteria; and d.) Scanning electron microscope (SEM) identification of iron sulfides. Our work has met three of those criteria; only sulfate-reducing bacteria have not been sought out.

Sulfide data should be regarded as minimum values due to rapid oxidation before analysis (Wersin et al., 1991).

Modeling a constant depth through time

The DMLS interval nearest 150 cm depth with a full data set was chosen for each sampling data for which sulfide data were available to compute pe. The solutions, a few tens of centimeters below the water table, are usually undersaturated with respect to ferrihydrite and lepidocrocite, although on three occasions low positive SI values were calculated with respect to lepidocrocite. The crystalline iron oxides goethite and hematite are not geologically reasonable in this environment (Matsunaga et al., 1991); their SI values are large, and are not plotted. In contrast, birnessite, the most common Mn oxyhydroxide in shallow sediments (Gilkes and McKenzie, 1988; Little et al., 1997),

has a very high negative SI. This is possibly because Mn^{2+} oxidizes at much higher Eh than Fe^{2+} at circumneutral pH (Tuhela et al., 1997).

Iron sulfide modeling indicates low positive SI for noncrystalline FeS and progressively higher SI for mackinawite and greigite, confirming that the least ordered phase is also the most thermodynamically reasonable under these conditions (Davison, 1991). Very high positive SI values for pyrite (not shown) suggest that pyrite is too insoluble to be active here; instead, Fe monosulfides are more likely (Wersin et al., 1991). No alabandite (MnS) can exist under these geological conditions (Berner, 1981a; Matsunaga et al., 1991). The most plausible sink for Mn(II), and an alternative fate for Fe(II), is as carbonates. These waters have low positive SI values for rhodochrosite ($MnCO_3$) and siderite ($FeCO_3$), although neither mineral was directly observed during the

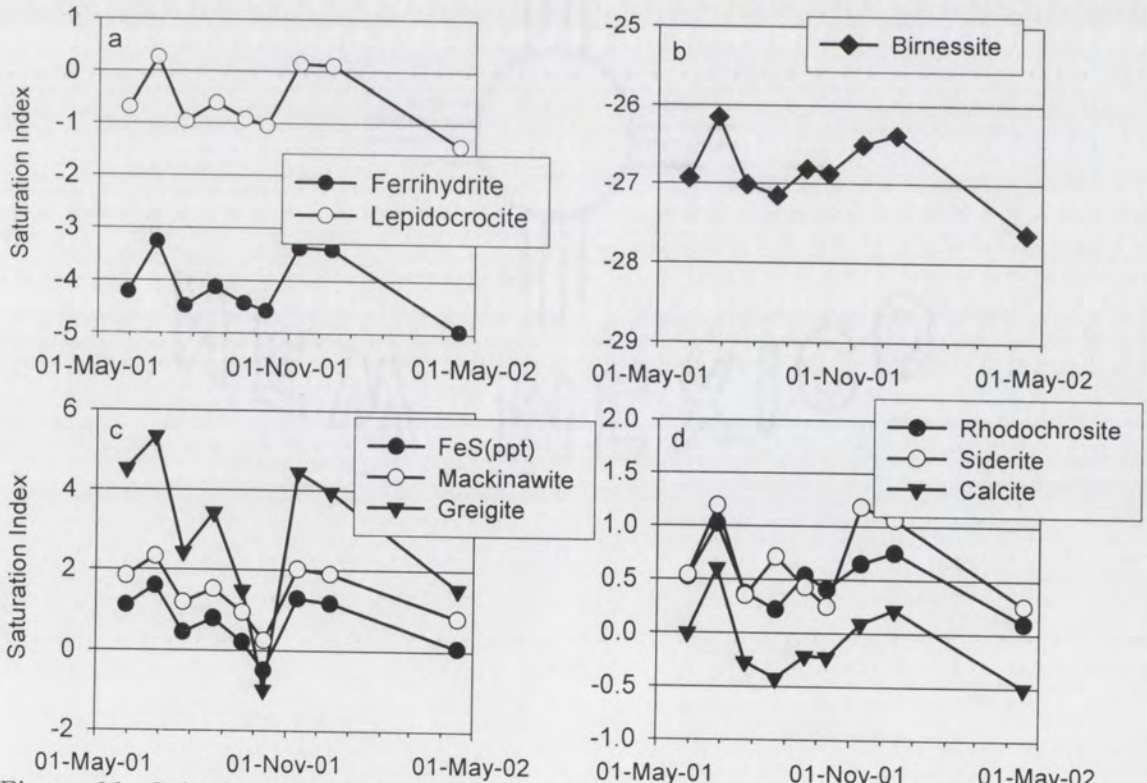

Figure 66. Calculated saturation indices near 150 cm depth for a.) Fe-oxyhydroxides; b.) Mn-oxyhydroxide; c.) Fe-sulfides; d.) reduced carbonates.

study. Siderite should only occur in methanogenic (post-sulfidic) environments because it is more soluble than Fe sulfides (Berner, 1981a), although this may not be true under all conditions (Lovley, 2000). Siderite and rhodochrosite precipitate very slowly in anoxic sediments, requiring hundreds of days to reach equilibrium. Thus, supersaturation is normal for these minerals and probably does not indicate that these minerals are precipitating in significant amounts (Jensen et al., 2002).

SI values for calcite are close to zero, suggesting that calcite can precipitate during ET or drying events, exerting an effect on alkalinity and pH. Immediately below the water table, excess Ca was often detected in water samples. Sample BLN2-091901-116-128, for which a Gran titration was performed, indicated that all parameters except Ca were consistent with the rest of the day's samples while Ca was more than two times the average value. This sample had an unresolvable charge balance error in excess of 25%. These factors indicate Ca contamination of the sample, rather than a real phenemenon; analytical error has been ruled out as a cause. Most likely, this Ca is calcite growth stimulated by evapoconcentration and drying at the water table. Having grown in the cells, this calcite would have been digested by HNO_3 addition prior to analysis. Vadose soils at Belén are somewhat calcic, containing $5.1 \pm 2.1\%$ $CaCO_3$ (N.M. Bailey, unpub. data).

Modeling depth profiles

When all of the samples along a DMLS profile are modeled in PHREEQC, it is possible to depict solubility trends with depth. SI profiles are not drastically different with depth through the study period (Figure 67-Figure 69). Lepidocrocite SI varies from slightly above to slightly below zero. On the other hand, these waters are substantially

undersaturated with respect to birnessite due to the relatively low pe throughout the study period. Most waters are slightly supersaturated with respect to amorphous FeS, making its formation throughout the study plausible. For some individual samples, both FeS and lepidocrocite are supersaturated, indicating the possible co-stability of Fe oxides and sulfides despite essentially anoxic conditions. All of the profiles show some degree of calcite supersaturation, and the warm periods (30 May and 19 September 2001) show this effect to be more pronounced near the water table. The 13 December 2001 profile shows no clear depth trend.

There is some redox stratification near the water table, where oxygen is available, resulting in a permanent but shifting oxic-anoxic interface at 20-30 cm below the water table. The PHREEQC model does not reflect this stratification because it does not incorporate the oxygen electrode data. Once in the anoxic sediments below the water table, redox-sensitive mineral solubilities are controlled primarily by distance along the flowpath, rather than distance below the water table. These two independent redox gradients, one horizontal and one vertical, create an opposing gradient system similar to the cultures described by Sobolev and Roden (2001). Oxygen diffusing from above diminishes in the 20-30 cm below the water table and meets typically sulfidic conditions occurring as a result of down-gradient TEAPs, creating an interface that hosts rapid biogeochemical cycling between iron(III) oxide-precipitating and iron(II) sulfide-precipitating conditions.

Inverse modeling

Traveling down-gradient, a parcel of water first encounters microbially-reducible Fe and Mn oxyhydroxides in the anoxic sediments. These oxides undergo reduction,

mobilizing Fe^{2+}, Mn^{2+}, phosphate, and trace metals. Sulfate reduction creates sulfide, which may release hydrogen sulfide and/or form FeS. Both of these TEAPs generate carbon dioxide, a microbial respiration product. Thus, iron and sulfur have two possible non-aqueous phases and manganese has one. H_2S and CO_2 leave the system as gases when those gases exceed saturation. During transport in the growing season, evapotranspiration removes water from the aquifer, concentrating solutes (Figure 70).

Inverse modeling attempts to account for chemical evolution caused by heterogeneous reactions along a flowpath. At Belén, these chemical differences usually include increased Fe_T, Mn_T, sulfide, alkalinity, and conservative ions, as well as decreased sulfate. The model simulates heterogeneous reactions involving Fe, open-system gas behavior involving carbon dioxide and hydrogen sulfide, and evapotranspiration (Parkhurst and Appelo, 1999). To simplify the model and reduce the number of non-unique solutions, only one Fe oxide, Fe sulfide, and Mn oxide phase were included as possibilities. ET was simulated by creating an outflux of water vapor that leaves remaining salts concentrated. PHREEQC was directed to consider amorphous Fe(III) oxyhydroxide and Fe(II) sulfide, birnessite, calcite, CO_2 *(g)*, H_2S *(g)*, and H_2O *(g)* as possible phases. The redox minerals were free to precipitate or dissolve, and calcite was constrained to precipitate. CO_2 and H_2S were constrained to leave the system. Before 11 November 2001, H_2O was constrained to leave, and on the later two dates H_2O was unconstrained because ET is minimal during that period. Because salts such as gypsum and halite remained strongly undersaturated throughout the study, the conservative ions (except for Ca^{2+}) were forced to remain in solution. This means that

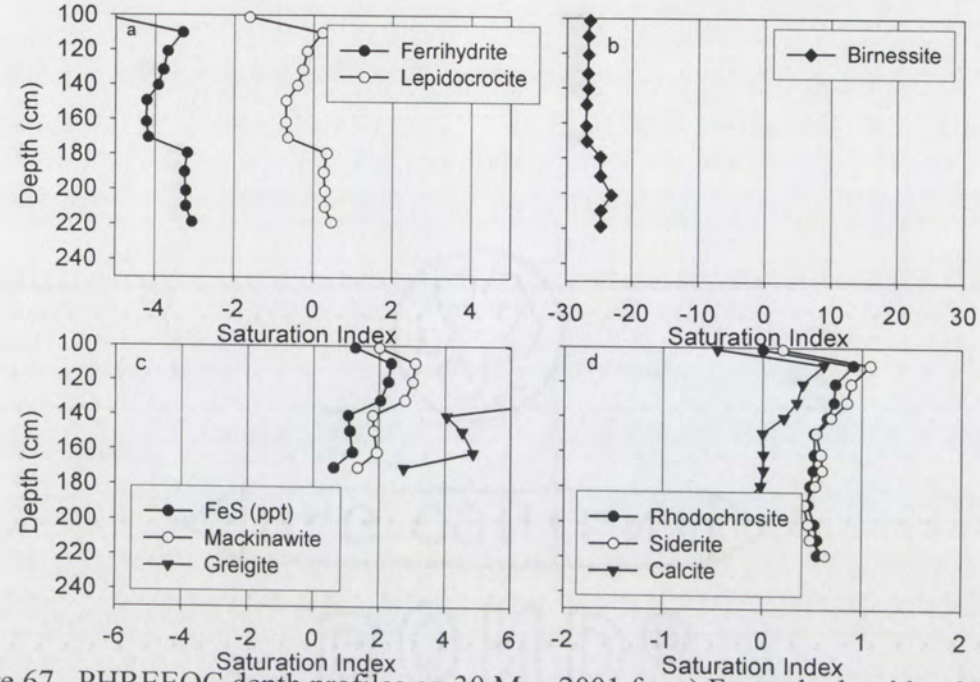

Figure 67. PHREEQC depth profiles on 30 May 2001 for a) Fe-oxyhydroxides, b) Mn-oxyhydroxide, c) Fe-sulfides, and d) reduced carbonates. The increase in SI of Fe-oxides at 180 cm depth is artificial because no sulfide was quantified in these lower samples. A very low sulfide concentration (10^{-10} mg L^{-1}) was used to calculate pe.

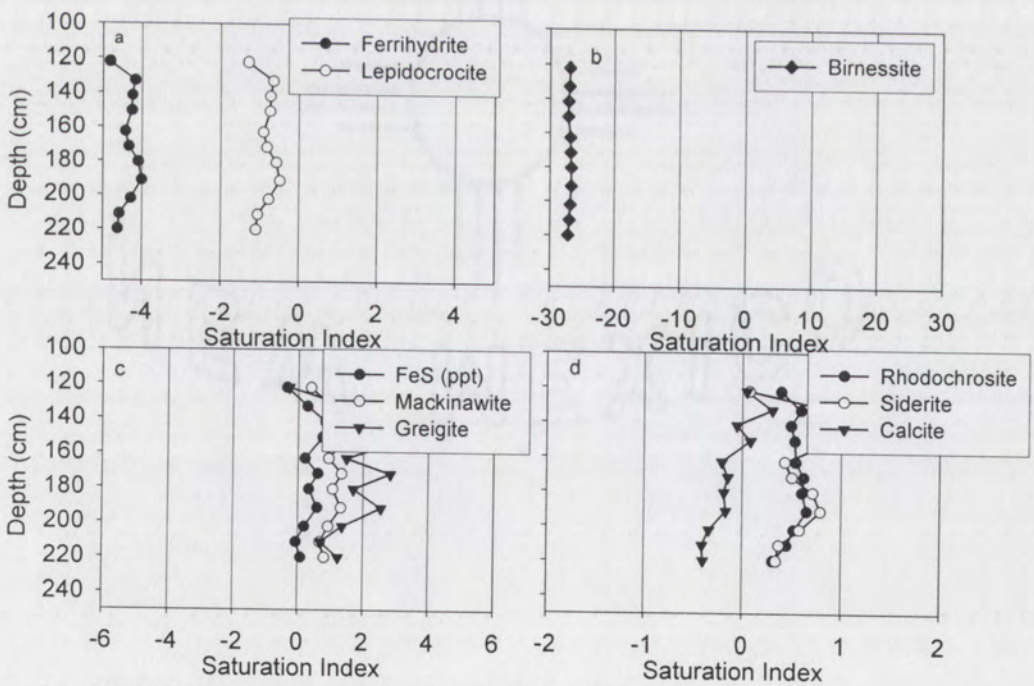

Figure 68. PHREEQC depth profiles for 19 Sep 2001.

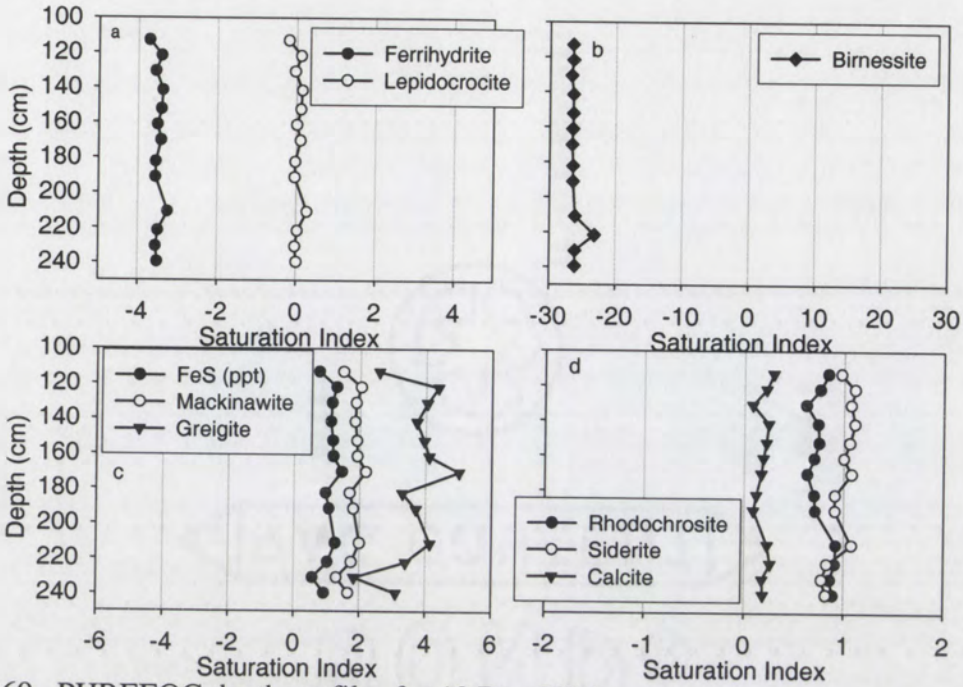

Figure 69. PHREEQC depth profiles for 13 Dec 2001.

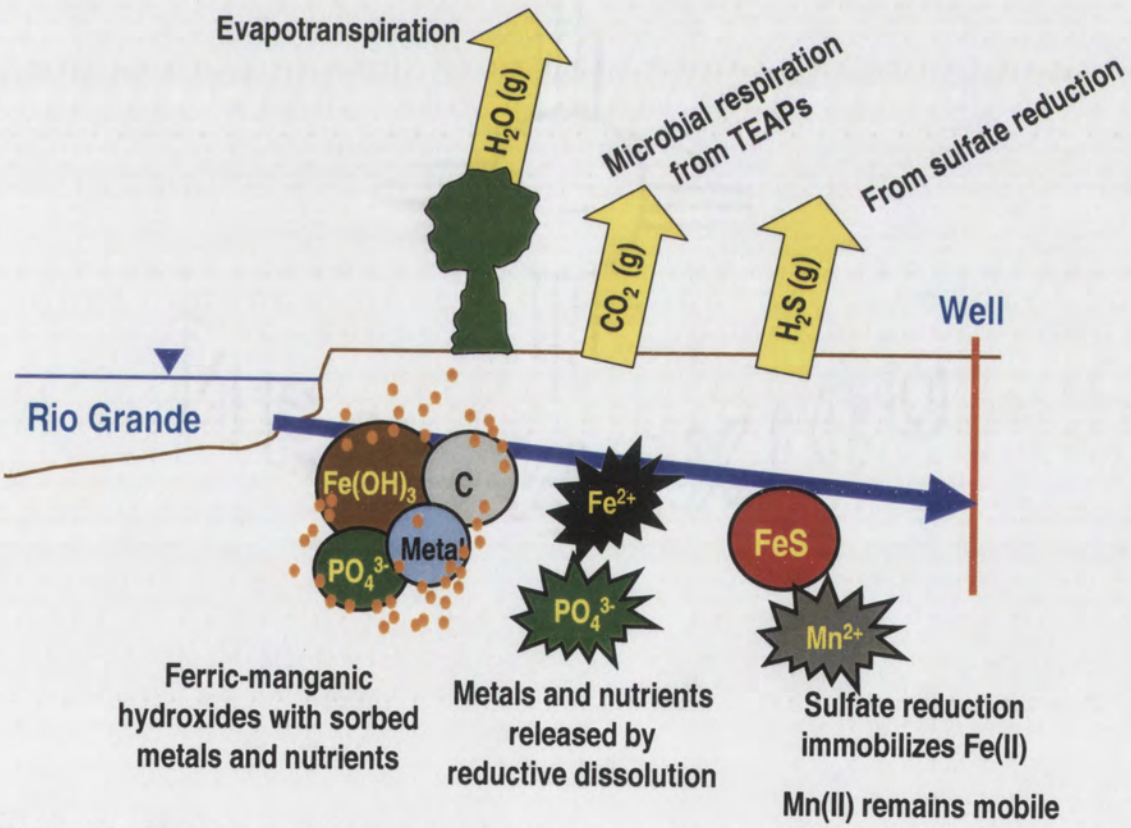

Figure 70. Heterogeneous reactions affecting water chemistry between Rio Grande and well samples.

chloride was treated conservatively and that reduction was the only possible fate for sulfate. Inverse modeling could not be performed on 2002 samples due to a lack of complete river data collection that included pH and temperature.

Another input parameter is analytical uncertainty in the water chemistry data. The smallest whole percent uncertainty was used that allowed PHREEQC to obtain a solution, usually around 10%. This uncertainty could be reduced to about 2.5% if large volume samples had been available to perform better analyses, especially for alkalinity. Using a smaller input uncertainty reduces the range of possible values in the solution, and it reduces the overall number of non-unique solutions produced by the model. In the model output, several non-unique solutions were obtained. I used the first solution in the output file, which has the lowest residuals, and is thus the most likely model. Non-unique solutions occur because there are too many unknown sinks, particularly for iron and sulfur. The other solutions usually involve unreasonably large gas fates instead of solid phases, and they are less plausible, especially in light of the abundant mineral phases observed with the SEM. Once mole transfers due to heterogeneous reactions were determined, they were used to calculate net rates at which heterogeneous redox reactions occur across the aquifer (Table 14):

$$\text{Reaction rate estimate} = \frac{\text{Mole transfer from model} \times \text{flow rate}}{\text{Flow length}} \qquad (3)$$

Manganese data are reliable because all reduced manganese can be accounted for as Mn^{2+}, which is soluble over the entire pH range seen in the study (Figure 71). On all six dates modeled, a similar Mn(IV) reduction rate is observed and is within an order of magnitude of rates for Fe(III) and S(VI). This modeling implies an irreversible transfer of manganese from buried deposits in the aquifer into the riverside drains.

Table 14. Net reduction rate estimates from inverse modeling, using minimum flow length of 125 m and average flow rate of 75 m day^{-1}.

	Electron acceptor reduction rate (μmol L^{-1} s^{-1})		
Date	Mn(IV) reduction	Fe(III) reduction	S(VI) reduction
5/30/01	1.044×10^{-4}	1.247×10^{-4}	4.169×10^{-5}
6/27/01	1.290×10^{-4}	1.893×10^{-4}	5.591×10^{-5}
7/24/01	1.042×10^{-4}	3.497×10^{-4}	6.972×10^{-5}
10/10/01	1.063×10^{-4}	7.097×10^{-5}	3.545×10^{-5}
11/11/01	9.000×10^{-5}	-2.333×10^{-3}	-2.691×10^{-4}
12/13/01	9.611×10^{-5}	2.377×10^{-4}	5.374×10^{-5}
	Organic carbon oxidation rate based on stoichiometry of Baker et al., 2000a (μmol L^{-1} s^{-1})		
Date	Mn(IV) reduction	Fe(III) reduction	S(VI) reduction
5/30/01	1.044×10^{-4}	3.116×10^{-5}	8.34×10^{-5}
6/27/01	1.290×10^{-4}	4.733×10^{-5}	1.12×10^{-4}
7/24/01	1.042×10^{-4}	8.741×10^{-5}	1.39×10^{-4}
10/10/01	1.063×10^{-4}	1.774×10^{-5}	7.09×10^{-5}
11/11/01	9.000×10^{-5}	-5.832×10^{-4}	-5.38×10^{-4}
12/13/01	9.611×10^{-5}	5.943×10^{-5}	1.07×10^{-4}

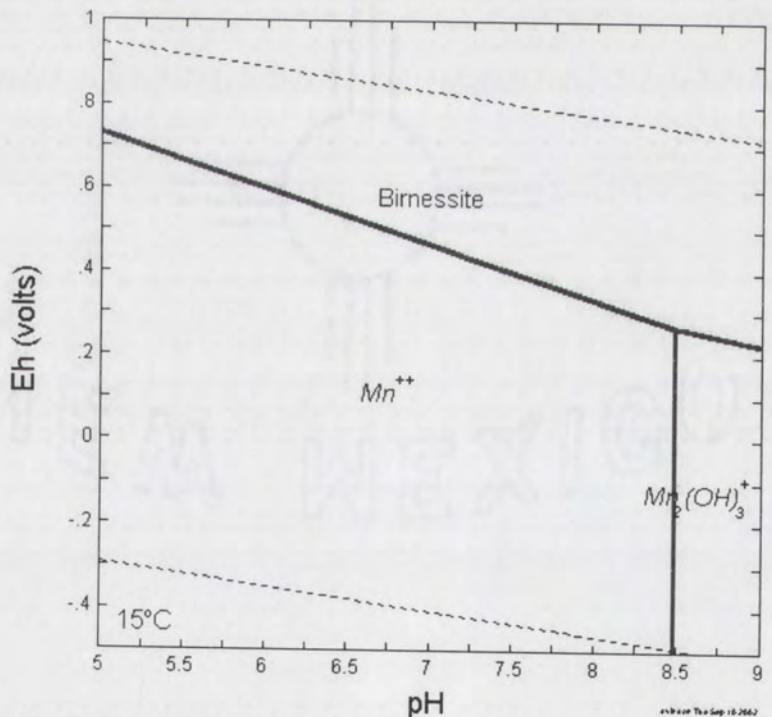

Figure 71. Eh-pH diagram for manganese redox reactions at circumneutral pH. Mn oxyhydroxides represented as birnessite. Temperature = 15°C, $[Mn_T]$ = 15 μM.

Iron data are least reliable because a solid-phase sink exists for both ferric and ferrous iron. Thus, not all iron can be accounted for with water analyses, making these

rate estimates minimum values. The ferrous – ferric boundary is influenced by both protons and electrons, so pH is as important as Eh for redox modeling of iron (Figure 72). In anoxic-sulfidic sediments, Fe(II) solubility is controlled by the availability of HS^-, which is pH-dependent (Figure 73). On five of the six dates modeled, net dissolution of Fe oxyhydroxides occured at a rate within an order of magnitude of Mn and S reduction (Table 14). The model for 11 November 2002 is anomalous, and is discussed below. Inverse modeling does not explain the visible encrustations of mixed Fe/Mn oxyhydroxides on DMLS membranes throughout the study period. Many of these oxyhydroxides form at the oxic-anoxic interface a few centimeters below the shifting water table, which the model does not consider, but other growths are too deep to be formed in this way. The sulfur redox couple produces a low estimate of redox potential; possibly, a low level of dissolved oxygen remains present at times to cause microbial Fe oxidation.

Sulfur data are reliable because all oxidized sulfur can be accounted for as sulfate. At typical iron concentrations, sulfide would appear as FeS (*s*) or as H_2S (*g*). The partition between these two species is pH-dependent and occurs at pH 7.7, a value straddled by these waters (Figure 73). On most occasions, river pH is slightly above 8, and BLN2 pH is as much as one unit lower. Thus, PHREEQC models the decline in sulfate from river to well by assigning it to iron monosulfides plus a small concentration of HS^-, or lost to the atmosphere as hydrogen sulfide gas. Estimated sulfate reduction rates are of similar orders of magnitude as manganese and iron reduction.

On five of the six dates modeled, the model depicts sulfate reduction products going to monosulfides rather than H_2S. 11 November 2001 is an unusual case because

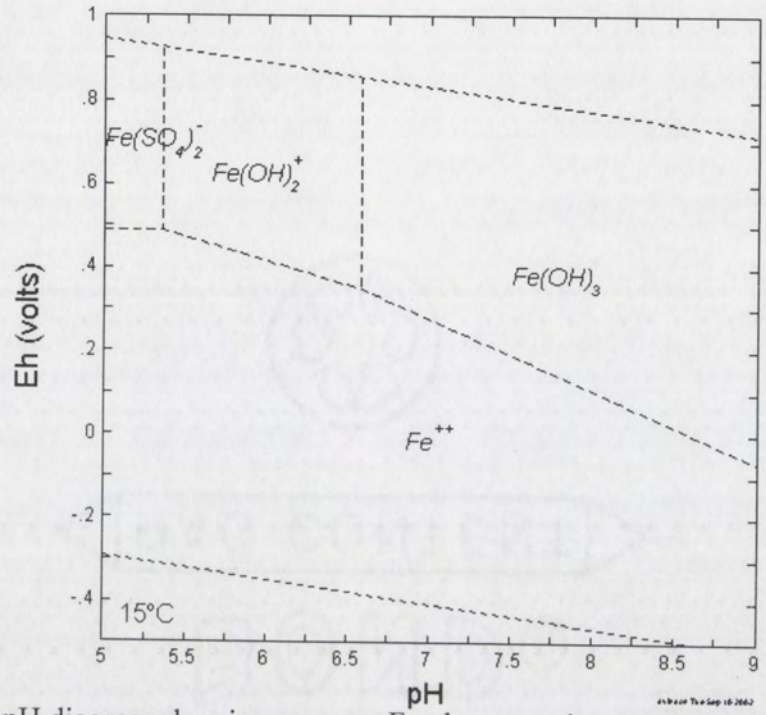

Figure 72. Eh-pH diagram showing aqueous Fe phases at circumneutral pH. Temperature = 15 °C, [Fe_T] = 25 μM.

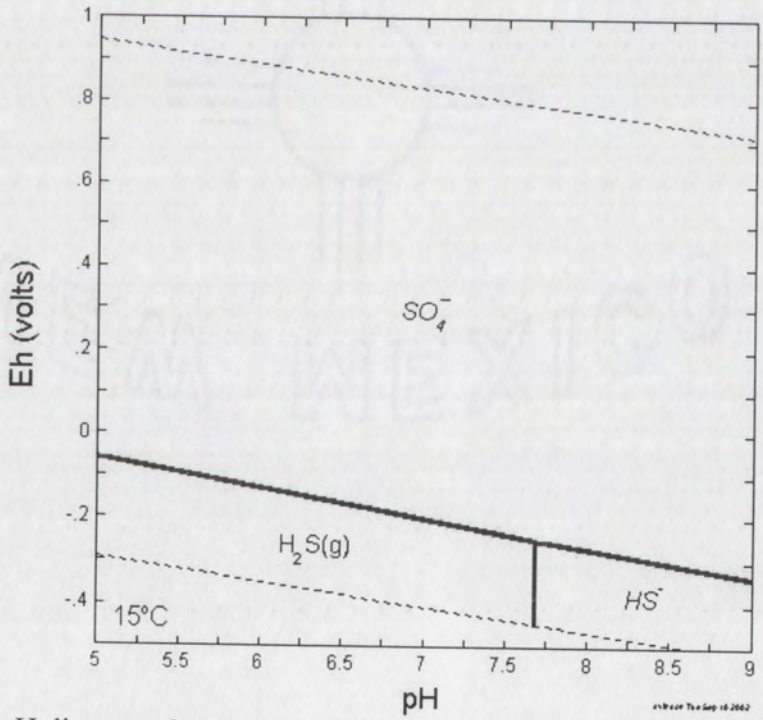

Figure 73. Eh-pH diagram showing speciation of sulfur at circumneutral pH. Temperature = 15°C, [S_T] = 500 μM.

observed river pH was 7.61, increasing to 7.71 at the well. A 10% decrease in the sulfate-to-chloride ratio indicates a modest amount of sulfate reduction. The model accounts for this by creating a small outflux of hydrogen sulfide due to the relatively low pH. The model then needs to dissolve a relatively large amount of FeS to account for the observed supersaturation with respect to that phase, which forces it to precipitate a similar amount of $Fe(OH)_3$ to remove the excess Fe. Mostly, this case points to the perils of using thermodynamic databases blindly, especially near phase boundaries.

Limitations

PHREEQC modeling suggests the importance of amorphous, nonstoichiometric oxyhydroxides and sulfides. However, these cannot be accurately modeled by published, ideal thermodynamic constants because composition, surface area, crystal structure, and metal valence vary between samples, and thus solubility varies greatly. Thermodynamic modeling does not incorporate metastable phases, which may buffer concentrations or create heterogeneous microenvironments, nor does the model consider reaction kinetics. Additionally, using pe to describe the state of every redox couple is an approximation in light of the wide range in pe values between redox couples (Lindberg and Runnels, 1984). The S(VI) : S (-II) couple is best, but it relies on difficult, low-level sulfide analyses. Although this problem applies more to iron because it is controlled by sulfide concentrations, SI values near zero should be interpreted qualitatively as near saturation.

The role of microbes

The sequence of TEAPs is believed to represent microbial competition in sediments. Each process is driven by the metabolic demands of heterotrophic bacteria competing for external energy sources; thus, competitive exclusion dictates that redox

zones will form, although zones will often overlap. In anoxic sediments, heterotrophs utilize alternative electron acceptors to oxidize electron donors such as low-molecular-weight organic acids (Chapelle, 2001). Electron donors are typically limiting, so bacteria compete for these compounds based on the Gibbs free energy of inorganic oxidants (electron acceptors) they are able to use. Thus, the documented TEAP sequence is good evidence of active microbial populations in the sediments. Although TEAPs occur in the expected, thermodynamic order, metal oxide reduction does not proceed to completion, as thermodynamics alone would indicate. Of the many possible amorphous and crystalline forms, some are more microbially reducible than others, probably due to differences in surface area. Microbial competitive relationships may dictate which metal oxides are reduced before sulfate reduction becomes dominant, at which point iron reducers are excluded (Lovley, 2000). Crystalline iron(III) oxides survive deep burial over geologic time because they have aged to stable phases such as hematite, which are unlikely to serve as microbial electron acceptors. In the shallow MRG sediments, however, labile iron and manganese oxidize and reduce on a short, probably seasonal time scale as microbes compete aggressively under shifting redox conditions.

Patterns observed in Fe oxyhydroxides also suggest a strong microbial role. In particular, the morphologies seen on many of the > 0.2 μm membranes are consistent with biological colonization. These amorphous, "biological-looking" Fe oxyhydroxides contain a disorderly mix of Fe, Mn, and P not consistent with pure, abiotic crystals. The helical stalks seen on many filters are strongly diagnostic of the Fe-oxidizer *Gallionella* spp., which is a strictly microaerophilic chemolithoautotroph (Tuhela et al., 1997; Emerson, 2000; Hanert, 2002). The presence of *Gallionella* is good evidence for

iron(II) oxidation at low O_2 concentrations (below 1 mg L^{-1}) because this organism specifically inhabits interfaces with low levels of oxygen. In general, low-oxygen conditions favor microbial Fe(II) oxidation, rather than abiotic oxidation (Emerson et al., 1999). Although suggestive morphologies alone are not sufficient evidence of biogenesis (Barton et al., 2001), geochemical evidence for microbial mineral processing is strong. Additionally, elevated oxalate-extractable Fe near the water table suggests increased microbial activity at the oxic-anoxic interface, since Fe_{ox} is a reasonable proxy for microbially-reducible ferrihydrite (Lovley, 1987).

Additional information about the role of bacteria comes from pore-size constraints in the experimental design. In general, the 0.2 μm filter precluded widespread Fe oxyhydroxide growth, an observation consistent with published findings on the pore-size constraints of bacteria in sedimentary rocks (Fredrickson et al., 1997). The outsides of these 0.2 μm filters accumulated profuse authigenic metal oxides. The interpreted nucleation sites of these oxides were associated with transported colloidal silicates a few microns in diameter. In the likely case that bacteria are agents in mineral precipitation, they are transported on this detrital material, thus making the effective pore size larger than 0.2 μm when their associated particles are considered. This is consistent with observations that most groundwater bacteria are not planktonic, but are attached to silt and clay particles (Harvey et al., 1984; Holm et al., 1992). The drastic difference in mineralization between the insides and outsides of filters was seen on 0.2 μm membranes, but not on 10 μm membranes. Thus, authigenic minerals grown *in situ* were associated with particles in the 0.2-10 μm size range that probably included bacteria. The documented groundwater chemistry provides geochemical evidence that these minerals

are probably the result of microbial competitive relationships in this oxic to sulfidic aquifer. The best evidence for specific bacterial identities or functions would be from culturing or molecular microbial analysis (Barton et al., 2001), but both techniques are beyond the scope of this work.

Conclusions

The Middle Rio Grande in central New Mexico has undergone hydrologic impairment with severe consequences for biogeochemistry. Although surface ecological effects are better-documented, biogeochemical processes in the (intermittently) saturated zone have not been thoroughly investigated until recently. For shallow aquifer biogeochemistry, the most severe human modifications have been the riverside drains built in the 1930s. These ditches have shortened groundwater flow lengths dramatically and increased hydraulic gradient (and possibly solute fluxes through the sediments) by up to an order of magnitude. This, combined with the almost total absence of flood sedimentation for sixty years, has altered drastically the organic carbon budget of the hyporheic zone. Thus, this study has examined biogeochemical processing of organic carbon, labile metals, and nutrients in a highly impaired hydrologic and geochemical environment.

Redox state along these "new" flowpaths is determined primarily by distance along flowpaths from the river to the riverside drains. Secondary effects include proximity to the water table, recent changes in river stage, and irrigation diversions. Terminal electron-accepting processes occur down-flow through the bosque aquifer in the thermodynamically-expected order: oxygen reduction, denitrification, Mn oxide reduction, Fe oxide reduction, and sulfate reduction. These processes oxidize much more organic carbon than is present in river water, indicating the importance of buried particulate organic carbon in the aquifer sediments. Redox processes are probably driven by microbial competition. Fine-grained, non-crystalline, microbially-reducible metal oxyhydroxides and iron(II) sulfides are the prevalent seasonal mineral phases, especially

in the zone of intermittent saturation. Amorphous Fe, Mn, and P are spatially related and frequently occur in mixed, disordered oxyhydroxide solids. These metal oxyhydroxides form under generally low oxygen concentrations, probably as a product of the respiration of microaerophilic, lithoautotrophic bacteria.

Mn^{2+} is more mobile than Fe^{2+} due to widespread sulfate reduction providing a seasonal iron sink as ferrous monosulfides. Manganese is carried to the riverside drains under reduced conditions. The spatial relationship between Fe^{2+} and Mn^{2+} was different in summer/fall 2001 than in winter/spring 2002, possibly due to higher water tables and/or differing degrees of oxide or sulfide formation. Iron and manganese behavior may control trace metals of potential interest, such as arsenic, which interacts with Fe/Mn oxides through adsorption processes (Driehaus et al., 1995; Drever, 1997; Breit, 2001), and is a water quality concern in the Albuquerque Basin.

This research has implications for river restoration by illustrating the connections between hydrology and biogeochemistry. For example, any reintroduction of flooding would affect the way organic carbon travels through the shallow aquifer. Modifications to the drainage system would alter water tables and nutrient fluxes. Hydrologic modifications made in the name of restoration should be monitored for subsurface physical and chemical changes in addition to desired biological and geomorphic effects. This could best be done at a surveyed well field, containing a closely spaced grid of wells, at which seasonal changes in chemistry, depth to water, and hydraulic gradient could be monitored throughout the year.

List of Appendices

Appendix I: Tracer data

Cell ID	Top (cm)	Btm (cm)	Br^- remaining (mg L^{-1})			q (cm s^{-1})			q (m day^{-1})			q_{avg} (m day^{-1})	st
			0.85 h	1.783 h	2.633 h	0.85 h	1.783 h	2.633 h	0.85 h	1.783 h	2.633 h		
1	*105.4*	*114.3*	*76.096*	*76.344*	*76.488*	*0.01*	*0.00*	*0.00*	*5.32*	*1.70*	*0.83*	*2.62*	*2*
2	*114.3*	*123.2*	*76.409*	*76.443*	*76.744*	*0.00*	*0.00*	*0.00*	*3.12*	*1.37*	*0.25*	*1.58*	*1*
3	*123.2*	*132.1*	*69.022*	*68.740*	*50.479*	*0.07*	*0.03*	*0.08*	*57.77*	*28.59*	*72.95*	*53.10*	*2*
4	132.1	144.8	65.789	58.238	51.271	0.10	0.08	0.08	83.56	71.07	70.25	74.96	7
5	144.8	153.7	65.130	58.414	46.714	0.10	0.08	0.10	88.97	70.30	86.41	81.89	1
6	153.7	162.6	65.292	57.374	50.533	0.10	0.09	0.08	87.64	74.90	72.77	78.44	8
7	162.6	171.5	65.736	55.375	49.964	0.10	0.10	0.09	83.99	83.99	74.73	80.91	5
8	174.8	183.7	67.484	61.493	46.228	0.08	0.07	0.10	69.89	57.13	88.23	71.75	1
9	183.7	192.6	67.298	61.477	47.759	0.08	0.07	0.10	71.37	57.20	82.57	70.38	1
10	192.6	201.5	67.070	59.901	49.302	0.08	0.07	0.09	73.19	63.86	77.05	71.37	6
11	201.5	214.2	65.212	59.700	49.070	0.10	0.07	0.09	88.30	64.72	77.87	76.96	1
12	214.2	223.0	LOST	59.807	52.532	LOST	0.07	0.08	LOST	64.26	66.03	65.14	N
13	223.0	231.9	64.053	58.576	53.380	0.11	0.08	0.07	97.94	69.59	63.25	76.93	1
14	231.9	240.8	67.804	56.100	52.510	0.08	0.09	0.08	67.34	80.66	66.10	71.37	8

Note: Cells, 1 and 2 above water table; cell 3 partially above water table. All (black rows) wer
excluded from analysis.
Blank values

Appendix II: Particle size distribution data for well BLN9

Depth (cm)	% gravel	% sand	% silt	% clay
15-23	0.41	7.82	48.03	43.74
23-41	0.47	6.59	64.80	28.14
41-51	0.00	12.20	64.50	23.30
51-61	0.00	39.55	48.88	11.57
61-71	0.00	69.05	23.35	7.60
71-81	0.00	92.00	5.72	2.28
81-91	0.00	90.65	7.07	2.28
91-102	0.00	91.10	6.69	2.21
102-112	0.07	93.36	4.52	2.05
112-122	0.18	92.83	5.38	1.61
122-132	0.03	93.72	5.00	1.25
132-142	0.01	95.94	2.80	1.25
142-152	0.09	96.94	2.11	0.86
152-163	0.00	94.80	4.58	0.62
163-168	0.00	93.70	5.92	0.38

Particle size data for BLN2 are presented in Block (2002).

Appendix III: Down-hole temperature and dissolved oxygen data for BLN2

Date	Depth below surface (cm)	Dissolved oxygen (mg L^{-1})	Temperature (°C)
5/30/01	107	1.11	14.3
5/30/01	117	0.91	14.3
5/30/01	127	0.77	13.2
5/30/01	137	0.61	12.7
5/30/01	147	0.55	12.3
5/30/01	157	0.37	11.8
5/30/01	167	0.35	11.8
5/30/01	177	0.27	11.4
5/30/01	187	0.28	11.4
5/30/01	197	0.31	11.4
5/30/01	207	0.27	11.2
5/30/01	217	0.26	11.1
5/30/01	227	0.28	11.0
5/30/01	237	0.25	10.9
5/30/01	247	0.24	10.9
6/27/01	127	0.60	15.7
6/27/01	137	0.26	14.9
6/27/01	147	0.22	14.2
6/27/01	157	0.21	13.7
6/27/01	167	0.15	13.5
6/27/01	177	0.14	13.2
6/27/01	187	0.12	13.0
6/27/01	197	0.13	12.8
6/27/01	207	0.15	12.7
6/27/01	217	0.14	12.5
6/27/01	227	0.14	12.4
6/27/01	237	0.14	12.3
6/27/01	247	0.10	12.2
6/27/01	257	0.11	12.1
6/27/01	267	0.14	12.1
6/27/01	277	0.10	12.1
6/27/01	287	0.11	12.0
7/24/01	136	0.62	16.3
7/24/01	146	0.35	15.7
7/24/01	156	0.23	15.2
7/24/01	166	0.17	15.0
7/24/01	176	0.16	14.8
7/24/01	186	0.16	14.6
7/24/01	196	0.13	14.5
7/24/01	206	0.11	14.3
7/24/01	216	0.12	14.2
7/24/01	226	0.13	14.1
7/24/01	236	0.14	13.9
7/24/01	246	0.15	13.8
7/24/01	256	0.10	13.7
7/24/01	266	0.11	13.7
7/24/01	276	0.14	13.6

Appendix III (continued)

Date	Depth below surface (cm)	Dissolved oxygen (mg L^{-1})	Temperature (°C)
7/24/01	286	0.15	13.6
7/24/01	296	0.12	13.5
7/24/01	306	0.12	13.5
7/24/01	316	0.11	13.4
8/22/01	127	4.61	18.2
8/22/01	137	0.58	17.6
8/22/01	147	0.37	17.2
8/22/01	157	0.25	17.0
8/22/01	167	0.20	16.8
8/22/01	177	0.16	16.6
8/22/01	187	0.17	16.4
8/22/01	197	0.18	16.1
8/22/01	207	0.17	15.9
8/22/01	217	0.13	15.7
8/22/01	227	0.14	15.5
8/22/01	237	0.15	15.4
8/22/01	247	0.12	15.3
8/22/01	257	0.12	15.3
9/19/01	120	1.18	18.2
9/19/01	130	1.20	17.6
9/19/01	140	0.97	17.2
9/19/01	150	0.95	17.0
9/19/01	160	0.80	16.8
9/19/01	170	0.83	16.6
9/19/01	180	0.74	16.4
9/19/01	190	0.79	16.1
9/19/01	200	0.76	15.9
9/19/01	210	0.75	15.7
9/19/01	220	0.76	15.5
9/19/01	230	0.79	15.4
9/19/01	240	0.74	15.3
9/19/01	250	0.79	15.3
10/10/01	126	1.48	17.7
10/10/01	136	1.25	17.3
10/10/01	146	0.97	17.0
10/10/01	156	0.81	16.8
10/10/01	166	0.79	16.7
10/10/01	176	0.69	16.7
10/10/01	186	0.67	16.7
10/10/01	196	0.63	16.7
10/10/01	206	0.64	16.7
10/10/01	216	0.53	16.6
10/10/01	226	0.54	16.6
11/11/01	89	0.51	16.3
11/11/01	96	0.30	16.3
11/11/01	106	0.22	16.3
11/11/01	116	0.18	16.3

Appendix III (concluded)

Date	Depth below surface (cm)	Dissolved oxygen (mg L^{-1})	Temperature (°C)
11/11/01	126	0.19	16.3
11/11/01	136	0.16	16.4
11/11/01	146	0.14	16.4
11/11/01	156	0.15	16.4
11/11/01	166	0.14	16.4
11/11/01	176	0.14	16.5
11/11/01	186	0.13	16.5
11/11/01	196	0.13	16.5
11/11/01	206	0.14	16.5
11/11/01	216	0.14	16.5
11/11/01	226	0.13	16.5
11/11/01	236	0.13	16.5
11/11/01	246	0.13	16.6
11/11/01	256	0.13	16.6
12/13/01	105	0.70	13.6
12/13/01	115	0.39	13.8
12/13/01	125	0.28	13.9
12/13/01	135	0.32	14.0
12/13/01	145	0.36	14.1
12/13/01	155	0.33	14.3
12/13/01	165	0.33	14.4
12/13/01	175	0.34	14.6
12/13/01	185	0.24	14.7
12/13/01	195	0.23	14.8
12/13/01	205	0.26	15.0
12/13/01	215	0.24	15.1
12/13/01	225	0.25	15.1
4/16/02	141	0.65	15.7
4/16/02	151	0.44	14.5
4/16/02	161	0.26	13.5
4/16/02	171	0.19	12.9
4/16/02	181	0.18	12.5
4/16/02	191	0.16	12.2
4/16/02	201	0.16	12.0
4/16/02	211	0.15	11.9
4/16/02	221	0.14	11.9
4/16/02	231	0.15	11.8
4/16/02	241	0.17	11.7
4/16/02	251	0.17	11.7
4/16/02	261	0.15	11.6
4/16/02	271	0.15	11.6
4/16/02	281	0.14	11.6
4/16/02	291	0.15	11.6

Appendix IV: DMLS water chemistry data

Date (MMDDYY)	Depth below surface (cm)	Ca^{2+}	Fe_T	Mg^{2+}	Mn_T	K^+	Na^+	F^-	Cl^-	NO_2^-	Br^-	NO_3^-	PO_4^{3-}	SO_4^{2-}	$S^{2-}{}_T$	$C_2H_3O_4^-$	$C_2O_4^{2-}$	HCO_3^-	CO_3^{2-}	pH	Eh (mV)	Alk (meq/kg as $CaCO_3$)	Charge balance error	Recalculated HCO_3^-
053001	88-97	74	1.50	12.0	0.80	12.0	57								0.82			333	0.06	6.78	427	5.45	NA	333
	97-106	68	2.22	11.5	0.72	10.5	54	0.47	30.51	0.18	0.10	0.59	0.44	95.68	1.01			212	0.23			3.49	5.22	231
	106-115	67	2.09	11.7	0.73	10.5	54	0.40	30.26	ND	0.09	0.34	0.45	95.29	0.90					8.10	142		NA	230
	115-127	65	1.82	11.2	0.67	10.0	55	0.40	29.98	ND	0.08	0.18	0.33	94.55	1.29					7.90	119		NA	225
	127-136	68	1.82	11.6	0.75	9.5	59	0.47	30.87	0.28	0.07	0.57	0.33	96.82	0.80					7.81	145		NA	240
	136-145	67	1.48	12.1	0.80	9.3	58	0.44	31.45	ND	0.07	0.10	0.23	98.26	0.10					7.70	162		NA	234
	145-154	68	1.68	10.9	0.89	8.9	59	0.44	32.43	0.21	0.09	0.13	0.24	100.66	0.16					7.52	144		NA	229
	157-166	72	1.95	11.6	0.93	8.9	63	0.44	33.73	0.16	0.07	0.20	0.12	103.76	0.19					7.49	155		NA	248
	166-175	74	2.03	12.5	0.93	10.4	72	0.41	37.25	ND	0.08	0.06	0.25	118.30	0.05					7.47	154		NA	259
	175-184	73	1.85	11.7	0.91	6.5	63	0.44	32.21	ND	0.08	0.11	0.08	95.17	ND					7.44	159		NA	262
	184-197	67	1.89	10.9	1.14	4.6	49	0.50	29.14	0.10	0.07	0.05	0.10	90.44	ND			224	0.09	7.38	155	3.67	1.66	214
	197-206	63	2.03	11.0	1.27	4.6	47	0.46	28.57	0.27	0.09	0.13	0.09	90.37	ND					7.34	165		NA	200
	206-214	64	2.23	10.8	1.42	4.5	47	0.45	28.30	0.12	0.07	0.01	0.11	91.06	ND					7.36	160		NA	202
	214-223	64	1.87	10.8	1.45	4.7	46	0.44	29.40	ND	0.09	0.10	0.19	89.06	ND			196	0.09	7.36	165	3.21	3.21	198
062701	92-100	88	0.56	11.4	0.01	7.0	49								ND					7.5	484		NA	
	100-109	71	6.71	10.5	0.03	5.0	46													7.8	381		NA	
	109-118	88	1.43	10.6	0.01	6.0	45								ND					7.5	381		NA	
	118-131	37	2.26	10.1	0.65	6.8	44		30.02	ND	0.09	0.10	0.18	78.41	0.03	ND	ND	236	0.17	7.9	94	3.87	-13.17	166
	131-140	66	2.31	10.2	0.93	4.3	46		31.45	ND	0.09	0.10	0.15	76.33	0.07	ND	ND			7.9	112		NA	264
	140-149	66	3.00	10.5	1.02	4.7	47		32.28	ND	0.08	0.09	0.17	76.99	0.04	ND	ND			7.9	95		NA	268
	149-158	70	2.18	10.4	1.02	4.0	47		34.26	ND	0.09	0.11	0.11	77.97	0.12	ND	ND			8.0	102		NA	273
	161-170	65	2.27	10.6	1.06	4.0	49											236	0.12	8.2	99	3.88	NA	
	170-179	69	1.89	10.2	1.26	4.0	54		37.66	ND	0.07	0.08	0.08	87.37	0.04	ND	ND			7.9	106		NA	271
	179-188	72	2.23	11.1	1.39	15.0	58		39.74	ND	0.08	0.06	0.12	91.87	0.03	ND	ND			7.9	101		NA	307
	188-200	70	3.82	11.4	1.66	4.7	56		41.11	ND	0.07	0.05	0.08	93.34	0.03	ND	ND	236	0.08	8.0	104	3.87	1.48	279
	200-209	69	2.95	11.3	1.29	4.0	56		35.26	ND	0.06	0.09	0.09	83.59	0.04	ND	ND			7.9	106		NA	294
	209-218	66	1.97	11.1	1.6	15.9	59		33.53	ND	0.10	0.14	0.14	80.89		ND	ND	238	0.09	7.9	118	3.91	1.67	316
	218-227	61	2.21	10.9	1.57	3.9	54		30.19	ND	0.07	0.06	0.18	74.54	ND	ND	ND			8.0	115		NA	279

Notes:

All concentrations in milligrams per liter.

ND indicates below instrumental detection limit.

NA indicates not applicable.

Blank cell indicates sample lost due to analytical problems or analysis not performed due to inadequate sample volume.

Appendix IV (continued)

Date (MMDDYY)	Depth below surface (cm)	Ca^{2+}	Fe_T	Mg^{2+}	Mn_T	K^+	Na^+	F^-	Cl^-	NO_2^-	Br^-	NO_3^-	PO_4^{3-}	SO_4^{2-}	$S^{2-}{}_T$	$C_2H_3O_4^-$	$C_2O_4^{2-}$	HCO_3^-	CO_3^{2-}	pH	Eh (mV)	Alk (meq/kg as $CaCO_3$)	Charge balance error	Recalculated HCO_3^-
	98-107	*7*	*0.32*	*ND*	*0.02*	*0.3*	*ND*	*0.47*	*0.62*	*ND*	*ND*	*216.35*	*0.17*	*0.45*	*ND*	*ND*	*ND*			*2.77*	*684*		*NA*	*-197*
	107-116	*5*	*0.41*	*ND*	*0.01*	*0.7*	*118*	*0.00*	*0.40*	*ND*	*ND*	*221.23*	*ND*	*0.36*	*ND*	*ND*	*ND*	*0*	*0.00*	*2.82*	*684*	*0.00*	*NA*	*73*
	116-125	*60*	*0.32*	*0.5*	*ND*	*ND*	*ND*	*0.69*	*0.53*	*ND*	*ND*	*223.31*	*0.04*	*0.44*	*ND*	*ND*	*ND*						*NA*	*-60*
072401	125-137	59	1.17	9.5	0.68	4.5	59	0.62	30.09	0.15	0.15	10.41	0.04	73.03	ND	ND	ND	202	0.05	6.39	407	3.98	4.75	192
	137-146	60	3.00	9.3	0.95	3.8	100	0.45	27.76	ND	0.11	0.41	0.20	76.24	0.03	ND	ND			6.80	445		NA	303
	146-155	61	4.10	9.9	0.98	4.2	61	0.64	31.19	ND	0.07	0.16	0.15	87.14	0.06	ND	ND			7.32	99		NA	199
	155-164	60	2.40	10.0	0.96	4.2	60	0.77	29.91	ND	0.08	0.45	0.13	82.34	0.05	ND	ND			7.34	101		NA	199
	167-176	60	4.10	9.6	0.95	3.8	62	0.65	28.99	ND	0.10	0.25	0.28	82.07	ND	ND	ND	199	0.12	7.28	112	3.26	7.27	207
	176-185	58	2.80	8.7	0.89	4.1	78	0.57	26.32	ND	0.11	0.28	0.11	77.30	ND	ND	ND			7.29	102		NA	244
	185-194	52	2.20	8.7	0.97	3.5	59	0.59	24.79	ND	0.12	0.13	0.27	76.46	ND	ND	ND			7.21	114		NA	185
	194-206	52	1.70	9.3	0.99	3.7	58	0.57	24.33	ND	0.07	0.13	0.18	78.41	ND	ND	ND	177	0.13	7.20	117	2.90	7.15	183
	206-215	46	1.70	8.3	0.98	3.4	58	0.68	18.93	ND	0.07	0.37	0.24	65.17	ND	ND	ND			7.15	133		NA	188
	215-224	44	1.40	7.9	0.99	3.4	53	0.71	18.53	ND	0.09	0.15	0.37	64.30	ND	ND	ND	172	0.09	7.12	141	2.83	5.85	170
	224-233	43	1.40	7.3	0.87	3.1	56	0.56	18.37	ND	0.09	0.12	0.49	64.00	ND	ND	ND			7.14	145		NA	172
	98-107	*3*	*0.14*	*ND*	*ND*	*ND*	*ND*	*0.48*	*1.05*	*0.02*	*0.22*	*639.40*	*0.42*	*0.54*	*0.00*	*ND*	*ND*			*2.27*	*680*		*NA*	*-626*
	107-116	*27*	*0.08*	*4.5*	*0.48*	*2.6*	*29*	*0.63*	*12.83*	*ND*	*0.12*	*150.28*	*0.16*	*26.54*	*0.00*	*ND*	*ND*			*2.44*	*656*		*NA*	*-36*
	116-125	*43*	*2.44*	*7.0*	*0.72*	*3.4*	*42*	*0.76*	*19.44*	*ND*	*0.11*	*15.76*	*0.27*	*57.04*	*0.00*	*ND*	*ND*			*6.41*	*569*		*NA*	*139*
082201	125-137	47	5.0	7.7	0.77	3.5	42	0.68	19.28	ND	0.10	0.26	0.25	61.62	ND	ND	ND	176	0.05	6.59	545	2.89	3.37	169
	137-146	49	3.62	8.1	0.77	3.7	44	0.77	19.33	ND	0.15	0.18	0.24	61.65	0.03	ND	ND			7.27	267		NA	178
	146-155	50	4.44	8.1	0.80	3.7	43	0.65	19.58	ND	0.07	0.25	0.24	61.87	0.05	ND	ND			7.28	229		NA	180
	155-164	50	4.10	8.1	0.81	3.4	42	0.66	20.16	ND	0.10	0.13	0.18	65.49	0.04	ND	ND			7.28	162		NA	171
	167-176	50	3.03	8.1	0.90	3.6	43	0.69	19.70	ND	0.11	0.15	0.24	58.61	0.03	ND	ND	182	0.10	7.30		2.98	4.61	181
	176-185	50	3.43	7.9	0.97	3.3	42	0.70	20.28	ND	0.09	0.11	0.16	57.48	0.02	ND	ND			7.19	122		NA	179
	185-194	52	2.36	8.2	1.08	3.8	43	0.62	20.93	ND	0.10	0.11	0.30	56.63	0.02	ND	ND			7.29	160		NA	187
	194-206	55	2.84	8.6	1.10	3.7	44	0.68	21.39	ND	0.10	0.07	0.29	55.86	0.06	ND	ND	199	0.09	7.33	138	3.26	4.91	201
	206-215	52	2.31	8.6	1.15	3.7	44	1.46	22.95	ND	0.12	0.09	0.22	56.49	0.07	ND	ND			7.18	127		NA	185
	215-224	56	1.94	9.0	1.22	3.8	46	0.78	21.99	ND	0.12	0.07	0.49	56.29	ND	ND	ND	198	0.08	7.18	118	3.25	5.96	206
	224-233	51	1.73	8.6	1.15	3.5	42	0.64	21.86	ND	0.09	0.17	0.35	55.17	0.02	ND	ND			7.11	141		NA	182

Notes:

All concentrations in milligrams per liter.

ND indicates below instrumental detection limit.

NA indicates not applicable.

Blank cell indicates sample lost due to analytical problems or analysis not performed due to inadequate sample volume.

Black rows were not used because cells were located above the water table and did not equilibrate with the aquifer.

Appendix IV (continued)

Date (MMDDYY)	Depth below surface (cm)	Ca^{2+}	Fe_T	Mg^{2+}	Mn_T	K^+	Na^+	F^-	Cl^-	NO_2^-	Br^-	NO_3^-	PO_4^{3-}	SO_4^{2-}	$S^{2-}{}_T$	$C_2H_3O_4^-$	$C_2O_4^{2-}$	HCO_3^-	CO_3^{2-}	pH	Eh (mV)	Alk (meq/kg as $CaCO_3$)	Charge balance error	Recalculated HCO_3^-
	89-98	*2*	*0.04*	*0.2*	*0.00*	*0*	*0*	*0.01*	*0.76*	*ND*	*ND*	*19.11*	*0.08*	*0.25*	*0.04*	*ND*	*ND*			*5.41*	*456*		*NA*	*NA*
	98-10"	*0*	*0.05*	*0.2*	*0.00*	*"*	*0*	*0.01*	*0.24*	*ND*	*0.03*	*13.19*	*0.0"*	*0.12*	*0.03*	*ND*	*ND*			*4.14*	*544*		*NA*	*NA*
	10"-116	*0*	*0.00*	*0.1*	*0.00*	*0*	*0*	*0.00*	*1.10*	*ND*	*0.00*	*11.19*	*0.1"*	*1.39*	*0.02*	*ND*	*ND*			*3.89*	*560*		*NA*	*NA*
091901	116-128	105	0.75	8.7	0.88	4	52	0.54	22.15	ND	0.11	0.13	0.57	58.29	0.02	ND	ND	180	0.16	7.31	301	2.95	26.67	NA
	128-137	117	3.50	9.7	0.97	5	51	0.57	22.27	ND	0.10	0.04	0.50	59.72	0.05	ND	ND			7.33	113		NA	NA
	137-146	74	4.40	8.6	1.05	5	50	0.51	23.63	ND	0.12	0.03	0.37	59.93	0.07	ND	ND			7.25	111		NA	266
	146-155	91	4.65	8.7	1.06	5	53	0.49	24.83	ND	0.13	0.17	0.36	61.31	0.06	ND	ND			7.24	161		NA	319
	158-167	54	1.59	8.1	1.16	4	53	0.54	26.04	ND	0.11	0.06	0.37	62.13	0.06	ND	ND	199	0.11	7.35	127	3.27	4.76	202
	167-176	55	1.67	8.7	1.26	4	48	0.52	26.06	ND	0.10	0.11	0.32	62.96	0.06	ND	ND			7.41	149		NA	196
	176-185	55	2.98	8.7	1.32	4	47	0.52	24.42	ND	0.11	0.09	0.38	62.25	0.02	ND	ND			7.37	127		NA	196
	185-198	53	3.25	8.8	1.36	4	49	0.51	24.12	ND	0.10	0.06	0.44	60.86	0.03	ND	ND	194	0.10	7.41	148	3.18	5.33	200
	198-207	51	2.88	8.2	1.38	3	46	0.48	22.76	ND	0.12	0.05	0.36	59.14	0.02	ND	ND			7.27	158		NA	189
	207-216	52	2.10	8.2	1.40	3	48	0.50	22.74	ND	0.08	0.09	0.30	59.41	0.02	ND	ND	201	0.10	7.19	155	3.30	3.09	193
	216-224	50	1.84	8.1	0.96	4	48	0.42	21.59	ND	0.10	0.42	0.40	55.12	0.03	ND	ND			7.21	165		NA	196
	105-114	*15*	*0.2*	*4.8*	*0.06*	*1.2*	*11*	*0.03*	*1.84*	*ND*	*0.04*	*59.38*	*0.12*	*0.58*		*ND*	*ND*			*3.18*			*NA*	*30*
	114-123	*34*	*0.2*	*4.5*	*0.02*	*3.8*	*52*	*0.33*	*13.41*	*ND*	*0.10*	*30.43*	*0.2*	*30.9"*	*0.02*	*ND*	*ND*			*3.4"*			*NA*	*152*
101001	123-132	200	0.7	12.8	0.87	4.0	68	0.56	22.15	ND	0.10	1.28	0.37	56.97	0.03	ND	ND			7.24	541		NA	670
	132-145	60	1.0	7.6	0.82	4.0	48	0.56	22.36	0.17	0.13	0.52	0.34	57.09	0.04	ND	ND	202	0.08	7.33	530	3.32	6.28	212
	145-154	59	1.2	8.0	0.96	4.6	46	0.55	22.46	0.14	0.09	0.49	0.24	58.01	0.03	ND	ND			7.31	448		NA	203
	154-163	59	1.2	7.7	0.87	4.4	47	0.52	22.87	0.13	0.10	0.25	0.26	59.14	0.03	ND	ND			7.26	417		NA	204
	163-172	54	2.1	6.9	0.86	3.8	63	0.49	21.83	ND	0.13	0.51	0.37	53.95	0.04	1.46	ND			7.25	417		NA	234
	175-184	55	1.0	7.3	0.95	3.9	41	0.52	20.16	ND	0.10	0.72	0.38	55.49	0.03	ND	ND			7.27	197		NA	184
	184-193	49	1.9	6.8	0.83	3.6	39	0.51	18.09	ND	0.12	0.08	0.38	51.74	0.07	ND	ND						NA	172
	193-202	51	1.4	6.8	0.84	3.8	36	0.53	15.57	ND	0.06	0.34	0.49	47.43	0.07	ND	ND			7.22	344		NA	178
	202-214	46	0.5	6.3	1.05	3.7	38	0.52	14.39	ND	0.07	0.42	0.46	46.36	0.04	ND	ND	177	0.10	7.34	274	2.90	3.20	168
	214-223	49	1.6	6.5	1.01	3.5	39	0.53	14.74	ND	0.07	0.06	0.50	46.19	0.04	0.32	ND			7.31	223		NA	183
	223-232	48	1.1	6.4	1.09	3.5	39	0.50	15.04	ND	0.09	0.13	0.54	46.18	0.03	0.31	ND	176	0.06	7.20	198	2.88	5.16	178
	232-241	51	0.4	7.3	1.01	3.9	41	0.56	14.58	ND	0.09	0.12	0.61	46.09	0.05	ND	ND			7.06	292		NA	194

Notes:

All concentrations in milligrams per liter.

ND indicates below instrumental detection limit.

NA indicates not applicable.

Blank cell indicates sample lost due to analytical problems or analysis not performed due to inadequate sample volume.

Black rows were not used because cells were located above the water table and did not equilibrate with the aquifer.

Appendix IV (continued)

Date (MMDDYY)	Depth below surface (cm)	Ca^{2+}	Fe_T	Mg^{2+}	Mn_T	K^+	Na^+	Ammonia (as NH_4^+)	F^-	Cl^-	NO_2^-	Br^-	NO_3^-	PO_4^{3-}	SO_4^{2-}	$S^{2-}{}_T$	$C_2H_3O_4^-$	$C_2O_4^{2-}$	HCO_3^-	CO_3^{2-}	pH	Eh (mV)	Alk (meq/kg as $CaCO_3$)	Charge balance error	Recalculated HCO_3^-
111101	108-117	63	0.5	8.6	1.02	8.8	41	0.60	0.65	20.70	ND	0.32	0.51	0.41	51.75	ND	ND	ND			7.54	488		NA	208
	117-126	47	2.8	7.8	0.82	8.4	41	0.82	0.54	18.26	ND	0.16	0.21	0.32	50.44	0.02	ND	ND			7.67	255		NA	173
	126-135	48	2.8	8.0	0.86	7.1	40	0.71	0.57	18.58	ND	0.14	0.12	0.55	51.16	0.10	ND	ND			7.83	259		NA	169
	135-147	50	2.7	8.0	0.75	6.9	42	0.87	0.52	18.14	ND	0.17	0.08	0.56	50.20	0.05	ND	ND	188	0.14	7.75	210	3.08	5.80	181
	147-156	50	4.3	8.0	0.77	6.9	42	0.92	0.57	17.71	ND	0.74	0.27	0.38	49.92	0.05	ND	ND			7.71	143		NA	186
	156-165	52	3.5	7.8	0.71	6.9	43	0.73	0.57	16.95	ND	0.12	0.11	0.35	48.78	0.04	ND	ND			7.71	129		NA	194
	165-174	50	2.8	6.8	0.71	7.1	39	0.89	0.55	15.21	ND	0.15	0.06	0.47	45.29	ND	ND	ND			7.68	123		NA	182
	177-186	46	2.7	6.8	0.83	6.9	38		0.54	14.06	ND	0.22	0.11	0.52	44.55	0.05	ND	ND	166	0.12			2.72	7.94	171
	186-195	45	2.6	6.6	0.86	6.1	36	0.57	0.48	14.19	ND	0.13	0.17	0.50	45.64	0.04	ND	ND			7.71	131		NA	160
	195-204	45	1.8	6.3	1.02	6.1	37	0.73	0.47	14.41	ND	0.25	0.11	0.56	46.52	0.02	ND	ND			7.69	150		NA	159
	204-217	45	2.5	6.3	1.01	6.2	37	0.67	0.48	14.66	ND	0.16	ND	0.77	47.01	0.04	0.06	ND	146	0.09	7.82	178	2.40	9.57	159
	217-226	45	2.2	6.3	0.95	6.0	36	0.62	0.51	14.57	ND	0.21	0.11	0.63	47.17	0.06	ND	ND			7.78	145		NA	156
	226-234	40	2.5	6.6	0.94	6.1	38	0.78	0.51	14.93	ND	0.15	0.03	0.74	47.02	0.04	ND	ND	157	0.09		180	2.57	4.98	147
	234-243	43	1.3	6.3	0.86	5.8	37		0.54	14.86	ND	0.19	0.14	0.51	47.34	ND	ND	ND			8.00	185		NA	150
121301	108-117	58	2.15	7.5	1.00	5.0	41		0.65	22.65	ND	0.27	0.24	0.48	29.04	0.03	ND	ND			7.72	59		NA	273
	117-126	50	2.90	7.3	0.81	3.8	40		0.50	19.61	ND	0.15	0.11	0.57	52.73	0.06	ND	ND			7.81	110		NA	219
	126-135	51	3.60	7.3	0.76	3.8	41		0.50	19.87	ND	0.11	0.06	0.35	55.12	0.05	ND	ND			7.67	89		NA	224
	135-148	51	2.81	7.4	0.75	3.8	41		0.51	19.53	ND	0.14	0.08	0.30	55.53	0.04	ND	0.08	274	1.21	7.82	74	4.54	-9.65	222
	148-157	48	2.43	6.9	0.76	3.5	40		0.47	18.23	ND	0.13	0.07	0.24	52.62	0.05	ND	ND			7.84	79		NA	212
	157-168	49	2.31	7.0	0.72	3.7	39		0.51	18.39	ND	0.15	0.52	0.14	55.83	0.06	ND	ND			7.80	85		NA	208
	168-175	48	2.81	6.6	0.62	4.3	37		0.52	17.81	ND	0.37	0.10	0.23	55.92	0.09	ND	ND			7.81	87		NA	200
	178-187	45	1.96	6.4	0.76	3.3	36		0.49	16.77	ND	0.11	ND	0.29	52.13	0.04	ND	ND	179	0.11	7.80	86	2.94	-0.13	191
	187-196	45	2.09	6.3	0.82	3.3	35		0.49	16.37	ND	0.15	0.07	0.32	53.56	0.05	ND	ND			7.78	82		NA	186
	196-205	45	1.49	6.6	0.93	3.5	37		0.49	17.24	ND	0.12	0.12	0.33	57.37	ND	ND	ND			8.11	104		NA	186
	205-217	44	2.31	6.5	1.03	3.8	37		0.44	17.30	ND	0.16	ND	0.36	59.31	0.05	ND	ND	164	0.10	7.93	107	2.70	1.15	183
	217-226	45	1.24	6.4	0.97	4.0	37		0.43	17.36	ND	0.15	0.07	0.28	59.88	0.05	ND	ND			7.95	103		NA	183
	226-235	46	1.30	6.4	0.99	3.3	35		0.48	17.50	ND	0.13	0.16	0.35	59.76	0.02	ND	ND	166	0.10	7.87	106	2.72	0.20	179
	235-244	45	1.39	6.4	1.02	3.1	35		0.56	17.14	ND	0.15	0.07	0.51	59.43	0.04	ND	ND			7.90	107		NA	176

Notes:

All concentrations in milligrams per liter.

ND indicates below instrumental detection limit.

NA indicates not applicable.

Blank cell indicates sample lost due to analytical problems or analysis not performed due to inadequate sample volume.

Black rows were not used because cells were located above the water table and did not equilibrate with the aquifer.

Appendix IV (continued)

Date (MMDDYY)	Depth below surface (cm)	Ca^{2+}	Fe_T	Mg^{2+}	Mn_T	K^+	Na^+	F^-	Cl^-	NO_2^-	Br^-	NO_3^-	PO_4^{3-}	SO_4^{2-}	$S^{2-}{}_T$	$C_2H_3O_4^-$	$C_2O_4^{2-}$	HCO_3^-	CO_3^{2-}	pH	Eh (mV)	Alk (meq/kg as $CaCO_3$)	Charge balance error	Recalculated HCO_3^-
022802	107-116	62	0.73	8.1	0.05	4.5	38	0.50	17.57	ND	0.14	1.07	0.30	36.26		ND	ND			7.62			NA	275
	116-125	43	1.61	8.9	0.71	4.0	34	0.49	16.48	ND	0.10	0.01	0.76	40.60		ND	ND			7.45			NA	207
	125-134	43	1.81	8.6	0.77	4.0	35	0.49	16.77	ND	0.12	0.16	0.31	44.15		ND	ND			7.45			NA	204
	134-146	44	ND	8.7	0.78	4.0	36	0.53	16.73	ND	0.12	ND	0.37	43.38		ND	ND			7.51			NA	
	146-155	49	1.79	9.6	0.78	4.5	35	0.50	16.88	ND	0.11	0.13	0.49	43.21		ND	ND			7.46			NA	230
	155-164	49	1.81	8.7	0.80	3.5	35	0.42	16.88	ND	0.12	0.05	0.41	44.05		ND	ND			7.49			NA	223
	164-173	45	1.60	10.6	0.67	5.0	35	0.45	17.07	ND	0.07	ND	0.36	45.54		ND	ND			7.52			NA	220
	176-185	45	1.92	9.0	0.84	4.0	34	0.49	17.61	ND	0.07	0.05	0.37	52.75		ND	ND	199	0.74	7.53		3.28	-2.59	198
	185-194	46	1.75	9.0	1.00	4.0	33	0.45	18.16	ND	0.08	0.08	0.43	56.28		ND	ND			7.48			NA	193
	194-203	46	ND	9.4	1.11	3.5	33	0.43	19.77	ND	0.13	0.10	0.33	64.83		ND	ND			7.46			NA	
	203-216	49	1.75	10.2	1.17	4.9	36	0.42	20.47	ND	0.12	ND	0.36	69.14		ND	ND	190	0.15	7.45		3.12	-0.81	199
	216-225	50	1.65	10.3	1.29	4.0	36	0.42	22.73	ND	0.11	0.07	0.35	75.13		ND	ND			7.47			NA	189
	225-234	51	1.74	10.5	1.34	4.5	38	0.57	25.22	ND	0.18	0.08	0.38	79.52		ND	ND	195	0.16	7.47		3.20	-3.12	189
	234-242	51	1.75	10.4	1.37	4.9	38	0.39	26.06	ND	0.13	ND	0.29	80.95		ND	ND			7.50			NA	186
041602	104-113	7	0.11	ND	0.04	4.3	6	0.22	11.31	ND	12.83	2.03	ND	1.98	ND	ND	0.03						NA	
	113-122	49	2.71	7.0	0.12	3.6	39	0.04	17.30	ND	0.30	0.42	0.12	47.15		ND	ND						NA	215
	122-131	62	ND	7.5	ND	3.8	40	0.45	19.11	ND	0.18	1.42	0.36	43.90	ND	ND	ND						NA	
	131-143	54	3.31	7.6	1.02	4.3	36	0.44	20.43	ND	0.18	0.17	0.25	51.19	ND	ND	ND	253	0.24	7.41		4.15	-5.89	222
	143-152		3.05		0.86			0.44	20.44	ND	0.10	0.74	0.19	52.18	0.04	ND	ND						NA	
	152-161	58	2.30	7.5	0.86	3.7	40	0.43	20.51	ND	0.17	0.04	0.29	54.99	0.02	ND	ND						NA	226
	161-170	56	2.98	8.5	0.97	3.7	39	0.39	21.74	ND	0.15	0.05	0.26	61.23	0.05	ND	ND						NA	
	173-182	59	2.33	9.5	1.24	3.8	38	0.37	22.32	ND	0.16	0.08	0.22	62.12	0.07	ND	ND	212	0.15	7.29		3.48	1.15	230
	182-191	64	4.88	9.0	1.36	4.3	30	0.32	20.80	ND	0.17	0.90	0.25	54.60	0.05	ND	ND						NA	242
	191-200	62	2.39	9.4	1.47	3.8	34	0.38	24.40	ND	0.17	0.04	0.17	68.79	0.02	ND	ND						NA	220
	200-213	65	2.46	9.5	1.70	3.8	38	0.38	26.74	ND	0.23	ND	0.28	81.37	ND	ND	ND	214	0.15	7.19		3.51	-0.43	221
	213-222	67	0.51	11.0	1.41	3.8	38	0.34	26.72	ND	0.14	0.06	0.18	82.99	0.03	ND	ND						NA	229
	222-231	64	1.91	10.0	1.65	3.6	38	0.40	26.09	ND	0.13	0.08	0.19	81.04	0.03	ND	ND	210	0.11	7.17		3.45	-0.21	218
	231-240	66	1.74	10.5	1.66	3.7	40	0.33	25.87	ND	0.15	0.02	0.14	80.12		ND	ND						NA	236

Notes:

All concentrations in milligrams per liter.

ND indicates below instrumental detection limit.

NA indicates not applicable.

Blank cell indicates sample lost due to analytical problems or analysis not performed due to inadequate sample volume.

Samples in italics were not used because cells were located above the water table and did not equilibrate with the aquifer.

Appendix IV (concluded)

Date (MMDDYY)	Depth below surface (cm)	Ca^{2+}	Fe_T	Mg^{2+}	Mn_T	K^+	Na^+	F^-	Cl^-	NO_2^-	Br^-	NO_3^-	PO_4^{3-}	SO_4^{2-}	$S^{2-}{}_T$	$C_2H_3O_4^-$	$C_2O_4^{2-}$	HCO_3^-	CO_3^{2-}	pH	Eh (mV)	Alk (meq/kg as $CaCO_3$)	Charge balance error	Recalculated HCO_3^-
031902 (10 µm filters)	77-86		1.82		0.16			0.63	39.58	ND	0.41	12.36	0.37	47.85		ND	ND							
	86-99		2.10		0.19			0.50	23.84	ND	0.24	5.67	0.53	38.52		ND	ND							
	99-108		0.49		0.13			0.46	17.89	ND	0.08	ND	1.00	35.40		ND	ND							
	108-116		6.00		0.53			0.43	18.50	ND	0.10	2.41	0.37	44.07		ND	ND							
	116-125		3.15		0.67			0.43	18.75	ND	0.13	ND	0.25	45.11		ND	ND							
	129-138		4.04		0.69			0.42	19.26	ND	0.11	ND	0.31	46.21		ND	ND							
	138-146		3.73		0.68			0.42	19.59	ND	0.13	ND	0.19	45.36		ND	ND							
	146-155		3.87		0.69			0.43	20.00	ND	0.09	ND	0.21	43.92		ND	ND							
	155-168		3.20		0.73			0.41	19.63	ND	0.13	0.03	0.36	44.04		ND	ND							
	168-177		3.70		0.87			0.41	19.55	ND	0.15	0.15	0.25	44.99		ND	0.03							
	177-186		14.90		0.90			0.40	19.70	ND	0.15	0.09	0.18	45.33		ND	ND							
	186-195		8.00		1.26			0.43	20.39	ND	0.13	0.11	0.32	57.18		ND	ND							
031902 (0.2 µm filters)	99-108		0.73		0.18			0.44	19.08	ND	0.15	0.05	1.30	34.62		ND	ND							
	108-116		1.24		0.03			0.46	18.40	ND	0.13	1.22	0.48	42.62		ND	ND							
	116-125		2.44		0.58			0.45	18.67	ND	0.07	0.04	0.25	44.92		ND	ND							
	129-138		2.39		0.61			0.52	19.30	ND	0.12	0.75	0.27	45.68		ND	ND							
	138-146		7.50		0.71			0.45	19.27	ND	0.14	0.06	0.37	45.07		ND	ND							
	146-155		2.75		0.69			0.46	19.54	ND	0.14	ND	0.19	44.28		ND	ND							
	155-168		2.62		0.67			0.43	19.55	ND	0.13	ND	0.24	43.82		ND	ND							
	168-177		2.61		0.82			0.44	19.32	ND	0.14	0.05	0.11	44.81		ND	ND							
	177-186		2.14		0.92			0.48	18.89	ND	0.14	0.03	0.33	48.91		ND	ND							
	186-195		1.99		1.17			0.39	20.16	ND	0.08	0.29	0.34	56.44		ND	ND							

Notes:

All concentrations in milligrams per liter.

ND indicates below instrumental detection limit.

NA indicates not applicable.

Blank cell indicates sample lost due to analytical problems or analysis not performed due to inadequate sample volume.

Samples in italics were not used because cells were located above the water table and did not equilibrate with the aquifer.

Appendix V: Transect and conventional well chemistry

Sample ID (concentrations in mg L^{-1})	Ca^{2+}	Fe_T	Mg^{2+}	Mn_T	K^+	Na^+	F^-	Cl^-	NO_2^-	Br^-	NO_3^-	PO_4^{3-}	SO_4^{2-}	$S^{2-}{}_T$	HCO_3^-	pH	Eh (mV)	Diss. O_2	Alk (meq/kg as $CaCO_3$)	% Charge balance error
BLN C 10/10/01	45	1.40	9.0	1.45	3.8	43	0.50	20.34	ND	0.11	ND	0.20	63.99		184	7.44		0.56	3.01	1.12
BLN 2 10/10/01	45	4.80	10.5	1.17	5.3	38	0.53	16.90	ND	0.19	0.09	0.50	47.96		190	7.40		0.63	3.12	4.82
BLN 3 10/10/01	42	0.04	8.0	0.88	3.8	38	0.54	16.43	ND	0.07	0.05	0.83	50.04		168	7.62		1.07	2.76	2.47
BLN 4 10/10/01	46	2.70	10.0	0.95	6.5	39	0.47	18.07	ND	0.23	0.14	0.65	54.57		167	7.79		1.89	2.73	7.02
Rio BLN 10/10/01	52	0.27	10.7	0.11	6.3	49	0.50	23.23	0.53	0.10	3.57	0.53	70.24		173	8.35		7.88	2.83	6.48
Rio BLN 11/11/01	55	0.08	9.4	0.07	10.8	43	0.49	26.69	ND	0.10	4.82	0.66	83.29		210	7.61			3.44	-3.23
USJRD BLN 11/11/01	60	0.11	14.0	1.78	8.1	58	0.49	28.70	ND	0.11	0.12	0.30	70.65		284	7.93			4.66	-0.39
BLN C 12/13/01	53	ND	5.8	0.78	7.3	54	0.49	14.49	ND	0.07	1.23	0.29	49.04		155	7.20			2.54	17.13
BLN 3 12/13/01	55	0.03	6.0	0.53	8.6	55	0.57	17.48	ND	0.12	0.28	0.73	60.95		149	7.62			2.45	15.49
BLN 4 12/13/01	55	ND	6.4	0.03	11.0	55	0.53	17.11	ND	0.09	0.74	0.49	57.53		149	7.70			2.44	17.58
Rio BLN 12/13/01	63	ND	8.2	ND	10.4	60	0.44	23.43	ND	0.17	2.95	0.47	77.52		201	8.33			3.29	8.29
USJRD BLN 12/13/01	68	ND	12.3	2.07	9.9	68	0.55	28.16	ND	0.20	0.04	0.23	61.80		295	7.68			4.84	4.92
BLN C 1/27/02	46	0.08	9.3	0.90	3.5	33	0.62	19.17	ND	0.10	1.72	0.20	63.13		117	7.08			1.92	9.20
BLN 3 1/27/02	60	0.09	12.5	0.67	5.0	43	0.47	41.03	ND	0.10	0.35	0.76	111.10		123	7.11			2.02	4.37
BLN 4 1/27/02	45	ND	9.4	0.07	4.0	34	0.46	20.17	ND	0.10	0.31	0.59	63.14		107	7.27			1.76	11.03
Rio BLN 1/27/02	47	0.03	12.3	0.04	6.0	44	0.47	28.51	ND	0.09	3.79	0.60	80.40		166	7.53			2.72	1.18
USJRD BLN 1/27/02	59	ND	14.4	1.51	5.0	50	0.53	35.78	ND	0.12	ND	0.27	77.35		193	7.39			3.17	5.36
BLN RIO 2/07/02	55	ND	11.7	0.86	5.5	40	0.42	25.13	ND	0.14	0.89	0.49	79.38	0.03	183	7.86	290		3.00	1.67
BLN TR-1 2/07/02	57	ND	12.0	1.37	4.5	41	0.40	25.79	ND	0.17	1.02	0.53	78.14	ND		8.03	290			
BLN TR-3 2/07/02	44	ND	8.8	0.82	5.0	42	0.49	21.90	ND	0.11	0.13	0.37	68.42	ND		8.01	252			
BLN TR-4 2/07/02	48	ND	9.7	0.80	3.0	34	0.68	17.94	ND	0.08	ND	0.48	11.42	0.07	200	7.36	-33		3.28	7.77
BLN TR-5 2/07/02	154	ND	38.8	0.36	112	188	1.17	256.13	ND	0.51	2.43	1.10	502.78	ND						
BLN USJRD 2/07/02	54	ND	13.8	1.75	5.0	63	0.52	30.60	ND	0.16	ND	0.33	76.34	0.02	225	7.54	76		3.69	4.35
BLN C 2/28/02	47	0.35	10.4	1.35	4.0	33	0.41	20.51	ND	0.14	0.38	0.23	61.36		186				3.04	-1.29
BLN 3 2/28/02	98	0.23	18.9	1.87	6.0	50	0.49	83.30	ND	0.28	0.13	0.56	162.03		229				3.76	-3.69
BLN 4 2/28/02	47	ND	9.9	0.17	5.5	38	0.33	22.82	ND	0.12	1.20	0.51	71.66							
USJRD BLN 2/28/02	64	0.05	14.5	1.75	5.0	46	0.42	34.24	ND	0.17	ND	0.27	89.07		223				3.66	0.55
BLN RIO 4/16/02	51	ND	8.7	0.05	6.0	45	0.54	25.68	ND	0.27	3.17	0.59	75.44	0.07	196		394		3.22	-2.41
BLN TR-1 4/16/02	58	ND	9.0	0.05	6.5	47	0.24	27.02	1.38	0.12	1.09	0.37	63.10				369			
BLN TR-3 4/16/02	82	ND	10.9	0.07	7.5	70	0.29	24.56	3.14	0.17	16.63	0.65	191.79				340			
BLN TR-4 4/16/02	47	0.01	8.0	0.65	2.5	40	0.40	16.93	ND	0.06	0.07	0.58	3.46	2.26	240		-48		3.94	3.12
BLN USJRD 4/16/02	70	0.03	12.8	1.60	4.5	50	0.47	39.30	ND	0.12	0.02	0.26	104.89	0.12	322		77		5.28	-11.00
BLN C 4/16/02	58	2.00	9.8	1.60	4.0	37	0.37	24.47	ND	0.13	ND	0.13	63.79					0.33		
BLN 3 4/16/02	64	0.09	9.8	1.44	4.3	41	0.35	26.58	ND	0.16	0.16	0.79	83.57					0.27		
BLN 4 4/16/02	47	ND	8.5	0.07	4.8	39	0.40	22.76	ND	0.09	1.46	0.48	71.54					1.94		

Appendix VI: Sediment extraction data

(All values in weight percent)			Dithionite extraction	Oxalate extraction		0.5 N HCl extraction (24 hr)			6 N HCl extraction (2 h)
Well ID	Top (cm)	Bottom (cm)	Fe_{dith} as Fe_2O_3	Fe_{ox} as Fe_2O_3	Al_{ox} as Al_2O_3	$Fe_{0.5N}$ as Fe_2O_3	$Mn_{0.5N}$ as MnO_2	$P_{0.5N}$ as P_2O_5	Fe_{6N} as Fe_2O_3
BLN9	15	23	2.71	0.237	0.21	0.302	0.1027	0.0131	0.49
BLN9	23	41	2.05	0.191	0.15	0.284	0.0635	0.0144	0.35
BLN9	23	41	2.05	0.183	0.11	0.261	0.0509	0.0153	0.32
BLN9	41	51	1.97	0.200	0.11	0.283	0.0614	0.0137	0.34
BLN9	51	61	0.97	0.085	0.06	0.154	0.0283	0.0130	0.20
BLN9	61	71	1.05	0.093	0.08	0.154	0.0265	0.0131	0.18
BLN9	61	71	0.69	0.060	0.06	0.113	0.0213	0.0108	0.14
BLN9	71	81	0.52	0.045	0.06	0.091	0.0183	0.0087	0.13
BLN9	81	91	0.40	0.038	0.04	0.085	0.0163	0.0080	0.13
BLN9	91	102	0.48	0.037	0.05	0.081	0.0155	0.0080	0.12
BLN9	102	112	0.54	0.106	ND	0.091	0.0151	0.0084	0.15
BLN9	102	112	0.44	0.100	ND	0.085	0.0144	0.0075	0.15
BLN9	112	122	0.46	0.051	ND	0.101	0.0073	0.0088	0.19
BLN9	122	132	0.64	0.098	ND	0.105	0.0059	0.0123	0.32
BLN9	132	142	0.46	0.099	ND	0.102	0.0067	0.0092	0.26
BLN9	142	152	0.40	0.033		0.069	0.0066	0.0092	0.22
BLN9	142	152	0.31	0.036		0.063	0.0057	0.0084	0.18
BLN9	152	163	0.29	0.036		0.064	0.0064	0.0075	0.16
BLN9	163	168	0.52	0.040		0.087	0.0081	0.0093	0.21
BLN2	0	15				0.067	0.0083	0.0065	
BLN2	30	46				0.053	0.0069	0.0047	
BLN2	61	76				0.053	0.0055	0.0050	
BLN2	91	107				0.067	0.0075	0.0076	
BLN2	122	137				0.062	0.0065	0.0070	
BLN2	122	137				0.064	0.0079	0.0069	
BLN2	152	168				0.067	0.0063	0.0058	
BLN2	183	198				0.057	0.0049	0.0054	
BLN2	213	229				0.058	0.0081	0.0065	
BLN2	244	259				0.079	0.0089	0.0076	
BLN2	274	290				0.070	0.0089	0.0081	
BLN2	274	290				0.073	0.0091	0.0071	
BLN2	305	320				0.059	0.0061	0.0051	
BLN2	335	351				0.053	0.0065	0.0055	
BLN2	366	381				0.066	0.0073	0.0080	
BLN2	396	411				0.062	0.0066	0.0063	
BLN2	427	442				0.068	0.0066	0.0068	
BLN2	427	442				0.069	0.0071	0.0062	
BLN2	457	472				0.085	0.0085	0.0066	
BLN2	488	503				0.078	0.0066	0.0065	
BLN2	518	533				0.085	0.0066	0.0072	

ND: Not detected

BLN2 dithionite extractions, presented on graphs in text, appear in Block (2002).

Appendix VII: X-ray fluorescence bulk chemistry data of size separates

Sand (subsample S)					All values in weight percent of oxides											
Sample ID	Well ID	Top (cm)	Btm (cm)	Avg depth (cm)	SiO_2	Al_2O_3	Fe_2O_3	MnO	MgO	CaO	Na_2O	K_2O	TiO_2	P_2O_5	H_2O-	L.O.I.
W-3	BLN2	30	46	38	86.916	6.785	1.412	0.023	0.418	1.159	1.492	2.135	0.198	0.015	0.13	0.80
renorm	BLN2	30	46	38	85.746	6.694	1.393	0.023	0.412	1.143	1.472	2.106	0.195	0.015	0.13	0.80
W-8	BLN2	107	122	114	83.728	6.777	1.465	0.025	0.409	1.141	1.528	2.195	0.209	0.017	0.19	0.87
renorm	BLN2	107	122	114	84.970	6.878	1.487	0.025	0.415	1.158	1.551	2.228	0.212	0.017	0.19	0.87
W-9	BLN2	122	137	130	83.919	7.667	1.908	0.035	0.402	1.062	1.455	2.138	0.253	0.015	0.28	0.59
renorm	BLN2	122	137	130	84.153	7.688	1.913	0.035	0.403	1.065	1.459	2.144	0.254	0.015	0.28	0.59
W-10	BLN2	137	152	145	83.555	8.173	1.637	0.029	0.393	0.990	1.497	2.088	0.237	0.013	0.11	0.67
renorm	BLN2	137	152	145	84.070	8.223	1.647	0.029	0.395	0.996	1.506	2.101	0.238	0.013	0.11	0.67
W-12	BLN2	168	183	175	83.468	8.395	1.595	0.028	0.400	1.067	1.506	2.117	0.226	0.014	0.14	0.70
renorm	BLN2	168	183	175	83.759	8.424	1.601	0.028	0.401	1.071	1.511	2.124	0.227	0.014	0.14	0.70
W-15	BLN2	213	229	221	87.019	6.380	1.492	0.027	0.385	1.054	1.402	2.004	0.224	0.013	0.12	0.74
renorm	BLN2	213	229	221	86.271	6.325	1.479	0.027	0.382	1.045	1.390	1.987	0.222	0.013	0.12	0.74
W-29	BLN2	427	442	434	89.534	9.013	1.010	0.017	0.355	0.864	1.671	2.264	0.147	0.014	0.06	0.55
renorm	BLN2	427	442	434	84.840	8.540	0.957	0.016	0.336	0.819	1.583	2.145	0.139	0.013	0.06	0.55
W-35A	BLN2	518	549	533	83.546	8.254	1.006	0.019	0.350	0.843	1.610	2.246	0.155	0.009	0.14	0.44
renorm	BLN2	518	549	533	84.724	8.370	1.020	0.019	0.355	0.855	1.633	2.278	0.157	0.009	0.14	0.44
Silt + Clay (subsample Z)					All values in weight percent of oxides											
W-3	BLN2	30	46	38	34.115	4.425	4.433	0.064	0.797	3.478	0.784	1.108	0.835	0.057	0.61	1.36
renorm	BLN2	30	46	38	67.173	8.713	8.729	0.126	1.569	6.848	1.544	2.182	1.644	0.112	0.61	1.36
W-8	BLN2	107	122	114	65.105	8.752	7.658	0.109	1.319	5.941	1.518	2.072	1.486	0.132	0.12	5.98
renorm	BLN2	107	122	114	65.055	8.745	7.652	0.109	1.318	5.936	1.517	2.070	1.485	0.132	0.12	5.98
W-9	BLN2	122	137	130	65.310	8.985	7.031	0.104	1.317	6.148	1.553	2.096	1.356	0.134	1.11	5.70
renorm	BLN2	122	137	130	65.495	9.010	7.051	0.104	1.321	6.165	1.557	2.102	1.360	0.134	1.11	5.70
W-10	BLN2	137	152	145	68.726	9.428	7.974	0.116	1.474	6.674	1.676	2.333	1.471	0.128	0.57	4.70
renorm	BLN2	137	152	145	65.497	8.985	7.599	0.111	1.405	6.360	1.597	2.223	1.402	0.122	0.57	4.70
W-12	BLN2	168	183	175	64.436	9.230	6.706	0.103	1.327	6.338	1.588	2.153	1.223	0.100	0.54	6.46
renorm	BLN2	168	183	175	64.668	9.263	6.730	0.103	1.332	6.361	1.594	2.161	1.227	0.100	0.54	6.46
W-15	BLN2	213	229	221	63.986	9.161	7.174	0.108	1.347	6.344	1.609	2.156	1.371	0.129	0.57	4.70
renorm	BLN2	213	229	221	65.299	9.349	7.321	0.110	1.375	6.474	1.642	2.200	1.399	0.132	0.57	4.70
W-29	BLN2	427	442	434	68.964	9.885	4.659	0.082	1.278	5.341	1.819	2.349	0.860	0.116	0.57	4.70
renorm	BLN2	427	442	434	68.927	9.880	4.657	0.082	1.277	5.338	1.818	2.348	0.860	0.116	0.57	4.70
W-35A	BLN2	518	549	533	67.636	11.285	4.278	0.073	1.084	4.454	2.378	2.887	0.747	0.111	0.47	3.99
renorm	BLN2	518	549	533	68.403	11.413	4.327	0.074	1.096	4.505	2.405	2.920	0.755	0.112	0.47	3.99

References

Action Committee of the Middle Rio Grande Water Assembly, 1999, Middle Rio Grande Water Budget (Where Water Comes From, and Goes, and How Much): Averages for 1972-1997, Albuquerque, October 1999.

Amann, R., Snaidr, J., Wagner, M., Ludwig, W., and Schleifer, K., 1996, In situ visualization of high genetic diversity in a natural microbial community: Journal of Bacteriology, v. 178, p. 3496-3500.

American Public Health Association 1995, Standard Methods for the Examination of Water and Wastewater, 19th ed: Washington, APHA.

Baird, D.C., 2001, Downstream effects of dams on the Middle Rio Grande, *in* Johnson, P.S., ed., Water, Watersheds, and Land Use in New Mexico: Impacts of Population Growth on Natural Resources, Santa Fe Region 2001: New Mexico Bureau of Mines and Mineral Resources, Decision Makers Field Guide 1, p. 106-107.

Baker, M.A., Dahm, C.N., Valett, H.M., Morrice, J.A., Henry, K.S., Campana, M.E., and Wroblicky, G.J., 1994, Spatial and temporal variation in methane distribution at the ground water/surface water interface in headwater catchments, *in* Stanford, J.A., and Valett, H.M., eds., Proceedings of the Second International Conference on Ground Water Ecology: Atlanta, U.S. Environmental Protection Agency/American Water Resources Association, p. 29-37.

Baker, M.A., Dahm, C.N., and Valett, H.M., 2000a, Anoxia, anaerobic metabolism, and biogeochemistry of the stream-water-ground-water interface *in* Jones, J.B., and Mulholland, P.J., eds., Streams and Ground Waters: San Diego, Academic Press, p. 259-283.

Baker, M.A., Valett, H.M., and Dahm, C.N., 2000b, Organic carbon supply and metabolism in a shallow groundwater ecosystem: Ecology, v. 81, p. 3133-3148.

Ball, J.W., and Nordstrom, D.K., 1991, WATEQ4F—User's Manual with Revised Thermodynamic Data Base and Test Cases for Calculating Speciation of Major, Trace and Redox Elements in Natural Waters: U.S. Geological Survey Open-File Report 90–129.

Banfield, J.F., Welch, S.A., and Edwards, K.J., 1998, Microbes as geochemical agents: The Geochemical News, no. 96, July, p. 11-17.

Barcelona, M.J., Holm, T.R., Schock, M.R., and George, G.K., 1989, Spatial and temporal gradients in aquifer oxidation-reduction conditions: Water Resources Research, v. 25, p. 991-1003.

Barns, S.M., and Nierzwicki-Bauer, S.A., 1997, Microbial diversity in ocean, surface, and subsurface environments *in* Banfield, J.F, and Nealson, K.H., eds., Geomicrobiology: Interactions between Microbes and Minerals, Reviews in Mineralogy, v. 35, Ribbe, P.H., series ed: Washington, Mineralogical Society of America, p. 391-428.

Bartlett, R.J., 1988, Manganese redox reactions and organic interactions in soils, *in* Graham, R.D., Hannam, R.J., and Uren, N.C., eds, Manganese in Soils and Plants: Dordrecht, Kluwer, p. 59-73.

Barton, H.A., Spear, J.R., and Pace, N.R., 2001, Microbial life in the underworld: Biogenicity in secondary mineral formations: Geomicrobiology Journal, v. 18, p. 359-368.

Bencala, K.E., 1993, A perspective on stream-catchment connections: Journal of the North American Benthological Society, v. 12, p. 44-47.

Berner, R.A., 1970, Sedimentary pyrite formation: American Journal of Science, v. 268, p. 1-23.

Berner, R.A., 1981a, Authigenic mineral formation resulting from organic matter decomposition in modern sediments: Fortschritte der Mineralogie, v. 59, p. 117-135.

Berner, R.A., 1981b, A new geochemical classification of sedimentary environments: Journal of Sedimentary Petrology, v. 51, p. 359-365.

Bethke, C.M., 1998, The Geochemist's Workbench, Release 3.0: Urbana, University of Illinois.

Beveridge, T.J., 1989, Metal ions and bacteria, *in* Beveridge, T.J., and Doyle, R.J., eds., Metal Ions and Bacteria: New York, Wiley, p. 1-29.

Block, S.E., 2002, Biogeochemistry of the Middle Rio Grande Bosque, NM—Links Among Surface Water, Groundwater and Sediments: M.S. thesis, University of New Mexico.

Borggaard, O.K., 1983, Effect of surface area and mineralogy of iron oxides on their surface charge and anion-adsorption properties: Clays and Clay Minerals, v. 31, p. 230-232.

Boulton, A.J., Findlay, S., Marmonier, P., Stanley, E.H., and Valett, H.M., 1998, The functional significance of the hyporheic zone in streams and rivers: Annual Reviews in Ecology and Systematics, v. 29, p. 59-81.

Bourg, A.C.M., and Bertin, C., 1994, Seasonal and spatial trends in manganese solubility in an alluvial aquifer: Environmental Science and Technology, v. 28, p. 868-876.

Breit, G.N., 2001, Early diagenetic ferric oxide accumulations formed along redox gradients: Examples from modern and ancient fluvial sedimentary units: Geological Society of America, Abstracts with Programs, v. 33, no. 6, p. 281.

Bricker, O.P., 1982, Redox potential: Its measurement and importance in water systems, *in* Minear, R.A., and Keith, L.H., eds., Water Analysis, v. 1: New York, Academic Press, p. 55-83.

Brown, E., Skougstad, M.W., and Fishman, M.J., 1970, Techniques of Water-Resources Investigations of the U.S. Geological Survey, Chapter A1: Methods for Collection and Analysis of Water samples for Dissolved Minerals and Gases: U.S. Geological Survey.

Bull, W.B., 1997, Discontinuous ephemeral streams: Geomorphology, v. 19, p. 227-276.

Champ, M.P., Gulens, J., and Jackson, R.E., 1979, Oxidation-reduction sequences in ground-water flow systems: Canadian Journal of Earth Science, v. 16, p. 12-23.

Chapelle, F.H., 2001, Ground-water Microbiology and Geochemistry, 2nd ed: New York, Wiley.

Chapelle, F.H., and Lovley, D.R., 1992, Competitive exclusion of sulfate reduction by Fe (III)-reducing bacteria: A mechanism for producing discrete zones of high-iron groundwater: Ground Water, v. 30, p. 29-36.

Chapelle, F.H., McMahon, P.B., Dubrovsky, N.M., Fujii, R.F., Oaksford, E.T., and Vroblesky, D.A., 1995, Deducing the distribution of terminal electron-accepting processes in hydrologically diverse groundwater systems: Water Resources Research, v. 31, p. 359-371.

Cline, J.D., 1969, Spectrophotometric determination of hydrogen sulfide in natural waters: Limnology and Oceanography, v. 14, p. 454-458.

Connell, S.D., and Love, D.W., 2001, Stratigraphy of middle and upper Pleistocene fluvial deposits of the Rio Grande (post-Santa Fe Group) and the geomorphic development of the Rio Grande Valley, northern Albuquerque Basin, central New Mexico, *in* Connell, S.D., Lucas, S.G., and Love, D.W., eds, Mini-papers, Geological Society of America, Rocky Mountain-South Central Section Meeting, Albuquerque, NM: New Mexico Bureau of Mines and Mineral Resources Open-File Report 454A, p. J1-J10.

Costigan, K.R., Bossert, J.E., and Langley, D.L., 2000, Atmospheric/hydrologic models for the Rio Grande Basin: Simulations of precipitation variability: Global and Planetary Change, v. 25, p. 83-110.

Crank, J., McFarlane, N.R., Newby, J.C., Paterson, G.D., and Pedley, J.B., 1981, Diffusion Processes in Environmental Systems: London, Macmillan.

Crawford, C.S., Cully, A.C., Leutheuser, R., Sifuentes, M.S., White, L.H., and Wilber, J.P., 1993, Middle Rio Grande Ecosystem: Bosque Biological Management Plan: Albuquerque, U.S. Fish and Wildlife Service.

Crill, P.M., Bartlett, K.B., Harriss, R.C., Gorham, E., Verry, E.S., Sebacher, D.I., Madzar, L., and Sanner, W., 1988, Methane flux from Minnesota peatlands: Global Biogeochemical Cycles, v. 2, p. 371-384.

Culbertson, J.K., and Dawdy, D.R., 1964, A Study of Fluvial Characteristics and Hydraulic Variables, Middle Rio Grande, New Mexico: U.S. Geological Survey Water-Supply Paper 1498-F.

Dahm, C.N., Cleverly, J.R., Allred Coonrod, J.E., Thibault, J.R., McDonnell, D.E., and Gilroy, D.J., 2002, Evapotranspiration at the land/water interface in a semi-arid drainage basin: Freshwater Biology, v. 47, p. 831-843.

Darke, A.K. and Walbridge, M.R., 2000, Al and Fe biogeochemistry in a floodplain forest: Implications for P retention: Biogeochemistry, v. 51, p. 1-32.

Davison, W., 1991, The solubility of iron sulphides in synthetic and natural waters at ambient temperature: Aquatic Sciences, v. 53/4, p. 309-329.

Day, P.R., 1965, Particle fractionation and particle-size analysis, *in* Blake, C.A., Evans, D.D., White, J.L., Ensminger, L.E., and Clark, F.E., eds, Methods of Soil Analysis, Part I, no. 9, p. 545-567.

Dionex Corporation 2000, Determination of inorganic anions in drinking water by ion chromatography: Dionex Technical Note 133.

Drever, J.I., 1997, The Geochemistry of Natural Waters: Surface and Groundwater Environments, 3rd ed: Upper Saddle River, Prentice-Hall.

Driehaus, W., Seith, R., and Jekel, M., 1995, Oxidation of arsenate(III) with manganese oxides in water treatment: *Water Research*, v. 29, p. 297-305.

Ehrlich, H.L., 1996, How microbes influence mineral growth and dissolution: Chemical Geology, v. 132, p. 5-9.

Emerson, D., 2000, Microbial oxidation of Fe(II) and Mn(II) at circumneutral pH, *in* Environmental Microbe-Metal Interactions, D.R. Lovley, ed.: Washington, American Society for Microbiology Press, p. 31-52.

Emerson, D., Weiss, J.V., and Megonigal, J.P., 1999, Iron-oxidizing bacteria are associated with ferric hydroxide precipitates (Fe-plaque) on the roots of wetland plants: Applied and Environmental Microbiology, v. 65, p. 2758-2761.

Fenchel, T., King, G.M., and Blackburn, T.H., 1998, Bacterial Biogeochemistry: The Ecophysiology of Mineral Cycling, 2nd ed: San Diego, Academic Press.

Ferris, F.G., 2000, Microbe-metal interactions in sediments, *in* Riding, R.E. and Awramik, S.M., eds, Microbial Sediments: Berlin, Springer-Verlag, p. 121-126.

Ferris, F.G., Fyfe, W.S., and Beveridge, T.J., 1987, Bacteria as nucleation sites for authigenic minerals in a metal-contaminated lake sediment: Chemical Geology, v. 63. p. 225-232.

Ferris, F.G., Schultze, S., Witten, T.C., Fyfe, W.S., and Beveridge, T.J., 1989a, Metal interactions with microbial biofilms in acidic and neutral pH environments: Applied and Environmental Microbiology, v. 55, p. 1249-1257.

Ferris, F.G., Shotyk, W., and Fyfe, W.S., 1989b, Mineral formation and decomposition by microorganisms, *in* Beveridge, T.J., and Doyle, R.J., eds., Metal Ions and Bacteria: New York, Wiley, p. 413-441.

Fortin, D., Ferris, F.G., and Beveridge, T.J., 1997, Surface-mediated mineral development by bacteria *in* Banfield, J.F, and Nealson, K.H., eds., Geomicrobiology: Interactions between Microbes and Minerals. Reviews in Mineralogy, v. 35. Ribbe, P.H., series ed: Washington, Mineralogical Society of America, p. 161-180.

Fredrickson, J.K., McKinley, J.P., Bjornstad, B.N., Long, P.E., Ringelberg, D.B., White, D.C., Krumholz, L.R., Suflita, J.M., Colwell, F.S., Lehman, R.M., and Phelps, T.J., 1997, Pore-size constraints on the activity and survival of subsurface bacteria in a Late Cretaceous shale-sandstone sequence, Northwestern New Mexico: Geomicrobiology Journal, vol. 14, p. 183-202.

Freedman, Y.E., Magaritz, M., Long, G.L., and Ronen, D., 1994, Interaction of metals with mineral surfaces in a natural groundwater environment: Chemical Geology, v. 116, p. 111-121.

Freeze, R.A., and Cherry, J.A.,1979, Groundwater: Englewood Cliffs, Prentice-Hall.

Gilkes, R.J., and McKenzie, R.M., 1988, Geochemistry and mineralogy of manganese in soils, *in* Graham, R.D., Hannam, R.J., and Uren, N.C., eds, Manganese in Soils and Plants: Dordrecht, Kluwer, p. 23-35.

Gilroy, D.J., Vinson, D.S., Thibault, J.R., Cleverly, J.R., Dahm, C.N., and Crossey, L.J., 2001, Intermittent saturation of shallow aquifer sediments along the Middle Rio Grande, New Mexico: Geological Society of America Abstracts with Programs, v. 33, no. 5, p. 53.

Goldstein, J.I., Newbury, D.E., Echlin, P., Joy, D.C., Romig, A.D., Lyman, C.E., Fiori, C., and Lifshin, E., 1992, Scanning Electron Microscopy and X-ray Microanalysis, 2nd ed: New York, Plenum.

Grassel, K., 2002, Taking Out the Jacks: Issues of Jetty Jack Removal in Bosque and River Restoration Planning, University of New Mexico Water Resources Program, Publication WRP-6, http://www.unm.edu/~wrp.

Groffman, A.R., 2001, Biogeochemical and Hydrochemical Structure of an Alluvial Aquifer with Emphasis on Redox Conditions and Cycling of Iron and Manganese: Ph.D dissertation, University of New Mexico.

Groffman, A.R., and Crossey, L.J., 1999, Transient redox regimes in a shallow alluvial aquifer: Chemical Geology, v. 161, p. 415-442.

Groffman, A.R., Crossey, L.J., and Fellows, C.S., 1998, The upper water table: A reactive interface between ground water and surficial biogeochemical processes in a shallow alluvial aquifer: Mineralogical Magazine, v. 62A, p. 543-544.

Gutzler, D.S. and Preston, J.W., 1997, Evidence for a relationship between spring snow cover in North America and summer rainfall in New Mexico: Geophysical Research Letters, v. 24, p. 2207-2210.

Hanert V. H., 1974, In situ-Untersuchungen zur Analyse und Intensität der Eisen(III)-Fällung in Dränungen: Z. Kulturtechnik und Flurbereinigung, v. 15, p. 80-90.

Hanert, H.H., 2002, Bacterial and chemical iron oxide deposition in a shallow bay on Palaea Kameni, Santorini, Greece: Microscopy, electron probe microanalysis, and photometry of in situ experiments: Geomicrobiology Journal, v. 19, p. 317-342.

Hansen, S., and Gorbach, C., 1997, Middle Rio Grande Water Assessment: Final Report: Albuquerque, U.S. Bureau of Reclamation.

Happ, S.C., 1948, Sedimentation in the Middle Rio Grande Valley, New Mexico: Bulletin of the Geological Society of America, v. 59, p. 1191-1214.

Harvey, R.W., Smith, R.L., and George, L., 1984, Effect of organic contamination upon microbial distributions and heterotrophic uptake in a Cape Cod, Mass., aquifer: Applied and Environmental Microbiology, v. 48. p. 1197-1202.

Hawley, J.W., and Whitworth, T.M., 1996, Hydrogeology of Potential Recharge Areas for the Basin- and Valley-fill Aquifer Systems, and Hydrogeochemical Modeling of Proposed Artificial Recharge of the Upper Santa Fe Aquifer, Northern Albuquerque Basin, New Mexico: New Mexico Bureau of Mines and Mineral Resources Open-File Report OF402-D.

Herbert, R.B., Benner, S.G., Pratt, A.R., and Blowes, D.W., 1998, Surface chemistry and morphology of poorly crystalline iron sulfides precipitated in media containing sulfate-reducing bacteria: Chemical Geology, v. 144, p. 87-97.

Holm, P.E., Nielsen, P.H., Albrechtsen, H., and Christensen, T.H., 1992, Importance of unattached bacteria and bacteria attached to sediment in determining potentials for degradation of xenobiotic organic contaminants in an aerobic aquifer: Applied and Environmental Microbiology, v. 58, p. 3020-3026.

Howe, W.H. and Knopf, F.L., 1991, On the imminent decline of Rio Grande cottonwoods in central New Mexico: The Southwestern Naturalist, v. 36, p. 218-224.

Jackson, M.L., 1969, Soil Chemical Analysis, Advanced Course (2nd ed., published by author, Madison, Wisconsin), p. 44-51.

Jackson, R.E., and Patterson, R.J., 1982, Interpretation of pH and Eh trends in a fluvial-sand aquifer system: Water Resources Research, v. 18, p. 1255-1268.

Jakobsen, R. and Postma, D., 1999, Redox zoning, rates of sulfate reduction and interactions with Fe-reduction and methanogenesis in a shallow sandy aquifer, Rømø, Denmark: Geochimica et Cosmochimica Acta, v. 63 p. 137-151.

Jensen, D.L., Boddum, J.K., Tjell, J.C., and Christensen, T.H., 2002, The solubility of rhodochrosite ($MnCO_3$) and siderite ($FeCO_3$) in anaerobic aquatic environments: Applied Geochemistry, v. 17, p. 503-511.

Kelley, V.C., 1977, Geology of Albuquerque Basin, New Mexico: New Mexico Bureau of Mines and Mineral Resources Memoir 33.

Klein, C., 2002, Manual of Mineral Science, 22nd ed: New York, Wiley.

Lagasse, P.F., 1981, Geomorphic response of the Rio Grande to dam construction, *in* Wells, S.G., and Lambert, W., eds., Environmental Geology and Hydrology in New Mexico: New Mexico Geological Society, Special Publication 10, p. 27-46.

Lindberg, R.D., and Runnels, D.D., 1984, Ground water redox reactions: An analysis of equilibrium state applied to Eh measurements and geochemical modeling: Science, v. 225, p. 925-927.

Little, B.J., Wagner, P.A., and Lewandowski, Z., 1997, Spatial relationships between bacteria and mineral surfaces, *in* Banfield, J.F, and Nealson, K.H., eds., Geomicrobiology: Interactions between Microbes and Minerals. Reviews in Mineralogy, v. 35. Ribbe, P.H., series ed: Washington, Mineralogical Society of America, p. 391-428.

Love, D.W., 2000, Preliminary Geologic Map of Veguita Quadrangle: New Mexico Bureau of Mines and Mineral Resources, open-file geologic map.

Lovley, D.R. and Klug, M.J., 1983, Sulfate reducers can outcompete methanogens at freshwater sulfate concentrations: Applied and Environmental Microbiology, v. 45, p. 187-192.

Lovley, D.R., 1987, Organic matter mineralization with the reduction of ferric iron: A review: Geomicrobiology Journal, v. 5., p. 375-399.

Lovley, D.R., 2000, Fe(III) and Mn(IV) reduction, *in* Environmental Microbe-Metal Reactions, D.R. Lovley, ed.: Washington, American Society for Microbiology Press, p. 3-30.

Lozinsky, R.P., 1994, Cenozoic stratigraphy, sandstone petrology, and depositional history of the Albuquerque Basin, central New Mexico, *in* Keller, G.R., and Cather, S.M., eds., Basins of the Rio Grande Rift: Structure, Stratigraphy, and Tectonic Setting: Geological Society of America Special Paper 291, p. 73-81.

Lozinsky, R.P., Hawley, J.W., and Love, D.W., 1991, Geologic overview and Pliocene-Quaternary history of the Albuquerque basin, central New Mexico, *in* Julian, B. and Zidek, J., eds., Field Guide to Geologic Excursions in New Mexico and Adjacent Areas: New Mexico Bureau of Mines and Mineral Resources Bulletin, v. 137, p. 157-162.

Magaritz, M., Wells, M., Amiel, A.J., and Ronen, D., 1989, Application of a multi-layer sampler based on the dialysis cell technique for the study of trace metals in groundwater: Applied Geochemistry, v. 4, p. 617-624.

Matsunaga, T., Karametaxas, G., von Gunten, H.R., and Lichtner, P.C., 1991, Redox chemistry of iron and manganese minerals in river-recharged aquifers: A model interpretation of a column experiment: Geochimica et Cosmochimica Acta, v. 57, p. 1691-1704.

McBride, E.F., 1963, A classification of sandstones: Journal of Sedimentary Petrology, v. 33, p. 664-669.

McKeague, J.A. and Day, J.H., 1966, Dithionate- and oxalate-extractable Fe and Al as aids in differentiating various classes of soils: Canadian Journal of Soil Science, v. 46, p. 13-22.

Mehra, O.P., and Jackson, M.L., 1960, Iron oxide removal from soils and clays by a dithionate-citrate system buffered with sodium bicarbonate, *in* Proceedings of the Seventh National Conference on Clays and Clays Minerals: New York, Permangon, p. 317-327.

Molles, M.C., 1999, Ecology: Concepts and Applications: Dubuque, WCB/McGraw-Hill.

Molles, M.C., and Dahm, C.N., 1990, A perspective on El Niño and La Niña: Global implications for stream ecology: Journal of the North American Benthological Society, v. 9, p. 68-76.

Molles, M.C., Crawford, C.S., Ellis, L.M., Valett, H.M., and Dahm, C.N., 1998, Managed flooding for riparian ecosystem restoration: BioScience, v. 48, p. 749-756.

Molles, M.C., Dahm, C.N., and Crocker, M.T., 1992, Climatic variability and streams and rivers in semi-arid regions *in* Robarts, R.D., and Bothwell, M.L., eds., Aquatic Ecosystems in Semi-Arid Regions: Implications for Resource Management: NHRI Symposium Series 7, Saskatoon, Environment Canada.

Mullet, M., Boursiquot, S., Abdelmoula, M., Génin, J., and Ehrhardt, J., 2002, Surface chemistry and structural properties of mackinawite prepared from reaction of sulfide ions with metallic iron: Geochimica et Cosmochimica Acta, v. 66, p. 829-836.

Murphy, J., and Riley, J.P., 1962, A modified single solution method for the determination of phosphate in natural waters: Analytica Chimica Acta, v. 27, p. 31-36.

Nealson, K.H., 1983, The microbial iron cycle, *in* Krumbein, W.E., ed., Microbial Geochemistry: Oxford, Blackwell, p. 159-190.

Nealson, K.H., and Stahl, D.A., 1997, Microorganisms and biogeochemical cycles: What can we learn from layered microbial communities? *in* Banfield, J.F, and Nealson, K.H., eds., Geomicrobiology: Interactions between Microbes and Minerals. Reviews in Mineralogy, v. 35. Ribbe, P.H., series ed: Washington, Mineralogical Society of America, p. 5-33.

Nordstrom, D.K., and Wilde, F.D., 1998, Reduction-oxidation potential (electrode method): National Field Manual for the Collection of Water-Quality Data, U.S. Geological Survey, Techniques of Water-Resources Investigations, Book 9, Section 6.5, http://water.usgs.gov/owq/FieldManual/Chapter6/6.5_contents.html.

Parkhurst, D.L., and Appelo, C.A.J., 1999, User's Guide to PHREEQC (Version 2) - A Computer Program for Speciation, Batch-Reaction, One-Dimensional Transport, and Inverse Geochemical Calculations: U.S. Geological Survey Water-Resources Investigations Report 99-4259.

Pemberton, E.L., 1964, Sediment investigations – Middle Rio Grande: Journal of the Hydraulics Division, Proceedings of the American Society of Civil Engineers, v. HY 2 (March), p. 163-185.

Peter, K.D., 1987, Ground-water Flow and Shallow-aquifer Properties in the Rio Grande Inner Valley South of Albuquerque, New Mexico: U.S. Geological Survey Water-Resources Investigations Report 87-4015.

Pósfai, M., Buseck, P.R., Bazylinski, D.A., and Frankel, R.B., 1998, Reaction sequence of iron sulfide minerals in bacteria and their use as biomarkers: Science, v. 280, p. 880-883.

Post, V.E.A., 2001, PHREEQC for Windows v. 1.5.08, http://www.geo.vu.nl/users/posv/phreeqc.html.

Postma, D., 1993, The reactivity of iron oxides in sediments: A kinetic approach: Geochimica et Cosmochimica Acta, v. 57, p. 5027-5034.

Postma, D., and Jakobsen, R., 1996, Redox zonation: Equilibrium constraints on the Fe(III)/SO_4-reduction interface: Geochimica et Cosmochimica Acta, v. 60, p. 3169-3175.

Rittenhouse, G., 1944, Sources of modern sands in the Middle Rio Grande valley, New Mexico: Journal of Geology, v. 52, p. 145-183.

Robbins, E.I., Corley, T.L., and Conklin, M.H., 1999, Manganese removal by the epilithic microbial consortium at Pinal Creek near Globe, Arizona: U.S. Geological Survey, Toxic Substances Hydrology Program, Proceedings of Technical Meeting, Charleston, S.C., Mar. 8-12, 1999: U.S. Geological Survey Water-Resources Investigations Report 99-4018A, vol. 1.

RockWare, Inc., 1999, RockWorks99: Golden, Colo.

Roden, E.E., and Edmonds, J.W., 1997, Phosphate mobilization in iron-rich anaerobic sediments: microbial Fe(III) oxide reduction versus iron-sulfide formation: Archiv fur Hydrobiologie, v. 139, p. 347-378.

Roden, E.E., Sobolev, D., Glazer, B., and Luther, G.W., in press, New insights into the biogeochemical cycling of iron in circumneutral sedimentary environments: Potential for rapid microscale bacteria Fe cycling at the aerobic-anaerobic interface, *in* The Biogeochemistry of Iron Cycling in Natural Environments, ed. Coates, J.D. and Zhang, C.: Kluwer.

Ronen, D., Magaritz, M., and Levy, I., 1986a, A multi-layer sampler for the study of detailed hydrochemical profiles in groundwater: Water Research, v. 20, p. 311-315.

Ronen, D., Magaritz, M., Paldor, N., and Bachmat, Y., 1986b, The behavior of groundwater in the vicinity of the water table evidenced by specific discharge profiles: Water Resources Research, v. 22, p. 1217-1224.

Russell, L.R., and Snelson, S., 1994, Structure and tectonics of the Albuquerque Basin segment of the Rio Grande rift: Insights from reflection seismic data, *in* Keller, G.R., and Cather, S.M., eds., Basins of the Rio Grande Rift: Structure, Stratigraphy, and Tectonic Setting: Geological Society of America Special Paper 291, p. 83-112.

Scurlock, D., 1998, From the Rio to the Sierra: An Environmental History of the Middle Rio Grande Basin: US Department of Agriculture, Forest Service, Rocky Mountain Research Station, General Technical Report RMRS-GTR-5, Fort Collins, Colo.

Sobolev, D., and Roden, E.E., 2001, Suboxic deposition of ferric iron by bacteria in opposing gradients of Fe(II) and oxygen at circumneutral pH: Applied and Environmental Microbiology, v. 67, p. 1328-1334.

Stanford, J.A., and Ward, J.V., 1993, An ecosystem perspective of alluvial rivers: connectivity and the hyporheic corridor: Journal of the North American Benthological Society, v. 12, p. 48-60.

Straub, K.L., Benz, M., and Schink, B., 2001, Iron metabolism in anoxic environments at near neutral pH: FEMS Microbiology Ecology, v. 34, p. 181-186.

Surman, S.B., Walker, J.T., Gottard, D.T., Morton, L.H.G., Keevil, C.W., Weaver, W., Skinner, A., Hanson, K., Caldwell, D., and Kurtz, J., 1996, Comparison of microscope techniques for the examination of biofilms: Journal of Microbiological Methods, v. 25, p. 57-70.

Tebo, B.M., and He, L.M., 1998, Microbially mediated oxidative precipitation reactions, *in* Sparks, D.L. and Grundl, T.J., eds., Mineral-Water Interfacial Reactions: Kinetics and Mechanisms: American Chemical Society Symposium Series, no. 715, p. 393-414.

Theis, C.V., 1938, Ground water in the Middle Rio Grande Valley, New Mexico, in National Resources Committee, ed., Regional Planning, Part VI-The Rio Grande Joint Investigation in the Upper Rio Grande Basin in Colorado, New Mexico, and Texas, 1936-1937, Pt. II, Section 3, p.268-291.

Thorstenstein, D.C., 1984, The Concept of Electron Activity and its Relation to Redox Potentials in Aqueous Geochemical Systems: U.S. Geological Survey Open-File Report 84-072.

Tuhela, L., Carlson, L., and Tuovinen, O.H., 1997, Biogeochemical transformations of Fe and Mn in oxic groundwater and well water environments: Journal of Environmental Science and Health, Part A, vol. A32, p. 407-426.

Titus, F.B., 1963, Geology and Ground-Water Conditions in Eastern Valencia County, New Mexico: New Mexico Bureau of Mines and Mineral Resources Ground-Water Report 7.

U.S. Fish and Wildlife Service, 2002, Middle Rio Grande Bosque Initiative website, http://mrgbi.fws.gov.

Wersin, P., Höhener, P., Giovanoli, R., and Stumm, W., 1991, Early diagenetic influences on iron transformations in a freshwater lake sediment: Chemical Geology, v. 90, p. 233-252.

Woodward, L.A., 1984, Tectonic map of the Rocky Mountain region of the United States, *in* Sloss, L.L., ed., Sedimentary Cover of the Craton: U.S. The Geology of North America, vol. D-2: Boulder, Geological Society of America, plate 2.

Zachara, J.M., Kukkadapu, R.K., Fredrickson, J.K., Gorby, Y.A., and Smith, S.C., 2002, Biomineralization of poorly crystalline Fe(III) oxides by dissimilatory metal reducing bacteria: Geomicrobiology Journal, v. 19, p. 179-207.